sciendo

Eur. Pharm. J. 2021, 68(1), 1-9.
ISSN 1338-6786 (online) and ISSN 2453-6725 (print version),
DOI: 10.2478/afpuc-2020-0015

EUROPEAN PHARMACEUTICAL JOURNAL

Sedative Effect and Standardization Parameters of Herbal Medicinal Product Obtained from the *Ocimum americanum* L. Herb

Original Paper

Shanaida M.[1]✉, Golembiovska O.[2], Jasicka-Misiak I.[3], Oleshchuk O.[1], Beley N.[1], Kernychna I. [1],Wieczorek P.P. [3]

[1]*I. Horbachevsky Ternopil National Medical University*
[2]*Institute of Organic Chemistry National Academy of Sciences of Ukraine*
[3]*Opole University*

Received 9 September, 2020, accepted 1 February, 2021

Abstract Sedative phytomedications continue to play an important role in the management of a considerable amount of anxiety symptoms because of the various side effects of synthetic sedatives and tranquilizers. However, developing new herbal drugs needs their appropriate quality control according to the relevant requirements. The aim of the study was to determine the sedative properties of the tinctures obtained from the American basil (*Ocimum americanum* L., *Lamiaceae* Martinov family) herb and to develop the standardization parameters for the promising herbal medicinal product. The open field test was used to evaluate the sedative effect of the prepared tinctures: (1) with the added of *O. americanum* essential oil (OATEs) and (2) without adding *O. americanum* essential oil (OAT). The standardization parameters for the OATEs were developed using validated High-Performance Thin Layer Chromatography (HPTLC) and High-Performance Liquid Chromatography (HPLC) methods. The HPTLC analysis was used for the chromatographic fingerprints of polyphenols and for identifying linalool in the OATEs. The HPLC analysis found the significant content of rosmarinic acid (RA) (0.26%) in the OATEs. In conclusion, the developed OATEs can be considered as the new herbal medicinal product with significant sedative properties.

Keywords *American basil – herb – tincture – sedative activity – polyphenols – linalool – chromatographic analysis*

INTRODUCTION

Rational phytotherapy is a modern concept of herbal medicines that uses the standardized herbal medicinal products (Choudhary et al., 2011). A significant number of components in the tinctures and extracts from the plant raw materials are accompanied by the problem of their standardization. Quality control of herbal drugs should be done according to the requirements of relevant regulations (American Herbal Pharmacopoeia, 2011; European Pharmacopoeia, 2016).

Anxiety and depression are the important health problems in a modern society leading to low quality of life (Gutiérrez et al., 2015). Sedatives continue to play an important role in managing many anxiety symptoms in the context of medical illness. However, the side effects of synthetic anxiolytic drugs such as various syndromes of withdrawal, dependencies, and impairment of cognitive function and memory are of concern to physicians and scientists. Searching of new sources of plant raw material with anxiolytic action among the *Lamiaceae* Martinov species is a promising direction of scientific investigations is the area of phytochemistry and ethnopharmacology (Rabbani et al., 2015; Caputo et al., 2018; Bittner Fialová et al., 2019). Pharmaceutical industries produce a lot of phytomedications of a sedative action using the aerial parts of the *Lamiaceae* representatives such as *Leonurus cardiaca, Melissa officinalis, Mentha×piperita*, *Lavandula angustifolia,* and so on (Kowalczyk et al., 2012; Derzhavnyi rejestr, 2020).

Tincture, as a water-ethanol extract of a plant material being prepared at room temperature, preserves the complex as non-volatile so as volatile compounds (Doughari, 2012). The quality of tinctures or any herbal medicinal products primarily depends on the presence and content of the certain ingredients with proven biological activity (Hudz et al., 2019).

* *E-mail: shanayda-mi@ukr.net*

High-Performance Thin Layer Chromatography (HPTLC) and High-Performance Liquid Chromatography (HPLC) methods have become increasingly practiced for routine analysis of herbal medicinal products obtained from the representatives of Mint Family (Staszek et al., 2013; Shafqatullah et al., 2014; Asha et al., 2015) as well as synthetic drugs (Logoyda et al., 2018).

American basil (*O. americanum* L.) belongs to the genus *Ocimum* L., subfamily *Nepetoideae* Burnett, family *Lamiaceae*. It is an annual essential oil-bearing plant native to Africa and Southeast Asia used locally as a spice or ornamental plant as well as a sedative, digestive, and anti-inflammatory remedy (The Genus *Ocimum*, 2006; Shanaida et al., 2017). Nowadays, this species is successfully naturalized on most continents. The aerial part of *O. americanum* accumulates several valuable groups of primary and secondary metabolites such as terpenoids, polyphenols, and amino acids, which are perspective for the sedative purpose (Koteswar and Babu, 2011; Shanayda, 2012; Shanaida et al., 2017; Shanaida and Golembiovska, 2018; Shanaida et al., 2018). Linalool (49.84%) that possesses significant sedative properties (Linck et al., 2009; Aprotosoaie et al., 2014) was the major component of essential oil hydrodistillated from the *O. americanum* herb collected in Ukraine (Shanayda, 2012). Rosmarinic acid (19.59 mg/g) was revealed by HPTLC as a predominant polyphenolic compound in the methanol extract of this plant raw material (Shanaida et al., 2020). However, the raw material of this species is not included in any Pharmacopoeias (American Herbal Pharmacopoeia, 2011; European Pharmacopoeia, 2016). Thus, studying the sedative properties of tinctures obtained from the herb of *O. americanum* and developing their quality parameters can be considered as quite a perspective.

The aim of the study was to determine the sedative effects of the tinctures obtained from the *Ocimum americanum* herb and to develop the standardization parameters for the promising herbal medicinal product by the validated HPTLC and HPLC methods.

MATERIALS AND METHODS

Plant material and preparing of tinctures

The herb of *O. americanum* was collected from the experimental plots in Ternopil region (Ukraine). Plants were grown from the seeds obtained from the collection of M. Hryshko National Botanical Garden (Kyiv, Ukraine). A voucher specimen (OM: 10011) has been deposited in the Herbarium of **I. Horbachevsky Ternopil National Medical University** for further references. The herb was harvested during the flowering stage, then dried in the shadow at 25–35°C. Two tinctures were prepared from the *O. americanum* herb using 70% ethanol (*V/V*): (1) with added *O. americanum* essential oil (OATEs) and (2) without adding *O. americanum* essential oil (OAT).

The powdered herb of the plant (20.0 g) was macerated with 200 mL ethanol (70%, *V/V*) at room temperature for 24 hours using forced periodic stirring. The supernatant was separated and filtered with a Buchner funnel, then placed for 2 days in the refrigerator (at 8–10 °C) for the sedimentation of ballast substances. The total ratio of raw material and tincture obtained by the described method was 1:10 (if necessary, 70% ethanol was added to get 200 mL of OAT). The OATEs was obtained by the adding 0.5 mL of *O. americanum* essential oil hydrodistillated from its herb to 100 mL of OAT. The volume of *O. americanum* essential oil chosen for dissolving into basic ethanol extract was analogous to the dose of *Mentha × piperita* (*Lamiaceae*) essential oil, which is added to the '*Menthae piperitae* tincture' to enhance its pharmacological effect (Derzhavnyi reiestr, 2020). The essential oil of *O. americanum* was first dissolved in ethanol (96%, *V/V*) in the ratio 1:4, and then this solution was added to 100 mL of OAT to obtain a homogeneous solution.

Drugs and chemicals

Ethanol, ethyl acetate, and formic acid were purchased from Merck (Kennborough, NJ, USA). Aluminium chloride, toluene, Tween-80, anisaldehyde were purchased from Sigma-Aldrich (Germany). HPLC-grade acetonitrile, methanol, and trifluoracetic acid were purchased from Sigma-Aldrich (USA). Double-distilled water prepared using a Milli-Q water purification system (Millipore system). Silica gel plates for HPTLC and reference standards such as linalool, rutin, caffeic acid, and rosmarinic acid (RA) were purchased from Merck (Germany). Diazepam (5 mg/mL) was obtained from the Elegant (India). All the chemicals used in this study were of analytical grade.

Open field test

The spontaneous locomotor activities of experimental animals were assessed according to Linck et al. (2009) and Sarker Apu et al. (2013). Open field device consisted of a wooden field of one square meter with a series of squares and holes at their intersection; the floor was divided into 25 marked small squares of equal dimensions (20 × 20 cm). This device was placed in a dimly lit room.

Animals: male albino rats (220–240 g) were obtained from the Vivarium of I. Horbachevsky Ternopil National Medical University (Ukraine). Animals were kept in the standard laboratory conditions: relative humidity 55±5%; room temperature 22±2°C under a 12 h light/dark cycle. The animals were provided with standard diet and clean water *ad libitum* during acclimatization period. They were fasted overnight, with free access to water before the experiments. All the experimental animals were conformed to internationally accepted standards, which were approved by the Bioethical Committee of I. Horbachevsky Ternopil National Medical University, in accordance with 'Ethical Principles and Guidelines for Experiments on Animals' (2005).

The tested animals were randomly divided into four groups (n = 6). The rats were fasted for 12 h before the experiment. The tinctures were dissolved in the vehicle (1% solution of Tween-80 in distilled water) to obtain the dose 100 mg/kg body weight, calculated in terms of dry residue of tincture. Each group of animals received a particular treatment. Group I: negative control (vehicle). Group II: treatment with OAT. Group III: treatment with OATEs. Group IV: positive control (reference drug Diazepam at a dose of 0.55 mg/kg body weight). After one hour of the treatment, each animal was placed individually at the centre of the device and observed for 3 min to count the number of actions. The open field arena was thoroughly cleaned between each test to avoid the influence of the urine odours and faeces of the previous animal.

HPTLC analysis of OATEs

The HPTLC method was performed as described by Shanaida et al. (2020) with some modifications. 5 µL of OATEs and 10 µL of standard solutions (0.25 mg/mL of phenolic compounds and 5 µL/mL of linalool) were applied to HPTLC plates using an automatic HPTLC application device (Linomat 5, CAMAG, Muttenz, Switzerland). The chromatographic separation was performed on 20 × 10 cm HPTLC plates. Two mobile phases were used for eluting process: the ethyl acetate – toluene (5:95, *V/V*) was used for method A, and the ethyl acetate – formic acid – water (15:1:1, *V/V*) was applied for method B. The chromatographic plates were evaluated after derivatization with anisaldehyde reagent (method A) or with 1% aluminium chloride solution in methanol (method B). The resulting bands were observed under the daylight (method A) and with UV at 254 and 366 nm. The obtained chromatograms were analysed using HPTLC software (vision CATS, CAMAG). The compounds were identified using their R_f values and colours of the fluorescence comparatively to those of the reference standards. The applied HPTLC method was validated using specificity and robustness parameters.

HPLC analysis of OATEs

The quantitative analysis of RA in the OATEs was performed with Shimadzu HPLC-DAD system (Shimadzu, Japan). Good separation was achieved by a Phenomenex Luna C18 column (Phenomenex Inc., 250 x 4.6 mm i.d., 5 µm particle size) at 35°C. The UV absorption spectra of the reference standards and test samples were recorded in the range from 190 to 400 nm. The mobile phase consisted of two solutions: A (0.1% trifluoroacetic acid in water) and B (0.1% trifluoroacetic acid in acetonitrile). The flow rate was 1.0 mL/min and injection volume was 5 µL. The developed HPLC method for analysis of RA content in the OATEs was validated according to the linearity, specificity, limit of detection (LOD), limit of quantification (LOQ), precision, accuracy, and robustness parameters**.**

Statistical analysis

The variables for parametric data were analysed by one-way analysis of variance (ANOVA). Statistical analyses were performed using Statistica 12 software (StatSoft Inc., Tulusa, OK, USA). The data were expressed as mean ± standard error of the mean (SEM). The statistical significance was set at $p \leq 0.05$.

RESULTS AND DISCUSSION

Sedative activity of OAT and OATEs

The obtained OATEs demonstrated the noticeable sedative effect when compared to OAT for all the studied parameters in the open field test (Table 1). Anxiety level of animals after the single administration of OATEs decreased significantly. Sedative effect for OAT compared to Diazepam was observed only for the influence on defecation. Thus, adding essential oils of *O. americanum* to OAT led to increasing sedative activity. It was established that linalool as a predominant compound of *O. americanum* essential oil (Shanayda, 2012) added to tincture to obtain OATEs, possess significant sedative properties (Linck et al., 2009). As it can be seen from the Table 1, the number of squares crossed by the rats was the smallest after the treatment with OATEs. The frequency of defecation as an important indicator of anxiety after the OATEs influence was at the same level as a reference drug. The levels of tentative research activities such as vertical racks and examined holes were also the least numerous in the OATEs group compared to OAT and control groups.

Chromatographic analyses and standardization procedures for OATEs

HPTLC analysis

The HPTLC method for the qualitative determination of phenolic compounds and linalool in the OATEs was developed for the first time. A number of solvent systems were tried for OATEs chromatographic analysis. The satisfactory resolutions were reached using such solvent systems as ethyl acetate – toluene (5:95, *V/V*) for linalool (method A) and ethyl acetate – formic acid – water (15:1:1, *V/V*) for phenolic compounds (method B).

The validation of HPTLC procedure for the identification of linalool in the OATEs (method A) included the specificity and robustness studies. During the specificity study, it was revealed that chromatograms of the reference solution had the violet zone of linalool at $R_f = 0.29$ at daylight (Fig. 1, Table 2). The chromatogram of the test solution showed the weak violet zone at the level of linalool spot. The additional violet bands of unknown compounds possessing the specific for terpenoids violet shades were also available at R_f values 0.03, 0.11, 0.19, and 0.85 in the chromatogram of test solutions. The maximum difference in the values of the R_f zones of linalool

Table 1. The influence of tinctures prepared from Ocimum americanum herb on the spontaneous behavior of rats in the open field test (n = 6).

Group	Number of squares crossed	Tentative research activity		Indicators of anxiety (emotional reactions)		
		Vertical racks	Examined holes	Defecations	Urinations	Grooming
Control	32.61 ± 2.29	9.52 ± 0.89	5.21 ± 0.47	1.03 ± 0.1	0.51 ± 0.05	2.32 ± 0.21
OAT	29.17 ± 1.09	8.83 ± 0.28	4.83 ± 0.35	0.67 ± 0.09[1]	0.5 ± 0.05	2.33 ± 0.24
OATEs	26.0 ± 1.02[1]	8.0 ± 0.42[1]	4.5 ± 0.21	0.5 ± 0.05[1]	0.33 ± 0.02[1,2]	2.17 ± 0.19
Diazepam	18.5 ± 0.54[1]	6.5 ± 0.18[1]	3.17 ± 0.09[1]	0.5 ± 0.02[1]	0[1]	1.17 ± 0.04[1]

Notation. [1] – the differences are statistically significant for the values of the control group ($p \leq 0.05$); [2] – the differences are statistically significant for the values of the Diazepam group ($p \leq 0.05$)

Table 2. The results of HPTLC analyses of biologically active compounds in OATEs.

Compound	R_f value	Colour	Presence in OATEs	Presence in essential oil of *O. americanum*
Method A				
Unknown compound	0.03	Violet	+	-
Unknown compound	0.11	Violet	+	-
Unknown compound	0.19	Violet	+	-
Linalool	0.29	Violet	+	+
Unknown compound	0.85	Violet	+	+
Method B				
Rutin	0.09	Yellow	+	*
Unknown compound	0.14	Blue	+	*
Unknown compound	0.27	Yellow	+	*
Unknown compound	0.29	Blue	+	*
Unknown compound	0.43	Dark blue	+	*
Unknown compound	0.64	Blue	+	*
Rosmarinic acid	0.75	Blue	+	*
Caffeic acid	0.79	Blue	+	*

*Notation. '+' compound is presented; * – parameter was not studied*

Table 3. The robustness testing for the identification of linalool in OATEs by HPTLC.

Indicator	Level of changes	Rf variability (RSD, %)
Mobile phase composition (*ethyl acetate – toluene*, V/V)	5:95	0.6
	5.2:95	1.3
	4.8:95	0.8
Development distance, cm	8	1.3
	18	1.8
Chamber	3 different containers	1.3
Analysts	2 different analysts	0.8

corresponding the test and reference solutions within one plate was not exceed 0.01 units of R_f. The robustness studies for method A are presented in Table 3.

The specificity study of the polyphenols identified in OATEs (method B) showed that the chromatograms of reference and test solutions had the prominent blue fluorescent zone of RA (at λ = 366 nm) in the upper part at R_f = 0.75 (Fig. 2, Table 2). The less intense blue zone of caffeic acid was found at R_f = 0.79 and the yellow band of rutin was revealed at R_f = 0.09. The unknown compounds of blue shades were identified at 0.14, 0.29, 0.43, and 0.64 of R_f values, and yellow one corresponding to flavonoids was found at 0.27 in the chromatogram of test solutions. The differences in the values of the R_f zones of RA as a predominant component corresponding the test and

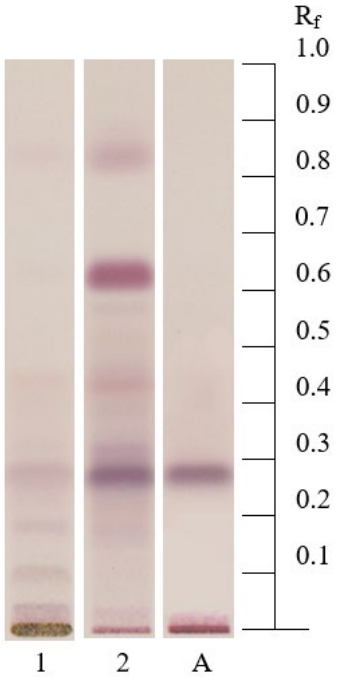

Figure 1. HPTLC chromatograms of the OATEs (1), Ocimum americanum essential oil (2), and linalool standard (A) after the derivatization with anisaldehyde solution at day light. Mobile phase: ethyl acetate – toluene (5:95).

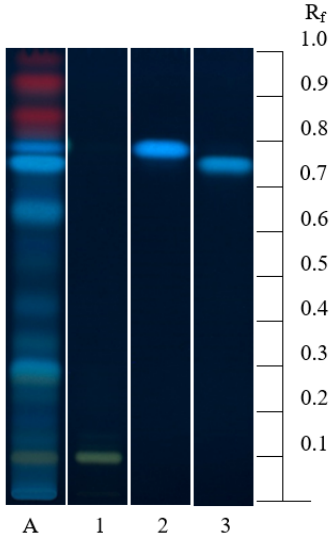

Figure 2. HPTLC chromatograms of the OATEs (A) and polyphenols standards (1 – rutin; 2 – caffeic acid; 3 – RA) after the derivatization with 1% methanolic $AlCl_3$ at λ=366 nm. Mobile phase: ethyl acetate – formic acid – water (15:1:1).

reference solutions within one plate did not exceed 0.01 units of R_f. The robustness studies of the RA identification in the OATEs are presented in Table 4.

Summarizing the abovementioned results, it was considered that the validated techniques for the identification of linalool and polyphenols in OATEs by the HPTLC method is a suitable procedure to control its quality in the 'Identification' test.

Table 4. The robustness testing of RA identification in OATEs by HPTLC.

Indicator	Level of changes	Rf variability (RSD, %)
Mobile phase composition *(ethyl acetate – formic acid – water, V/V)*	15:1:1	0.8
	15:1.05:1	1.3
	15:0.95:1	1.7
	15:1:1.05	1.3
	15:1:0.95	1.3
Development distance, cm	8	0.8
	18	1.3
Chamber	3 different containers	1.7
Analysts	2 different analysts	0.6

HPLC analysis

The content of RA as a predominant biologically active ingredient in the OATEs was assayed and validated by the HPLC for the first time. The mobile phase for HPLC consisted of two solutions: A (trifluoroacetic acid 0.1% in water), and B (trifluoroacetic acid 0.1% in acetonitrile) at 1.0 mL/min flow rate, volume of injection: 5 µL. All the solvents should be filtered through a 0.45 µm Millipore filter before use and degassed in an ultrasonic bath. Detection was made with spectrophotometer at 330 nm. HPLC was performed at 35°C column temperature. RA was determined using external standard method. The gradient elution was provided by mixing mobile phases A and B.

The validation of the HPLC test procedure for the analysis of RA content in the OATEs included specificity, linearity, accuracy, precision, and robustness studies. The specificity of the test was confirmed by the coincidence of retention time of the RA peak on the chromatogram of OATEs test solution with the retention of this peak on the chromatogram of RA standard solution (Fig. 3, 4). The chosen chromatographic conditions allowed to separate the peak of the RA from the peaks of other phenolic components. The values for the system suitability were an average of 6 replicates (Table 5). The linearity, recovery, accuracy, and range of HPLC method were defined on model mixtures with known content of active ingredients in the range of 80% to 120% of the RA nominal value (Table 6). The regression equation was calculated from the calibration curve for nine concentrations of the RA reference standard. The LOD and LOQ calculated for signal to noise ratio of 3 and 10, respectively. The aliquots of OATEs test solution was split and stored at 4°C. The aliquots were compared against the fresh-prepared reference standards at various intervals to determine the standard stability. It was recommended to perform all the experiments during a maximum of 3 days and to store stock and standard solutions in a refrigerator.

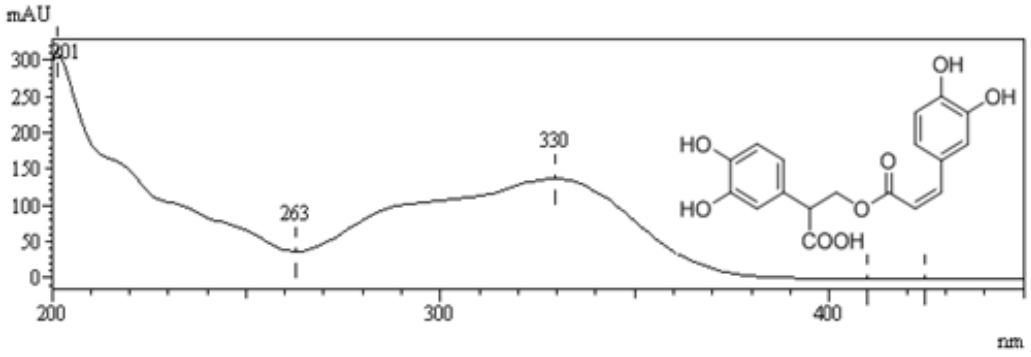

Figure 3. UV absorption spectrum of RA in the HPLC method.

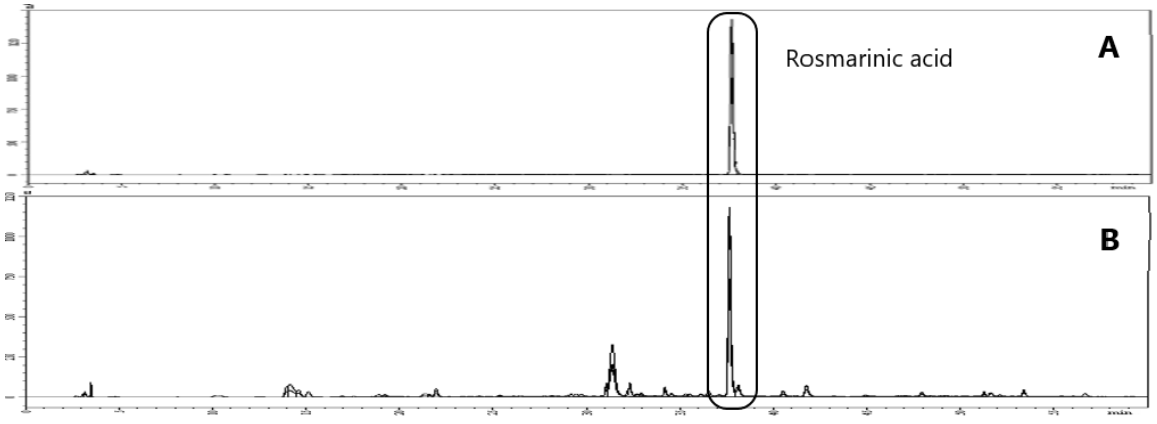

Figure 4. HPLC chromatogram of the RA standard solution (A) and OATEs (B) (λ=330 nm).

Table 5. The system suitability parameters for the determination of RA by HPLC.

Standard	Retention time (Rt)	Tailing factor (T)	Theoretical plates (N)
Rosmarinic acid	38.0	1.2	2399586

Table 6. The linearity, regression equation, limit of detection, limit of quantitation, precision parameters of RA standard in the HPLC analysis.

Standard	Linearity range [μg/ml]	Regression equation	R^2	LOD [μg/ml]	LOQ [μg/ml]	RSD [%]	
						Inter-day	Intra-day
Rosmarinic acid	5–50	Y = 0.235x + 0.164	0.9998	0.005	0.015	0.16	0.04

According to the results of the robustness study, the column temperature and the mobile phase flow within ±5% did not affect the test results significantly.

Standardization procedure

The standardization of the OATEs as a perspective herbal medicinal product has been carried out in accordance with the requirements of European Pharmacopoeia (2016) using such a scheme: definition (source of a plant material); production (method of extraction and solvent); characters (appearance, taste, odour), identification (by HPTLC); assay (content of the main biologically active compound by HPLC).

Definition. Tincture is produced from the *O. americanum* herb and its essential oil (OATEs).

Production. Tincture is produced from one part of dried herb using ethanol (70%, *V/V*) by a maceration method to obtain 10 parts of the finished product. Essential oil was dissolved first in ethanol (96%, *V/V)* in ratio 1:4, and then added to the tincture until 0.5% solution was obtained.

Characters. Greenish-brown transparent liquid with a specific aromatic small and bitter-burning taste.

Identification. Method A

Test solution. The tincture (OATEs) to be examined (10 µL).
Reference solution. Dissolve 25 µL of linalool in 5 mL of toluene.
Plate: TLC silica gel F_{254} plate (10 × 20 cm).
Mobile phase: *ethyl acetate – toluene* (5:95, *V/V*); *application*: 5 µL, as bands; *development*: 8 cm from the line of start; *drying*: in air.
Detection: treat with *anisaldehyde solution*, heat at 100–105°C for 5 min and examine in daylight immediately.
Results of TLC analysis. The chromatogram of the test solution in the lower third should be characterized by the weak violet zone of linalool (R_f = 0.29). Furthermore, other faint violet zones may be present in the chromatogram obtained with the test solution. Sequence of the zones present in the chromatograms obtained with the reference and test solutions (comparatively with the essential oil of *O. americanum*) are shown in Fig. 1.

Identification. Method B

Test solution. The tincture (OATEs) to be examined (10 µL).
Reference solutions. Dissolve (separately) 1 mg of rutin, 1 mg of caffeic acid, and 1 mg of RA in 4 mL of methanol.
Plate: TLC silica gel F_{254} plate (10 × 20 cm).
Mobile phase: *ethyl acetate – formic acid – water* (15:1:1, *V/V*); *application*: 5 µL, as bands; *development*: 8 cm from the line of start; *drying*: in air.
Detection: Visualization should be performed under UV light (254 nm, 366 nm) after spraying with 1% *aluminium chloride solution* and heating at 100–105°C for 5 min.
Results of TLC analysis. The chromatogram of the test solution should be characterized by intense blue zone of RA (R_f= 0.75) and less intense blue zone of caffeic acid (R_f= 0.79) just above it. The yellow zone of rutin should be evaluated at the bottom (R_f = 0.09). Furthermore, other faint blue and yellow zones may be present in the chromatogram obtained with the test solution. Red zones of chlorophyll may be present at the top. Sequence of the zones present in the chromatograms of the reference and test solutions are shown in Fig. 2.

HPLC analysis of RA content

Test solution. Introduce 1 mL of OATEs into a volumetric flask (100 mL) and dilute it by adding 70% ethanol to the mark. Filter the obtained solution through 0.45 µm Millipore filter.
Reference solution. Dissolve 15 mg of RA standard in 70% ethanol and dilute to 100.0 mL with the same solvent.
Column: Phenomenex Luna C18 column (250 x 4.6 mm i.d., 5 µm particle size) at 35°C as appropriate.
Mobile phase: Trifluoroacetic acid 0.1% in water (solution A), and trifluoroacetic acid 0.1% in acetonitrile (solution B) at 1.0 mL/min flow rate in a gradient elution mode (Table 7).
Detection: DAD (330 nm).

Table 7. The gradient mode in the HPLC analysis.

Time (min)	Mobile phase A (vol%)	Mobile phase B (vol%)
0–5	95	5
5–35	95 → 75	5 → 25
35–40	75	25
40–60	75 → 50	25 → 50
60–65	50 → 20	50 → 80
65–70	20	80
70–85	95	5

Results of HPLC analysis: 0.26 ± 0.01% of RA. Identification of RA achieved by comparison of the retention time on the chromatogram and the absorption spectra obtained for its peak in tincture with those obtained for the standard. The quantification of RA made by measuring its peak area at λ = 330 nm. The content of RA in tincture should be at minimum 0.2%.
As it is known, the healing properties of the herbal medicinal products can be viewed as a result of the synergistic effect of a lot of biologically active compounds (Yang et al., 2014). As the complexes of active compounds in the obtained tinctures can interact synergistically, the dominating of both RA and linalool in the OATEs could be the reason for the manifestation of its noticeable sedative action. A number of different pharmacologically active compounds with the possible sedative action was established in the *Ocimum americanum* water-ethanol extracts and essential oil (Shanayda, 2012; Shanaida and Golembiovska, 2018). The noticeable reduction in locomotor activity of the OATEs could either be due to the effect of its biologically active compounds on the central nervous system or a direct influence on the periphery as it was established for the related species *Ocimum sanctum* (Richard et al., 2016). Researchers observed a marked anxiolytic dose-dependent effect, similar to Diazepam, after using the water-ethanol extracts and essential oil of *Ocimum basilicum* herb (Rabbani et al., 2015). The sedative influence of the essential oil released by *Ocimum basilicum* plants was found in mice using open field test (Hirai and Ito, 2019). The sedative, anxiolytic, and antidepressant-like effects were established after the inhalation of *Ocimum gratissimum* essential oil in mice (Tankam et al., 2014).
The obtained data about the prevalence of RA among phenolic compounds in the OATEs revealed by the chromatographic methods correlates with the results of phytochemical analyses of the *O. americanum* herb (Shanaida et al., 2018; Shanaida et al., 2020). RA was also the 'marker component' of the ethanol extracts obtained from a lot of plants belonging to the *Lamiaceae* family such as *Origanum vulgare, Melissa officinalis, Rosmarinus officinalis, Ocimum basilicum, Salvia officinalis,* and *Hyssopus officinalis* (Staszek et al., 2013;

Benedec et al., 2015). RA can potentiate the pentobarbital-induced sleeping through the activation of $GABA_A$-ergic systems (Yeong et al., 2017). It can also demonstrate the antioxidant effect and other valuable biological activities similar to the other polyphenols containing more than 3 OH-groups in their molecules (Gontova et al., 2016; Rytsyk et al., 2020). Polyphenols possess free radicals scavenging activity, which can prevent neurodegenerative diseases (Cory et al., 2018). The methanol extract of *Stachytarpheta cayennensis* (order *Lamiales*) and its butanol, aqueous, and ethylacetate fractions demonstrated the sedative effect in a dose-dependent manner (Olayiwola et al., 2013).

Linalool as a key volatile molecule of many essential oils of the *Ocimum* species possess the sedative activity (Aprotosoaie et al., 2014). Linalool and other terpenoids can modify the function of $GABA_A$ receptors (Kessler et al., 2014). It was found that linalool and linalool-containing essential oil obtained from *Lavandula angustifolia* (*Lamiaceae*) aerial part were useful alternative tools to the available traditional treatments for social stress-induced mental illnesses such as anxiety and depression (Caputo et al., 2018; Agatonovic-Kustrin et al., 2020). The relationships between the contents of certain bioactive compounds of terpenoid and polyphenol nature in the *Leonurus cardiaca* (*Lamiaceae*) tinctures and their sedative effect were revealed by Romanenko et al. (2018).

The sedative properties of the obtained tinctures can be enhanced by some amino acids, which are extracted from the plant raw material with water and water-ethanol solutions (Shafaei et al., 2017; Shanaida et al., 2017). Besides γ-aminobutyric acid and glycine as the famous inhibitory neurotransmitter in the central nervous system, it was also established that the sedative effect of a lysine, arginine, alanine, serine, and cysteine acting via γ-aminobutyric acid receptors (Yamane et al., 2009). All these amino acids were found in the *Ocimum americanum* herb (Shanaida et al., 2017). The triterpenic ursolic acid possessing sedative action (Colla et al., 2015) was revealed in the 70% ethanol extract of *Ocimum americanum* (0.12%) (Shanaida and Golembiovska, 2018). Thus, the revealed sedative properties of the OATEs can be due to synergistic effects of RA and linalool as well as some amino acids and triterpenoids extracted from the *Ocimum americanum* raw material with water-ethanol solutions.

CONCLUSIONS

This study demonstrates the significant sedative effect of the OATEs developed from *O. americanum* herb using 70% ethanol and essential oil isolated from this plant. Such sedative property could be due to the common influence of RA and linalool as the predominant biologically active compounds in OATEs as well as some amino acids and triterpenoids. More tests and studies are needed to clarify the exact components with sedative activity in the developed herbal medicinal product. The necessary standardization parameters for the chromatographic analysis of the OATEs were established. The validated HPTLC method was successfully applied for identifying linalool and RA as the predominant compounds of the OATEs. The HPLC method was developed and validated to quantify the RA content in the OATEs. The current study provides a basis for the assessment of developed OATEs as the new perspective herbal medicinal product with sedative action.

CONFLICT OF INTEREST

There are no conflicts of interest declared by the authors.

References

[1] Agatonovic-Kustrin S, Kustrin E, Gegechkori V, Morton DW. Anxiolytic Terpenoids and Aromatherapy for Anxiety and Depression. Adv Exp Med Biol. 2020; 1260:283–296. doi: 10.1007/978-3-030-42667-5_11.

[2] American Herbal Pharmacopoeia. Botanical pharmacognosy – microscopic characterization of botanical medicines. CRC Press, 2011. 735 p.

[3] Aprotosoaie AC, Hancianu M, Costache Ii, Miron A. Linalool: a review on a key odorant molecule with valuable biological properties. Flavour Frag J. 2014; 29:193–219.

[4] Asha D, Mathew L, Kalappurakkal R. Evaluation of HPTLC fingerprints of flavonoids and antioxidant activity of selected medicinal plants of *Lamiaceae* Family. Int Journal of Pharmacognosy and Phytochemical Research. 2015; 7(2):240–245.

[5] Benedec D, Hanganu D, Oniga I, Tiperciuc B, Olah NK et al. Assessment of rosmarinic acid content in six *Lamiaceae* species extracts and their antioxidant and antimicrobial potential. Pak J of Pharm Sci. 2015; 28(6):2297–2303.

[6] Bittner Fialová S, Harris Ch, Ordsmith V, Nagy M, Jonáš F, Mučaji P. Polar phenolic compounds in peppermint rhizomes and leaves. Eur. Pharm. J. 2019; 66(1): 28–31.

[7] Caputo L, Reguilon MD, Mińarro J, De Feo V, Rodriguez-Arias M. *Lavandula angustifolia* essential oil and linalool counteract social aversion induced by social defeat. Molecules. 2018; 19; 23(10). pii: E2694. doi: 10.3390/molecules23102694.

[8] Choudhary N, Sekhon BS. An overview of advances in the standardization of herbal drugs. J Pharm Edu Res. 2011; 2 (2):55–70.

[9] Colla ARS, Rosa JM, Cunha MP, Rodrigues ALS. Anxiolytic-like effects of ursolic acid in mice. European Journal of Pharmacology. 2015; 758(5):171–176.

[10] Cory H, Passarelli S, Szeto J, Tamez M, Mattei J. The role of polyphenols in human health and food systems: A mini-review. *Front. Nutr.* 2018; 5(87).

[11] Derzhavnyi rejestr likarskyh zasobiv Ukrainy (2020). [ONLINE] Available at: http://www.drlz.com.ua (in Ukrainian)

[12] Doughari HJ. Phytochemicals: extraction methods, basic structures and mode of action as potential chemotherapeutic agents. *In:* Phytochemicals – a global perspective of their role in nutrition nd health. Ed. by V. Rao. 2012:1–32.

[13] European Pharmacopoeia. 2016. 8th Ed. [ONLINE] Available at: https://www.edqm.eu/en/european-pharmacopoeia-ph-eur-8th-edition

[14] Ethical Principles and Guidelines for Experiments on Animals. 2005. 3rd ed. Available at: https://publisher.medfak.ni.ac.rs/ASN_1/Ethical%20Principles-S.pdf

[15] Gontova T, Ilyinska N, Golembiovska O, Mashtaler V. Study of the component composition of phenolic compounds obtained from *Dahlia* varieties Ken's Flame herb. Der Pharma Chemica. 2016; 8(18):455–459.

[16] Gutiérrez SL, Chilpa RR, Jaime HB. Medicinal plants for the treatment of "nervios", anxiety, and depression in Mexican Traditional Medicine. Rev Bras Farmacogn. 2014; 24 (5):591–608.

[17] Hirai M, Ito M. Sedative effects of the essential oil and headspace air of *Ocimum basilicum* by inhalation in mice. J Nat Med. 2019; 73(1):283–288.

[18] Hudz N, Yezerska O, Shanaida M, Horčinová Sedláčková V, Wieczorek PP. Application of the Folin-Ciocalteu method to the evaluation of *Salvia sclarea* extracts. Pharmacia. 2019; 66(4):209–215.

[19] Kessler A, Sahin-Nadeem H, Lummis SC, Weigel I, Pischetsrieder M et al. GABA(A) receptor modulation by terpenoids from *Sideritis* extracts. Mol. Nutr. Food Res. 2014; 58:851–862. doi: 10.1002/mnfr.201300420

[20] Koteswar SB, Babu AV. Pharmacognostic and phytochemical studies of *Ocimum americanum*. J Chem Pharm Res. 2011; 3(3):337–347.

[21] Linck VM, da Silva AL, Figueiró M, Piato AL, Herrmann AP et al. Inhaled linalool-induced sedation in mice. Phytomedicine. 2009; 16:303–307.

[22] Logoyda L, Abdel-Megied A, Kondratova Y, Trofimenko O, Korobko D, Dakhym I. Development and validation of HPLC method for the simultaneous determination of enalapril maleate in present of their impurities: application to tablet analysis. International Journal of Applied Pharmaceutics. 2018; 10(1):98–102.

[23] Olayiwola G, Ukponmwan O, Olawode D. Sedative and anxiolytic effects of the extracts of the leaves of *Stachytarpheta cayennensis* in mice. Afr J Tradit Complement Altern Med. 2013; 10(6): 568–579.

[24] Rabbani M, Sajjadi SE, Vaezi A. Evaluation of anxiolytic and sedative effect of essential oil and hydroalcoholic extract of *Ocimum basilicum* L. and chemical composition of its essential oil. Res Pharm Sci. 2015; 10 (6):535–543.

[25] Richard EJ, Illuri R, Anandhakumar B, Anandhakumar S, Bhaskar A et al. Anti-stress activity of *Ocimum sanctum*: possible effects on hypothalamic–pituitary-adrenal axis. Phytotherapy Research. 2016; 30(5):805–814.

[26] Romanenko Ye, Koshovyi O, Kireyev I, Tryshchuk N, Ilyina T, Borodina N. Study of the relations between the main BAS groups content in *Leonurus cardiaca* tincture and its psychotropic activity. Ukraïns'kij bìofarmacevtičnij žurnal. 2018; 4 (57): 69–74 (in Ukrainian).

[27] Rytsyk O, Soroka Y, Shepet I, Vivchar Z, Andriichuk I et al. Experimental evaluation of the effectiveness of resveratrol as an antioxidant in colon cancer prevention. Natural product communications. 2020; 15(6):1934578X2093274

[28] Sarker Apu A, Hossan Bhuyan S, Matin M, Hossain F, Khatun F, Taiab A. Analgesic, neuropharmacological, anti-diarrheal, and cytotoxic activities of the extract of *Solanum sisymbriifolium* (Lam.) leaves. Avicenna J Phytomed. 2013; 3(4):302–312.

[29] Shafqatullah, Khan R, Hassan W. Development of HPLC method by UV-VIS detection for the quantification of phenolic acids in different *Ocimum sanctum* Linn. extracts. Pak J Pharm Sci. 2014; 27(5):1271–1275.

[30] Shafaei A, Ab Halim NH, Zakaria N, Ismail Z. Analysis of free amino acids in different extracts of *Orthosiphon stamineus* leaves by high-performance liquid chromatography combined with solid-phase extraction. Pharmacogn Mag. 2017; 13(Suppl 3):385–391.

[31] Shanaida M, Kernychna I, Shanaida Y. Chromatographic analysis of organic acids, amino acids, and sugars in *Ocimum americanum* L. Acta Poloniae Pharmaceutica – Drug Research. 2017; 74(2):729–734.

[32] Shanaida M, Golembiovska O. Identification and component analysis of triterpenoids in *Monarda fistulosa* L. and *Ocimum americanum* L. (*Lamiaceae*) aerial parts. ScienceRise: Pharmaceutical Science. 2018; 3(13):26–31.

[33] Shanaida M, Golembiovska O, Hudz N, Wieczorek PP. Phenolic compounds of herbal infusions obtained from some species of the *Lamiaceae* family. Current Issues in Pharmacy and Medical Sciences. 2018; 31(4):194–199.

[34] Shanaida M, Jasicka-Misiak I, Makowicz E, Stanek N, Shanaida V, Wieczorek PP. Development of high-performance thin layer chromatography method for identification of phenolic compounds and quantification of rosmarinic acid content in some species of *Lamiaceae* family. J Pharm Bioall Sci. 2020; 12 (2):139–145.

[35] Shanayda MI. Comparative analysis of essential oils components of *Ocimum* L. genus. Farmatz zhurnal. 2012; 4: 99–102. (in Ukrainian).

[36] Staszek D, Orłowska M, Waksmundzka-Hajnos M, Sajewicz M, Kowalska T. Marker fingerprints originating from TLC and HPLC for selected plants from the *Lamiaceae* family. J Chromatography. 2013; 36 (17):2463–2475.

[37] Tankam JM, Ito M. Sedative, anxiolytic and antidepressant-like effects of inhalation of the essential oil of *Ocimum gratissimum* L. from Cameroon in mice. Journal of Pharmacognosy and Phytochemistry. 2014; 2(5):1–9.

[38] The Genus *Ocimum* (Basil) / Ed. by R. Hiltunen and Y. Holm. Taylor & Francis e-Library. 2006.

[39] Yamane H, Kurauchi I, Denbow DM, Furuse M. Central functions of amino acids for the stress response in chicks. Asian-Aust. J. Anim. Sci. 2009; 22(2): 296–304.

[40] Yang Y, Zhang Z, Li S, Ye X, Li X, He K. Synergy effects of herb extracts: pharmacokinetics and pharmacodynamic basis. Fitoterapia. 2014; 92:133–147.

[41] Yeong Ok Kwon, Jin Tae Hong, Ki-Wan Oh. Rosmarinic acid potentiates pentobarbital-induced sleep behaviors and non-rapid eye movement (NREM) sleep through the activation of $GABA_A$-ergic systems. Biomol Ther (Seoul). 2017; 25(2):105–111.

sciendo

Eur. Pharm. J. 2021, 68(1), 10-16.
ISSN 1338-6786 (online) and ISSN 2453-6725 (print version),
DOI: 10.2478/afpuc-2020-0017

EUROPEAN PHARMACEUTICAL JOURNAL

Synthesis and Correlation of Aggregation and Antimicrobial Properties of Homochiral Quaternary Ammonium Bromides Derived from Camphoric Acid

Original Paper

Mikláš R.[1]✉, Miklášová N.[1], Bukovský M.[1]

[1]Department of Chemical Theory of Drugs, Faculty of Pharmacy, Comenius University, Odbojárov 10, 832 32 Bratislava, Slovak Republic

Received 25 November, 2020, accepted 12 February, 2021

Abstract A group of homochiral quaternary ammonium salts bearing hydrophobic camphoric acid-derived moiety was synthesized and characterized. The aggregation properties of the prepared compounds were evaluated by surface tension measurements, and the critical micelle concentration (CMC) was calculated. The novel quaternary ammonium bromides were tested as antimicrobial and antifungal agents, and their minimal inhibitory concentration (MIC) was evaluated and compared to clinically used benzalkonium bromide (BAB). Correlation of MIC with CMC reveals that monomers of prepared cationic surfactants, instead of micelles, are primarily responsible for antimicrobial activity.

Keywords *quaternary ammonium salts – antimicrobial activity – camphoric acid – critical micelle concentration*

INTRODUCTION

Quaternary ammonium salts (QASs) have found practical applications in many fields such as textile finishes (excellent fabric softeners), antielectrostatic agents and wood preservatives (Bureš, 2019; Gilbert & Moore, 2005, Kim & Sun, 2002, Piętka-Ottlik et al., 2012), catalysts (Shirakawa et al., 2012, Brak & Jacobsen, 2013), ionic liquids (Truong et al., 2012, Morel et al., 2013). Since it was found that cationic lipids, known as cytofectins, are efficient for delivering functional genes (Brigham et al., 1989), the use of cationic surfactants for mediating DNA transfection has increased (Sajomsang et al., 2013, Zhi et al., 2012, Cortesi et al., 2012). QAS with at least one long, hydrophobic chain attached to positively charged nitrogen belongs to the group of cationic surfactants (Rosen 1989). These salts possess properties such as adsorption at interfaces and self-aggregation in the bulk phase. In addition, the QASs with long alkyl chain show a strong biological activity against a broad range of microorganisms such as bacteria (both G+ and G-) and fungi (Lukáč *et al*., 2010; Mikláš *et al*., 2012, 2014; Soukup et al., 2020), certain viruses (Soukup et al., 2020; Wong *et al*., 2002), not excluding SARS-CoV (Schrank et al., 2020), anticancer agents (Kaushik *et al*., 2012), and many others.

The attraction of cationic surfactants for a negatively charged bacteria surface gives them the ability to intercalate into phospholipid membranes, thus causing the leakage of intercellular materials into the environment and cell death (Devínsky et al., 1985; Kopecká-Leitmanová et al., 1989; Mlynarčík et al., 1981). The disruption of membrane, and subsequent solubilization of its interior, plays an essential role in the mode of antimicrobial action of cationic surfactants and firmly depends on the ability of surfactant molecules to form micelles. Whereas micellization properties are linearly related to the length of the alkyl chains of cationic surfactant, the antimicrobial activity also depends on the number of carbon atoms in the long alkyl chain of surfactant molecule (Marek et al., 2018). The optimal antimicrobial activity for gram-positive bacteria is achieved when the carbon chain length is C12–C14, while for gram-negative bacteria, the highest activity is obtained for the chain length of C14–C16 (Feder-Kubis & Tomczuk 2013; Pernak and Skrzypczak, 1996; Thebault et al., 2009). Molecules with *n*-alkyl chain length below C4 and above C18 are antimicrobially ineffective. In the series of structurally related QASs, the antimicrobial activity increases with the growing chain length until it reaches the maximum. From this point, with a continuous growing chain length, the antimicrobial activity starts to decrease. This phenomenon, called cut-off effect, is typical for many of the biologically active compounds, and it can be caused by many

* *E-mail: miklas@fpharm.uniba.sk*

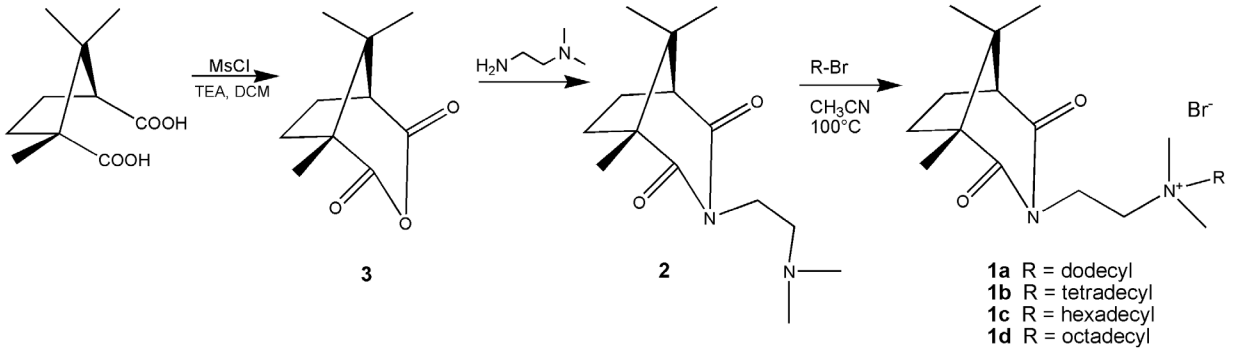

Figure 1. Synthesis of QASs derived from (1R,3S)-(+)-camphoric acid.

reasons (limited aqueous solubility, kinetic effects, interaction with lipid bilayers or proteins) (Balgavý & Devínsky, 1996).

The alkyl chain length is not the only factor affecting the antimicrobial activity of QASs. The other hydrophobic groups in the molecule of surfactant also influence the aggregation properties, so they can also affect the biological activity. The study of this effect on antimicrobial properties could help in the development of new active QASs (Benkova et al., 2019; Malinak et al., 2014).

In addition, introduction of new structural motives such as heteroatoms or aromatics (Semenov et al., 2011; Pernak et al., 2001) may result in potential antimicrobial agents with higher biological activities, and they could even conquer the growing resistance phenomenon (Jennings 2015). As long as essential oils containing bicyclical camphor or borneol moiety exhibit antibacterial effect (Ruiz-Navajas et al., 2012; Miguel et al., 2011), we decided to design and synthesize QASs bearing hydrophobic bicyclic moiety, hoping that incorporation of two important antimicrobially active structures in one compound will improve their bioactivity. In this study, we have prepared, as illustrated in Fig. 1, three new optically active amphiphilic QASs starting from (1*R*,3*S*)-(+)-camphoric acid. The aggregation properties of prepared surfactants were studied by tensiometry and critical micelle concentration (CMC); surface tension at CMC (γ_{CMC}) and efficiency of adsorption at the surface (pC_{20}) were calculated for each compound from a break in the plot of logarithm of surfactant's concentration versus surface tension. Their antimicrobial activity was tested against gram-negative bacteria *Escherichia coli*, gram-positive human pathogenic bacteria *Staphylococcus aureus*, and human fungal pathogen *Candida albicans*.

EXPERIMENTAL

Materials and methods

All compounds used ((1*R*,3*S*)-(+)-camphoric acid, methanesulfonyl chloride (MsCl), triethylamine (TEA), *N,N*-dimethylethane-1,2-diamine, acetone, dichloromethane (DCM), ethyl acetate, bromoalkanes) are commercially available. DCM was pre-dried over $CaCl_2$ and then distilled from CaH_2 under nitrogen atmosphere. ^1H and ^{13}C NMR spectra were measured on a Varian Gemini 300 spectrometer at 300 MHz and 75 MHz, respectively. Chemical shifts have been reported in ppm relative to an internal reference (TMS). IR spectra were recorded on NICOLET 6700 FT-IR instrument. Polarimetric measurements were obtained using a Jasco P-1010 polarimeter at 589 nm. Elemental analyses were carried out on a Carlo Erba 1108A instrument. All melting points reported were uncorrected and measured on Kofler hot stage. The surface tension measurements were performed on Krüss processor tensiometer K100 (Wilhelmy plate method). The temperature was kept constant at the desired level using thermostatted (Thermo Haake SC100) water bath. Double-distilled water was used for the preparation of all samples. Measurements of equilibrium surface tension were taken repeatedly until the change in surface tension was less than 0.08 mNm^{-1}. The values of surface tension decrease with increasing concentration and the break point provides the CMC value.

Microbiology

The antimicrobial activity was tested against gram-negative bacteria *Escherichia coli* CNCTC 377/79, gram-positive bacteria *Staphylococcus aureus* CNCTC 29/58, and fungi *Candida albicans* CCM 8186. Solutions of compounds studied were prepared in water (5%). A suspension of the standard microorganism, prepared from 24 h cultures of bacteria in blood agar and from 24 h cultures in the Sabouraud agar for fungi had a concentration of 5×10^7 cfu mL^{-1} of bacteria and 5×10^5 cfu mL^{-1} of *Candida*. The concentration of microorganisms was determined spectrophotometrically at 540 nm and adjusted to absorbance A = 0.35. The microorganism suspension was added to solutions containing the tested compound and to double concentrated peptone broth medium (8%) for bacteria or Sabouraud medium (12%) for *Candida*. The stock solution of the tested compounds was serially diluted by half. The cultures were done in 96-well microliter plates. The microorganisms were incubated for 24 h at 37°C, and then, from each well, 5 µL of suspension

Table 1. Characterization of camphoric acid-derived QAS 1.

Compound	Formula / $[\alpha]_D^{21}$ (conc[g/100 mL]., solvent)	w_i(calc.)/% w_i(found)/%			Yield	M.p.
		C	H	N	%	°C
1a	$C_{26}H_{49}BrN_2O_2$/ +7.99 (0.85, $CHCl_3$)	62.26 62.34	9.85 9.81	5.58 5.61	80	82–83.5
1b	$C_{28}H_{53}BrN_2O_2$/ +6.75 (0.809, $CHCl_3$)	63.50 63.26	10.09 9.96	5.29 5.15	87	85–85.5
1c	$C_{30}H_{57}BrN_2O_2$/ +7.2 (c = 0.799, $CHCl_3$)	64.61 64.36	10.30 9.96	5.02 4.85	84	95–96.8
1d	$C_{32}H_{61}BrN_2O_2$/ +6,7d (c = 0.80, $CHCl_3$)	65.62 65.68	10.50 10.45	4.78 4.82	85	96.8–97.5

were cultured on blood agar (bacteria) or on Sabouraud agar (fungi). After 24 h at 37°C, the lowest concentration of QAS that prevented colony formation was determined as minimal inhibitory concentration (MIC). Clinically used benzalkonuim bromide (BAB) was used as a standard.

Synthesis

1,8,8-trimethyl-3-oxa-bicyclo[3.2.1]octane-2,4-dione (**3**). (Eagles & Hitchcock, 2010)
30 g (150 mmol) of (1*R*,3*S*)-camphoric acid was dissolved in 750 mL of dry DCM in the argon purged vessel. TEA (62.6 mL, 450 mmol, 3 equiv.) was added to the mixture and stirred to give homogenous solution. Then MsCl (11.6 mL, 150 mmol) was added dropwise for several minutes and allowed to stir overnight. The mixture was transferred to a separatory funnel and washed with 3 M HCl (3 × 100 ml) followed by 100 mL of brine. The organic phase was dried over anhydrous Na_2SO_4, and the solvents were removed on rotary evaporator to give yellow crystals. Recrystallization from ethyl acetate gave 20.2 g (74%) of white needles. M.p. = 223–225°C; $[\alpha]_D^{21}$= -0.99 (1.0, $CHCl_3$). Spectral data were in agreement with the literature (Eagles & Hitchcock, 2010).

3-(2-(dimethylamino)ethyl)-1,8,8-trimethyl-3-aza-bicyclo[3.2.1]octane-2,4-dione (2). (Rice & Grogan, 1957)
20 g (0.11 mol) of anhydride **3** and 12.1 mL (0.11 mol) of *N,N*-dimethylethane-1,2-diamine were mixed and gently heated (90–100 °C) until a clear reaction mixture was obtained. The resulting partially reacted mass was heated to a temperature of 180°C and maintained at that temperature for 7 h. Reaction mixture was allowed to cool, and the resulting oil was vacuum distilled. The fraction distilled at 165–168°C / 10 mmHg was identified as a final product which was obtained in 94% yield as colorless oil. Spectral data were in agreement with the literature (Rice & Grogan, 1957).

General procedure for the synthesis of QAS 1
8 mmol of imide **2** was dissolved in 15 mL of acetonitrile. To this solution was added 9.6 mmol (1.2 eqiv.) of bromoalkene, and the reaction mixture was heated at 100°C for 24 h. After the reaction, the mixture was allowed to cool, and the solvent was removed by rotary evaporation. To the resulting mixture, orange oil was added 40 mL of anhydrous benzene, and again, it was evaporated. This procedure was repeated three times. The resulting material, solidified by cooling, was repeatedly crystallized from acetone/hexane mixture, filtered, washed with anhydrous diethyl ether, and dried in vacuum to afford final salts **1**. Structural and spectral characterization of prepared QASs are summarized in the Table 1 and Table 2.

3. RESULTS AND DISCUSSION

Enantiopure QASs of the compounds in series **1** were synthesized, as illustrated in Fig. 1, starting from (1*R*,3*S*)-(+)-camphoric acid. In the first step of the synthesis, (1*R*,3*S*)-(+)-camphoric acid was dehydrated using MsCl to yield anhydride **3** (Eagles & Hitchcock, 2010). The prepared anhydride **3** was subsequently heated with *N,N*-dimethylethane-1,2-diamine **(**Rice & Grogan, 1957). This nucleophilic attack followed by dehydration at 180°C gives as a product *N*-substituted imide of camphoric acid **2**. The final step of the synthesis was nucleophilic substitution of bromide in bromoalkanes by tertiary amino group of derivative **2**. QASs **1** were isolated after several crystallizations from acetone/hexane mixture as white solids in the yields 80–87%. All of the prepared QASs **1** were identified and characterized thoroughly from spectral and analytical data summarized in Table 1 and Table 2.
The antimicrobial activities of synthesized QASs were determined as a MIC, [μmol l^{-1}] against the gram-positive human pathogenic bacteria *S. aureus*, gram-negative bacteria *E. coli*, and human fungal pathogen *C. albicans,* the values for which are given in Table 3. The MIC values were determined as lowest concentration of the salts **1** that completely prevented visible colony formation. All the compounds were dissolved in water for biological evaluation. Clinically used BAB was used as a standard.

According to the results, it can be observed that all of the synthesized QASs exhibit growth inhibition effect against

Table 2. Spectroscopic data of camphoric acid-derived QASs 1.

Compound	Spectral data
1a	IR, $\widetilde{\nu}$ /cm^{-1}: 2921, 2843, 1723, 1669, 1469, 1373, 1343, 1332, 1179, 1002, 929, 823, 724 ^{1}H NMR (300 MHz, $CDCl_3$) δ: 0.88 (t, 3H, J = 7.04 Hz), 0.95 (s, 3H), 0.99 (s, 3H), 1.20 (s, 3H), 1.26 (s, 13H), 1.37 (s, 4H), 1.77 (s, 2H, broad), 1.88–2.11 (m, 4H), 2.17–2.29 (m, 1H), 2.74 (d, 1H, J = 7.04 Hz), 3.51 (s, 6H), 3.60–3.70 (m, 4H), 4.11 (t, 2H, J = 8.21 Hz) ^{13}C NMR (75 MHz, $CDCl_3$) δ: 13.9; 14.1; 19.5; 21.9; 22.7; 22.8; 25.1; 26.2; 29.2; 29.3; 29.4; 29.5; 29.6 (2C); 31.9; 32.9; 34.0; 44.7; 51.7 (2C); 54.6; 56.2; 60.0; 64.1; 176.0; 178.2
1b	IR, $\widetilde{\nu}$ /cm^{-1}: 2919, 2849, 1723, 1668, 1469, 1373, 1344, 1331, 1179, 989, 927, 822, 723 ^{1}H NMR (300 MHz, $CDCl_3$) δ: 0.89 (t, 3H, J = 6.45 Hz), 0.96 (s, 3H), 0.99 (s, 3H), 1.21 (s, 3H), 1.27 (s, 15H), 1.38 (s, 4H), 1.74–2.12 (m, 8H), 2.19–2.33 (m, 1H), 2.76 (d, 1H, J = 6.45 Hz), 3.52 (s, 6H), 3.59–3.70 (m, 4H), 4.11 (t, 2H, J = 7.62 Hz) ^{13}C NMR (75 MHz, $CDCl_3$) δ: 13.9; 14.2; 19.5; 21.9; 22.7; 22.8; 25.1; 26.2; 29.3; 29.4 (2C); 29.5; 29.7 (4C); 31.9; 32.9; 34.0; 44.7; 51.8 (2C); 54.6; 56.2; 60.0; 64.1; 176.0; 178.3
1c	IR, $\widetilde{\nu}$ /cm^{-1}: 2918, 2849, 1723, 1669, 1469, 1373, 1344, 1331, 1179, 990, 925, 820, 722 ^{1}H NMR (300 MHz, $CDCl_3$) δ: 0.88 (t, 3H, J = 6.45 Hz), 0.95 (s, 3H), 0.99 (s, 3H), 1.20 (s, 3H), 1.25 (s, 21H), 1.37 (s, 4H), 1.77 (s, 2H, broad), 1.85–2.11 (m, 4H), 2.17–2.30 (m, 1H), 2.75 (d, 1H, J = 6.45 Hz), 3.51 (s, 6H), 3.56–3.70 (m, 4H), 4.11 (t, 2H, J = 7.62 Hz) ^{13}C NMR (75 MHz, $CDCl_3$) δ: 13.9; 14.1; 19.5; 21.9; 22.7; 22.8; 25.1; 26.2; 29.3; 29.4 (2C); 29.5; 29.7 (6C); 31.9; 32.9; 34.0; 44.6; 51.7 (2C); 54.5; 56.2; 60.0; 64.1; 176.0; 178.2
1d	IR, $\widetilde{\nu}$ /cm^{-1}: 2918, 2848, 1723, 1668, 1469, 1373, 1344, 1331, 1179, 1001, 927, 820, 721 ^{1}H NMR (300 MHz, $CDCl_3$) δ: 0.88 (t, 3H, J = 6.45 Hz), 0.95 (s, 3H), 0.99 (s, 3H), 1.20 (s, 3H), 1.25 (s, 27H), 1.37 (s, 2H), 1.77 (s, 2H, broad), 1.85–2.11 (m, 4H), 2.17–2.30 (m, 1H), 2.74 (d, 1H, J = 6.45 Hz), 3.51 (s, 6H), 3.59–3.70 (m, 4H), 4.11 (t, 2H, J = 7.04 Hz) ^{13}C NMR (75 MHz, $CDCl_3$) δ: 13.9; 14.1; 19.5; 21.9; 22.7; 22.8; 25.1; 26.2; 29.2; 29.4 (2C); 29.5; 29.7 (8C); 31.9; 32.9; 34.0; 44.6; 51.7 (2C); 54.5; 56.2; 60.0; 64.1; 176.0; 178.2

Table 3. Minimal inhibitory concentrations [μmol L^{-1}] of prepared QAS 1.

Compound	*S. aureus* CNCTC 29/58	*E. coli* CNCTC 377/79N	*C. albicans* CCM 8186
1a	6.1	24.3	12.2
1b	0.7	5.8	0.7
1c	0.6	5.5	0.6
1d	324.1	665.8	324.1
BAB	26	260	26

all three types of microbes, with higher efficiency against *S. aureus* and *C. albicans* (Table 3). Gram-negative *E. coli* was found to be most resistant to the prepared salts among the tested microorganisms. This is presumably due to the cell membrane composition. Gram-negative bacteria contain an outer membrane with an external component that consists mainly of lipopolysaccharides, which acts as a barrier and prevents antimicrobial agents and biocides from entering the cell (Pérez et al., 2009).

The main target site of QASs is the cytoplasmic membrane comprised of a phospholipid bilayer. QASs are able to insert into the phospholipid bilayer, which is accompanied by membrane disorganization and structural and functional changes in the cell membrane, inducing leakage of intracellular components (Gilbert and Moore, 2005). In addition, QASs were also found to inhibit ATP synthesis by neutralizing the proton motive force (PMF) (Denyer & Hugo, 1977). The PMF is initiated by a proton gradient across the cytoplasmic membrane and is responsible for many respiratory and photosynthetic processes, including ATP synthesis. As long as QASs are surface active agents, they can cause denaturation of proteins anchored in the cytoplasmic membrane or dissociation of an enzyme from its prosthetic group. Because this effect was observed at concentrations much higher than lethal ones, the enzyme inhibition is not the primary injury caused by cationic surfactants (Merianos 1991). If we take a deeper look into the mechanism of action of QASs, for the most of them, no specific target site has been recognized. However, it is not excluded that there can exist some target specificities, like DNA binding, as shown by

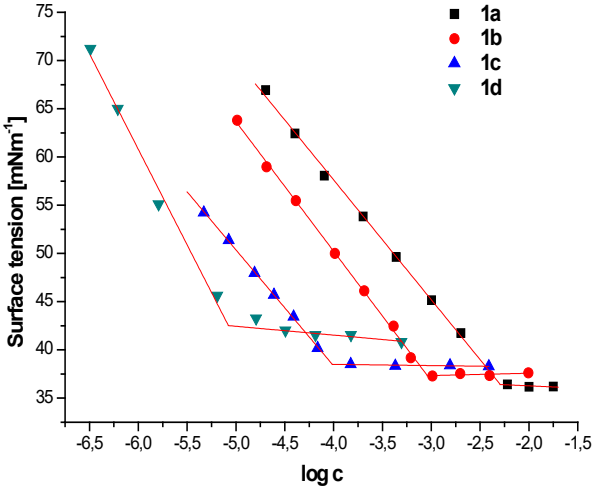

Figure 2. Surface tension versus the logarithm of the aqueous molar concentration of 1a–1d at 25°C.

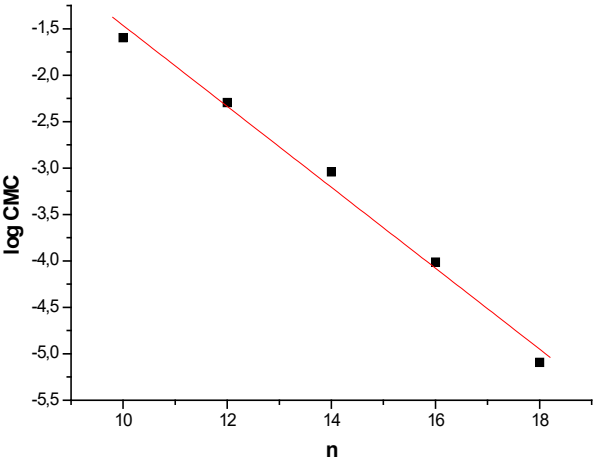

Figure 3. Variation of log CMC with chain length of 1a–1d at 25°C.

Menzel (2011) and Zhang (2013), because the antimicrobial activity of QASs changes significantly against various types of microorganisms and explanation only by the cationic charge and hydrophobic tail cannot be used.

The antimicrobial activity of surfactants generally depends on the alkyl chain length, although this correlation is not linear. In the series of prepared QASs **1a**–**1d,** maximum antimicrobial activity was observed for compound **1c** with 16 carbon atoms in alkyl chain, though salt **1b** with 14 carbon atoms in alkyl chain exhibits the similar antimicrobial activity. It is noteworthy that among the salts examined in this study, all of the prepared QASs inhibited the growth of microorganisms at the concentrations lower than clinically used BAB.

QASs **1a**–**1d** exhibit surface activities such as surface tension lowering and micelle formation. The surface properties of prepared QASs were investigated by surface tension

Table 4. CMC, g(CMC) and pC_{20} values of prepared QASs calculated from tensiometry measurements.

	1a	1b	1c	1d
CMC [molL^{-1}]	5.07×10^{-3} $\pm0.23\times10^{-3}$	9.13×10^{-4} $\pm0.98\times10^{-4}$	0.97×10^{-4} $\pm0.05\times10^{-4}$	8.09×10^{-6} $\pm1.13\times10^{-6}$
$\gamma_{(CMC)}$ [mNm^{-1}]	36.36	37.32	38.49	42.51
pC_{20}	3.5	4.1	5.1	5.5

measurements. The plots of surface tension against the logarithm of surfactant's concentration are presented in Fig. 2. CMC, surface tension at CMC (γ_{CMC}), and efficiency of adsorption at the surface (pC_{20}) (pC_{20} – the negative log of C_{20}, the surfactant molar concentration required to reduce surface tension by 20 mNm^{-1}) of QASs were calculated from the break in the plots and are shown in Table 4.

The surfactant concentration required to reduce the surface tension of pure water by 20 mNm^{-1} was used to compare the efficiency of surfactant (pC_{20}). Higher values indicate that the surfactant adsorbs at the interface more efficiently. The values of pC_{20} in Table 4 show that with increasing alkyl chain length the pC_{20} increases. This means that better reduction in surface tension is achieved for surfactants with longer alkyl chain used at a smaller concentration. It is known that by increasing the alkyl chain length of a surfactant the CMC values decrease (Rosen 1989). It can be seen from Fig. 3 that values of the log CMC decrease linearly with number of carbon atoms in the chain from **1a** to **1d**. This linear relationship between chain length and CMC for homologous series of surfactants is known as Kleven's equation: log CMC = A – Bn, where n is the number of carbon atoms in the long alkyl chain and A and B are constants (Klevens, 1953). For prepared QASs **1**, the linear relationship was found to be log CMC = 2.89 – 0.43n. The surface tension at CMC values (γ_{CMC}) are in the range of 36.36–42.51 mNm^{-1}.

With regard to better understanding of the relation between the antimicrobial activities and micelle forming ability, the MIC values [mmolL^{-1}] of the prepared QASs were correlated with their CMC values [mmolL^{-1}] (Fig. 4). As seen, the CMC curve intersects the MIC curve at the cut-off point (16 carbon atoms chain length) for all the microorganisms tested. In addition, MICs of the prepared cationic surfactants with the alkyl chain length shorter than 16 carbon atoms were found below the CMCs, while above the cut-off point, the MICs appear above the CMC. A similar behavior was observed also in the study of cationic surfactants derived from amino acids (Joondan et al., 2014), alkyl betaines, and *N*-oxides (Birnie et al. 2000). This observation could be explained according to Joondan et al. that at the concentration under the CMC, the surfactant molecules are soluble; therefore, monomers predominate and participate in the interaction

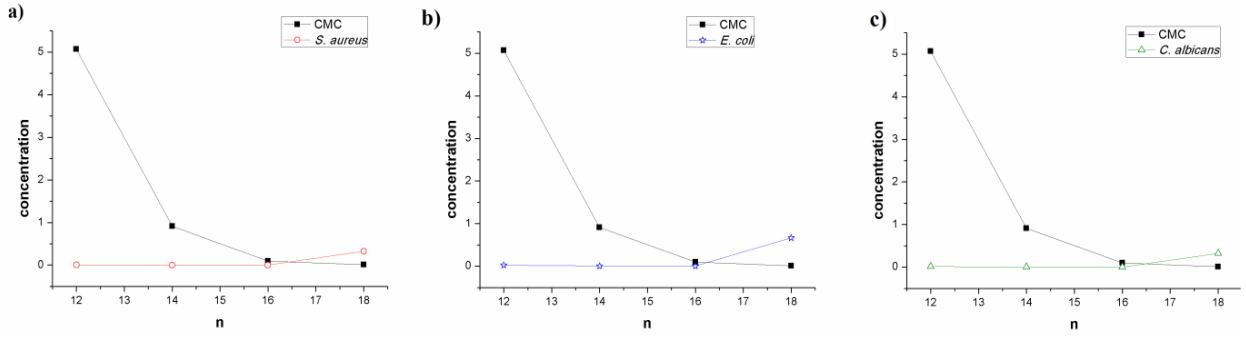

Figure 4. Correlation of CMC [mmolL^{-1}] and MIC [mmolL^{-1}] of QASs 1a–1d for a) S. aureus; b) E. coli; c) C. albicans.

with phospholipid bilayer in the bacterial cell wall. On the contrary, molecules with longer chain length aggregate into the micelles at much lower concentration, thus decreasing the concentration of monomers. To achieve bactericidal effect, the higher concentration of the surfactant is needed (Joondan et al., 2014).

CONCLUSIONS

In summary, we have designed and synthesized a new amphiphilic ammonium salt that could be classified as potential antimicrobials. All of the prepared QASs showed higher antimicrobial activity on gram-positive bacteria and fungi than on gram-negative strain. The maximum antimicrobial activity was observed for compound **1c** with 16 carbon atoms in alkyl chain. QASs **1a**–**1c** exhibit higher antimicrobial and antifungal activity than clinically used BAB. Aggregation parameters like CMC, γ_{CMC}, pC_{20} of synthesized cationic surfactants **1a**–**1d** were studied by tensiometry, and based on the correlation between CMC and MIC, we can conclude that monomers of surfactants are mainly responsible for antimicrobial activity.

ACKNOWLEDGMENT

Financial support of this work by the Ministry of Education, Science, Research, and Sport of the Slovak Republic under the contract No VEGA-1/0145/20 is gratefully acknowledged by the authors.

References

[1] Balgavý P. Devínsky F. Cut-off effects in biological activities of surfactants. Adv Colloid Interface Sci. 1996;66:23-63.
[2] Benkova M. Soukup O. Prchal L. et al. Synthesis, antimicrobial effect and lipophilicity-activity dependence of three series of dichained N-alkylammonium salts. Chemistry 2019;4:12076-12084.
[3] Birnie CR. Malamud D. Schnaare RL. Antimicrobial evaluation of *N*-alkyl betaines and *N*-alkyl-*N,N*-dimethylamine oxides with variations in chain length. Antimicrob Agents Chemother. 2000;44:2514-2517.
[4] Brak K. Jacobsen EN. Asymmetric ion-pairing catalysis. Angew Chem Int Ed. 2013;*52*(2):534-561.
[5] Brigham KL. Mezrick B. Christman B. Magnuson M. King G. Berry LC. In vivo Transfection of Murine Lungs with a Functioning Prokaryotic Gene Using a Liposome Vehicle. Am J Med Sci. 1989; 298: 278-281.
[6] Bureš F. Quaternary Ammonium Compounds: Simple in Structure, Complex in Application. Top Curr Chem. 2019;377:14.
[7] Cortesi R. Bergamini P. Ravani L. et al. Long-chain cationic derivatives of PTA (1,3,5-triaza-7-phosphaadamantane) as new components of potential non-viral vectors. Int J Pharm. 2012; 431:176-182.
[8] Denyer SP Hugo WB. The mode of action of cetyltrimethylammonium bromide (CTAB) on *Staphylococcus aureus*. J Pharm Pharmacol. 1977;29:66P.
[9] Devínsky F. Lacko I. Mlynarčík D. Račanský V. Krasnec Ľ. Relationship between critical micelle concentrations and minimum inhibitory concentrations for some non-aromatic quaternary ammonium salts and amine oxides. Tenside Deterg. 1985;22:10-15.
[10] Eagles JB. Hitchcock SR. Synthesis of D-camphor based γ-amino acid (1S,3R)-3-amino-2,2,3-trimethylcyclopentane carboxylic acid. Tetrahedron: Asymmetry. 2010;21(5):519-523.
[11] Feder-Kubis J. Tomczuk K. The effect of the cationic structures of chiral ionic liquids on their antimicrobial activities. Tetrahedron 2013;69(21):4190-4198.
[12] Gilbert P. Moore LE. Cationic antiseptics: diversity of action under a common Epithet. J. Appl Microbiol 2005; 99: 703-715.
[13] Jennings MC. Minbiole KPC. Wuest WM. Quaternary Ammonium Compounds: An Antimicrobial Mainstay and Platform for Innovation to Address Bacterial Resistance. ACS Infect Dis. 2015;1:288-303.
[14] Joondan N. Jhaumeer-Laulloo S. Caumul P. A study of the antibacterial activity of L-Phenylalanine and L-Tyrosine esters in

relation to their CMCs and their interactions with 1,2-dipalmitoyl-sn-glycero-3-phosphocholine, DPPC as model membrane. Microbiol Res. 2014;169:657-685.

[15] Kaushik NK, Attri P, Kaushik N, Choi EH. Synthesis and Antiproliferative Activity of Ammonium and Imidazolium Ionic Liquids against T98G Brain Cancer Cells. Molecules 2012;17(12):13727-13739.

[16] Kim YH. Sun G. Functional Finishing of Acrylic and Cationic Dyeable Fabrics: Intermolecular Interactions. Text Res J. 2002; 72: 1052-1056.

[17] Klevens HB. Structure and aggregation in divte solutions of surface aktive agents. J Am Oil Chem Soc. 1953;30:74-80.

[18] Kopecká-Leitmanová A. Devinsky F. Mlynarčík D. Lacko I. Interaction of amine oxides and quaternary ammonium salts with membrane and membrane-associated processes in E. Coli cells: mode of action. Drug Metabol Drug Interact. 1989;7(1):29-51.

[19] Lukáč M, Lacko I, Bukovský M et al. Synthesis and antimicrobial activity of a series of optically active quaternary ammonium salts derived from phenylalanine. Cent Eur J Chem. 2010;8:194-201.

[20] Malinak D. Dolezal R. Marek J. et al. 6-Hydroxyquinolinium salts differing in the length of alkyl side-chain: synthesis and antimicrobial activity. Bioorg Med Chem Lett. 2014;24:5238-5241.

[21] Marek J. Joskova V. Dolezal R. et al. Synthesis, antimicrobial effect and surface properties of hydroxymethyl-substituted pyridinium salts. Lett Drug Des Discov. 2018;15:828-842.

[22] Menzel TM. Tischer M. Francois P. et al. Mode-of-Action studies of the Novel Bisquaternary Bisnaphthalimide MT02 against *Staphylococcus aureus*. Antimicrob Agents Chemother. 2011;55:311-320.

[23] Merianos JJ. Quaternary ammonium antimicrobial compounds. In *Disinfection, sterilization, and preservation*, 4th Edition, 1991, Lea & Febiger, Philadelphia. ISBN: 0-8121-1364-0.

[24] Miguel G. Cruz C. Faleiro ML. Simoes MTF. Figueiredo AC. Barroso JG. Pedro LG. *Salvia officinalis* L. essential oils: effect of hydrodistillation time on the chemical composition, antioxidant and antimicrobial activities. Nat Prod Res. 2011;25(5):526-541.

[25] Mikláš R, Miklášová N, Bukovský M, Devínsky F. Synthesis and antimicrobial properties of binaphthyl derived quaternary ammonium bromides. Acta Facult Pharm Univ Comenianae. 2012;59:39-47.

[26] Mikláš R, Miklášová N, Bukovský M, Horváth B, Kubincová J, Devínsky F. Synthesis, surface and antimicrobial properties of some quaternary ammonium homochiral camphor sulfonamides. Eur J Pharm Sci. 2014;65:29-37.

[27] Mlynarčík D. Denyer SP. Hugo WB. A study of the action of a bisquaternary ammonium salt, an amine oxide and an alkoxy phenylcarbamic acid ester on some metabolic functions in Staphylococcus aureus. Microbios 1981;30:27-35.

[28] Morel A. Silarska E. Trzeciak A M. Pernak J. Palladium-catalyzed asymmetric Heck arylation of 2,3-dihydrofuran – effect of prolinate salts. Dalton Trans. 2013; *42*(4): 1215-1222.

[29] Pérez L. Pinazo A. García MT et al. Cationic surfactants from lysine: Synthesis, micellization and biological evaluation. Eur J Med Chem. 2009;44:1884-1892.

[30] Pernak J. Skrzypczak A. 3-Alkylthiomethyl-1-ethylimidazolium chlorides. Correlation between critical micelle concentrations and minimum inhibitory concentrations. Eur J Med Chem. 1996;31:901-903.

[31] Pernak J. Kalewska J. Ksycińska H. Cybulski J. Synthesis and antimicrobial activities of some pyridinium salts with alkoxymethyl hydrophobic group. Eur J Med Chem. 2001;36:899-907.

[32] Piętka-Ottlik M. , Frąckowiak R., Maliszewska I., Kołwzan B., Wilk KA. Ecotoxicity and biodegradability of antielectrostatic dicephalic cationic surfactants. Chemosphere 2012; 89: 1103-1111.

[33] Rice LM. Grogan CH. Hypotensive agents VI. Substitued 3-Azabicyclo[3.2.1]octane derivates. J Org Chem. 1957;22:185-189.

[34] Rosen MJ. Surfactants and interfacial phenomena, 2nd Edition, New York, John Wiley & Sons. ISBN: 0-471-83651-6; 1989.

[35] Ruiz-Navajas Y. Viuda-Martos M. Sendra M. Perez-Alvarez JA. Fernandez-Lopez J. Chemical characterization and antibacterial activity of *Thymus moroderi* and *Thymus piperella* essential oils, two Thymus endemic species from southeast of Spain. Food Control 2012;27(2):294-299.

[36] Sajomsang W. Gonil P. Ruktanonchai UR. Petchsangsai M. Opanasopit P. Puttipipatkhachorn S. Effects of molecular weight and pyridinium moiety on water-soluble chitosan derivatives for mediated gene delivery. Carbohydr Polym. 2013; 91(2): 508-517.

[37] Schrank CL. Minbiole KPC. Wuest WM. Are Quaternary Ammonium Compounds, the Workhorse Disinfectants, effective against Severe Acute Respiratory Syndrome-Coronavirus-2? ACS Infect Dis. 2020;6(7):1553-1557.

[38] Semenov VE. Mikhailov AS. Voloshina AD. Et al. Antimicrobial activity of pyrimidinophanes with thiocytosine and uracil moieties. Eur J Med Chem 2011;46(9):4715-4724.

[39] Shirakawa S. Liu K. Maruoka K. Catalytic Asymmetric Synthesis of Axially Chiral *o*-Iodoanilides by Phase-Transfer Catalyzed Alkylations. J Am Chem Soc. 2012; 134(2): 916-919.

[40] Soukup O. Benkova M. Dolezal R. et al. The wide-spectrum antimicrobial effect of novel N-alkyl monoquaternary amonium salts and their mixtures; the QSAR study against bakteria. Eur J Med Chem. 2020;206:112584.

[41] Thebault P. de Givenchi ET. Levy R. Vandenberghe Y. Guittard F. Géribaldi S. Preparation and antimicrobial behaviour of quaternary ammonium thiol derivatives able to be grafted on metal surfaces. Eur J Med Chem. 2009;44:717-724.

[42] Truong TKT. Olivier NVB. Aupoix A. Pegot B. Vo-Thanh G. Chiral Ionic Liquids Derived from (-)-Ephedrine and Carbohydrates: Synthesis, Properties and Applications to Asymmetric Synthesis and Catalysis. Curr Org Synth. 2012; *9*(1): 53-64.

[43] Wong Y-L, Hubieki MP, Curfaman CL et al. A Structure–Activity Study of Spermicidal and Anti-HIV Properties of Hydroxylated Cationic Surfactants. Bioorg Med Chem. 2002;10:3599-3608.

[44] Zhang Y. Zhu W. Liu Y-L. et al. Chemo-Immunotherapeutic Antimalarials Targeting Isoprenoid Biosynthesis. ACS Med Chem Lett. 2013;4:423-427.

[45] Zhi DF. Zhang SB. Qureshi F. et al. Synthesis and biological activity of carbamate-linked cationic lipids for gene delivery in vitro. *Bioorg Med Chem Lett*. 2012; 22(11): 3837-3841.

sciendo

Eur. Pharm. J. 2021, 68(1), 17-23.
ISSN 1338-6786 (online) and ISSN 2453-6725 (print version),
DOI: 10.2478/afpuc-2020-0019

EUROPEAN PHARMACEUTICAL JOURNAL

Study of the solubilisation process of bacterial model membranes induced by DDAO

Original Paper

Želinská K.✉, Gallová J.

Department of Physical Chemistry of Drugs,
Faculty of Pharmacy, Comenius University in Bratislava,
Odbojárov 10, 832 32 Bratislava, Slovakia

Received 30 November, 2020, accepted 1 March, 2021

Abstract Solubilisation of two bacterial model membranes induced by *N,N*-dimethyl-1-dodecanamine-*N*-oxide (DDAO) was studied. The first model membrane consisted of a mixture of palmitoyloleoylphosphatidylethanolamine (POPE) and palmitoyloleoylphosphatidylglycerol (POPG) in a molar ratio 0.6:0.4 mol/mol, and a second model membrane was enriched with tetraoleoylcardiolipin (TOCL) with a composition POPE-POPG-TOCL = 0.67:0.23:0.1 mol/mol/mol. Solubilisation of these model membranes was studied by static light scattering (nephelometry). Effective ratio R_e (the amount of DDAO integrated into the bilayer to the amount of lipid) at different steps of the solubilisation process was determined. The molar partition coefficient of DDAO was calculated – in case of the POPE-POPG membrane, K_p = 5,300 ± 400, for the POPE-POPG-TOCL membrane, K_p = 6,500 ± 500.

Keywords *N,N-dimethyl-1-dodecanamine-N-oxide – solubilisation – bacterial model membranes – cardiolipin*

INTRODUCTION

Increasing number of bacteria resistant against conventionally used antibiotics poses a serious health threat for the society. Conventional antibiotics have a specific target within a bacterial cell. Many bacteria have developed resistance to these specific mechanisms of action, rendering the antibiotics no longer effective. Particularly dangerous are the bacteria that are resistant to several conventional antibiotics (Pontali et al., 2013; Xu et al., 2014). In order to overcome multi-drug-resistant bacterial infections, research of substances targeting bacterial cells non-specifically is essential. An example of such substances are long-chain amphiphilic surfactants, such as the one used in the presented study.

N,N-dimethyl-1-dodecanamine-*N*-oxide (DDAO) is a surfactant with 12 carbon hydrophobic chains and a highly polar N-O group. It is widely commercially used in home cleaning detergents, personal hygiene products and pharmaceutical formulations as well (Singh et al., 2006). Within the research applications, DDAO is used to reconstitute, crystallise and purify membrane proteins, as well as to solubilise membranes, which is the focus of this study. DDAO is an amphiphilic molecule with pK ~ 5, meaning that at physiological pH, DDAO is in a non-ionic form (Búcsi et al., 2014; Herrmann, 1962). DDAO manifests various biological effects, such as antimicrobial (Devínsky et al., 1990) and antiphotosynthetic (Murín et al., 1990) activity or phytotoxic (Šeršeň et al., 1992) and immunomodulatory (Bukovský et al., 1996) effect. In contact with the biological membrane, DDAO interacts mostly with its phospholipids (Kragh-Hansen et al., 1998). DDAO molecules incorporate themselves into the bilayer, influence physical properties of bilayer, and induce formation of defects and pores (Memoli et al., 1999; Ruiz et al., 1988), followed by complete disintegration of the bilayer after a certain concentration of surfactant is reached (Lichtenberg et al., 2013a; Lichtenberg et al., 2013b). For the interaction studies, a binary and ternary mixture of phospholipids was used. Interaction of DDAO with model membranes of various phosphatidylcholines (PCs) or PCs mixed with cholesterol (lipids typical for the mammalian model membranes) was studied in several papers (Belička et al., 2014a; Belička et al., 2014b; Hrubšová et al., 2003; Huláková et al., 2013, 2015; Karlovská et al., 2004a; Karlovská et al., 2004b; Uhríková et al., 2001). The aim of this study was to determine how different

* *E-mail: katarina.zelinska@uniba.sk*

is the interaction of DDAO with bacterial model membranes. For most bacteria, phosphatidylethanolamines (PEs) are the most predominant phospholipids. All bacteria have at least 15% of anionic phospholipids such as phosphatidylglycerols (PGs) or cardiolipins (CLs) (Epand & Epand, 2009). PEs are zwitterionic phospholipids with a molecular shape of a truncated cone. Their polar headgroup is smaller in diameter in comparison with its hydrocarbon chain area. Therefore, they tend to form structures with negative curvature, which leads to the formation of non-lamellar phases at higher temperatures. PGs at physiological conditions are negatively charged, and because of their cylindrical molecular shape, they tend to form non-curved bilayers, even at higher temperatures. CLs have a double negative charge at physiological pH and relatively rigid (regarding mobility of the molecule) cylindrical molecular shape (Lopes et al., 2012). As a model organism for our experiments, G^- bacteria *Escherichia coli (E. coli)* were selected. Membrane lipids of *E. coli* are a mixture of PEs (57%), PGs (15%), CLs (10%) and other lipids (18%) (such mixture of lipids is commercially available as *E. coli* Total Lipid Extract). Frequently used models are two-component PE and PG mixtures (Lopes et al., 2010). The fatty acids found in the *E. coli* membrane phospholipids are predominantly 16–18 carbon long, with a substantial portion of them being unsaturated (Meister et al., 2014). For this reason, we chose to use a mixture of palmitoyloleoylphosphatidylethanolamine (POPE) and palmitoyloleoylphosphatidylglycerol (POPG) as our model system, in a molar ratio of POPE/POPG = 0.6/0.4 mol/mol. Gel phase–liquid-crystalline phase transition of this mixture is approximately at 20°C (Lopes et al., 2010; Pozo Navas et al., 2005). The temperature during the experiment was well-maintained at 25°C, ensuring our liposomes are in a liquid-crystalline phase.

An extract of polar lipids of *E. coli* (commercially prepared from total lipid extract by precipitation with acetone and extraction with diethyl ether) contains PEs (67%), PGs (23%) and CLs (10%). The POPE/POPG/CL three-component mixture (0.67:0.23:0.1) shows the highest similarity with the *E. coli* extracts based on phase transitions (Lopes et al., 2010). Despite CLs having 4 fatty acids in its molecules (in our case, 4 oleic acids), the dominant types of cardiolipin usually contain only one or two kinds of fatty acids. It was found that the fatty acid composition is relatively resistant to dietary manipulations, suggesting a specific composition is needed for its biological functions (Schlame et al., 2005). Tetraoleoylcardiolipin has a gel to liquid-crystalline phase transition at approximately -15°C (Chen, 2012). Therefore, we assume that our ternary mixture was in liquid-crystalline phase during the experiment as well.

In the present paper, the solubilising effect of a surfactant DDAO on two bacterial model membranes was studied using static light scattering (nephelometry). Because of the amphiphilic nature of the DDAO surfactant and relatively high amount of anionic phospholipids in model membranes, all experiments were performed in phosphate-buffered saline (PBS, pH 7.5).

MATERIALS AND METHODS

Chemicals

1-palmitoyl-2-oleoyl-sn-glycero-3-phosphoethanolamine (POPE), 1-palmitoyl-2-oleoyl-sn-glycero-3-phospho-(1'-rac-glycerol) (sodium salt) (POPG), 1',3'-bis[1,2-dioleoyl-sn-glycero-3-phospho]-glycerol (sodium salt) (TOCL) purchased from Avanti Polar Lipids (USA), and *N,N*-dimethyl-1-dodecanamine-*N*-oxide (DDAO) obtained from Sigma-Aldrich (Germany) were >99% pure and were used without further purification. Other used chemicals: K_2HPO_4 (CentralChem, Slovakia), KH_2PO_4 (Merck, Germany) and NaCl (Slavus, Slovakia) were of analytical grade.

Liposomes preparation

POPE-POPG (n_{POPE}:n_{POPG} = 0.6:0.4 mol/mol) and POPE-POPG-TOCL (n_{POPE}:n_{POPG}:n_{TOCL} = 0.67:0.23:0.1 mol/mol/mol) model membranes were prepared. Weighted amounts of dry lipids in glass tubes were co-solubilised by dissolving in chloroform. Chloroform was evaporated under a stream of gaseous nitrogen to dryness, followed by evacuation in a vacuum chamber using rotary oil pump for 8 h. 50 mmol/dm^3 PBS buffer with pH 7.5, consisting of 7.6 mmol/dm^3 KH_2PO_4, 42.4 mmol/dm^3 K_2HPO_4 and 150 mmol/dm^3 NaCl was prepared using redistilled water. Adequate amount of dry lipid film was hydrated with 1.3 ml of PBS buffer to obtain lipid concentration 10 mmol/dm^3. Spontaneous formation of multilamellar liposomes (MLLs) was accompanied by occasional vortexing until a homogenous dispersion was obtained. MLLs dispersion was extruded (LiposoFast-Basic Extruder) through a 100 nm polycarbonate filter 51 times (MacDonald et al., 1991; Olson et al., 1979). Unilamellar liposomes (ULLs) dispersion was then used to prepare a set of 25 samples with constant concentration of lipid and increasing concentration of DDAO from 0 to 3.12 mmol/dm^3. 5 sets of samples, with lipid concentrations 0.02, 0.04, 0.06, 0.08 and 0.1 mmol/dm^3 were prepared for each type of model membrane.

Static light scattering method

Typical three-stage (Lichtenberg et al., 2013a; Lichtenberg et al., 2013b; Želinská et al., 2020) solubilisation experiment is shown in Figure 1. In the first stage, the surfactant partitions into the membrane, until it is saturated (we will refer to this concentration as D_t^{SAT}). Further increase in the DDAO concentration causes a phase transition from lamellar structures (in our case, ULLs) to smaller micelles. This transition continues until all the lamellar structures are completely solubilised (we will call this concentration D_t^{SOL}).

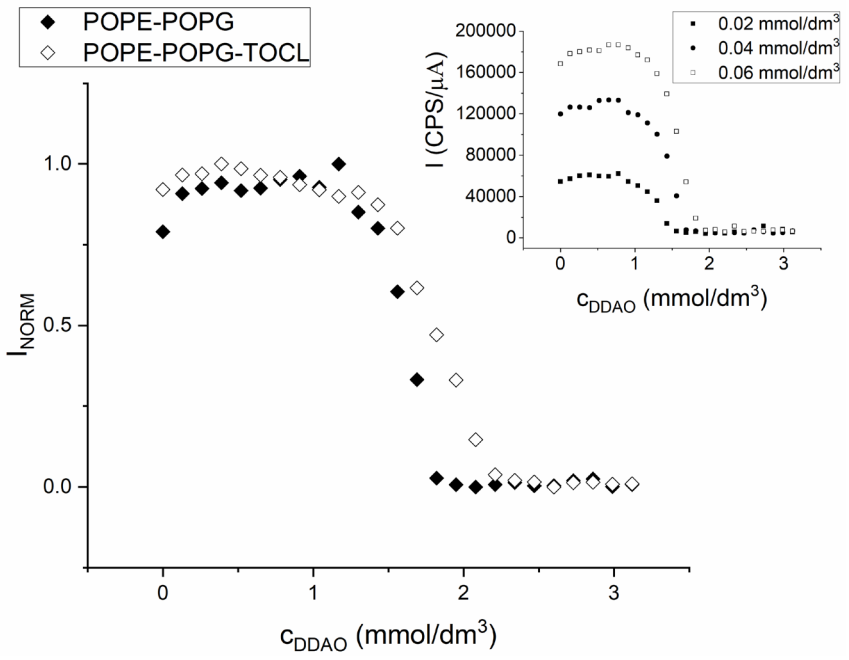

Figure 1. Dependence of normalised intensity of scattered light (I_{NORM}) on the concentration of added DDAO (c_{DDAO}), both types of membrane at a lipid concentration of 0.1 mmol/dm^3. Inset shows a comparison of the experiment at three different concentrations of POPE-POPG-TOCL (intensity (I) was not normalised).

In the last stage, only lipid–surfactant mixed micelles and residual surfactant monomers are present. Typical feature of this transition is the decrease of the size of the particles, which can be observed using static light scattering (nephelometry). We have also evaluated a concentration of DDAO that causes the scattered light intensity to decrease by 50% compared to the value in the first phase. We will refer to this parameter as D_t^{MID}. We will use the term "critical concentration" for all three D_t parameters.

Static light scattering experiments were carried out using Fluoromax 4 spectrofluorometer (Horiba Jobin Yvon, USA) with a controlled temperature of 25°C. Scattering of the light with 600 nm wavelength at a 90° angle was measured for 6 seconds with a step 0.1 second. Average intensity of the scattered light was calculated. Samples were measured 2 h after the DDAO was added to the ULLs dispersion.

Data evaluation and partition coefficient calculation

The method used to evaluate the data and perform the calculations was previously described in Želinská et al. (2020). To determine the D_t^{SAT} and D_t^{SOL} parameters, the nephelometry data were fitted using two bilinear functions (each parameter was fitted individually):

$$y = (kx + q)0.5(1 - (x - D_t)/|x - D_t|) + (mx + D_t(k - m) + q)0.5(1 + (x - D_t)/|x - D_t|) \quad (1)$$

where y = kx + q represents the equation of the straight line before the critical concentration (D_t), and y = mx + r is the equation of the straight line after the critical DDAO concentration was passed. Using the bilinear function, the searched for parameter, D_t, is found as an intersection point of these two straight lines. An example of the fitting is shown in the Figure 2 (full line). We can see that both fits (one for D_t^{SAT} and the other for D_t^{SOL}) overlap perfectly creating a continuous line, because the equation for the straight line in the second stage is identical for both fits.

The numerical value of D_t^{MID} was determined by fitting the dependence of scattered light intensity (I) on the DDAO concentration (c_{DDAO}) with reverse sigmoid function (Figure 2, dashed line):

$$I = I_{min} + (I_{max} - I_{min})/(1 + \exp(-(c_{DDAO} - D_t^{MID})/dc_{DDAO})) \quad (2)$$

where I_{max} is the maximum intensity, I_{min} is the minimum intensity and dc_{DDAO} represents the width of the second stage. Molar partition coefficient (K_p) is defined as the ratio of molar concentration of amphiphile in the lipid phase to its molar concentration in the aqueous phase in the equilibrium state. To determine K_p of DDAO between the POPE-POPG or POPE-POPG-TOCL bilayers and our water-based buffer, we used a method previously described in more detail in Želinská et al. (2020). The experimentally acquired dependence of the critical DDAO concentrations (D_t) on the concentration of lipid (c_L) was fitted with the function:

$$D_t = R_e . \frac{\rho_B}{M_L} . \frac{1}{K_p} + R_e . c_L \quad (3)$$

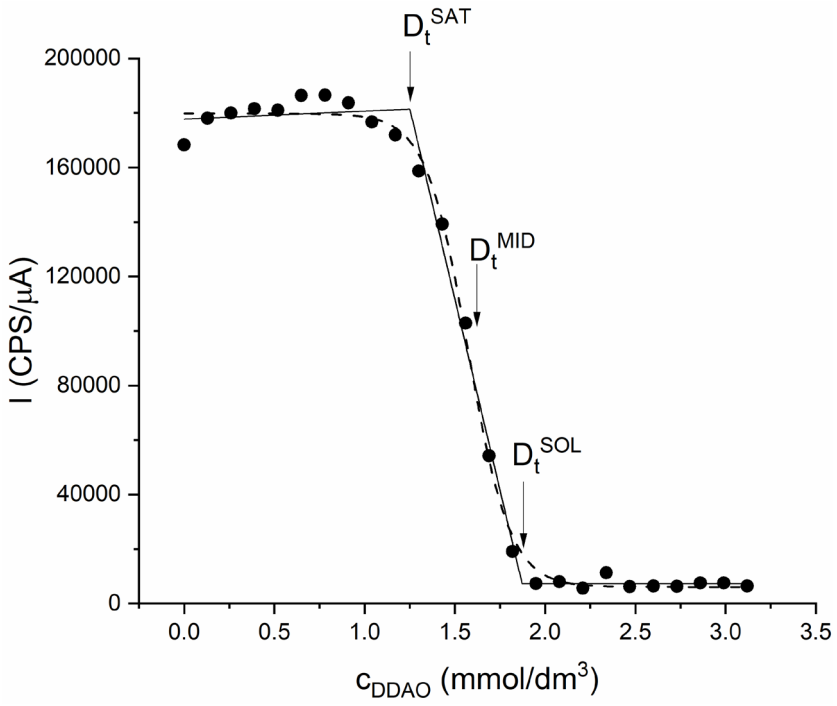

Figure 2. Dependence of scattered light intensity (I) on the concentration of added DDAO, $c_{POPE+POPG+TOCL}$ = 0.06 mmol/dm³. Arrows indicate the critical concentrations D_t^{SAT}, D_t^{SOL} acquired using bilinear functions (full line) and D_t^{MID} using reverse sigmoid function (dashed line).

where the slope of this linear dependence is the effective molar ratio (R_e) of the amount of DDAO integrated into the bilayer to the amount of lipid. The density of bilayer (ρ_B) was measured using vibrational densitometer DMA 4500M (Anton Paar, Austria), following the same procedure as in our previous study (Gallová et al., 2017). Molar mass (M_L) of the bilayer was calculated using mole fractions of lipids (X_L) constituting the bilayer. For example, $M_{POPE+POPG} = X_{POPE}M_{POPE} + X_{POPG}M_{POPG}$. The constant ratio of the density of bilayer (ρ_B) and its molar mass (M_L) was denoted as a fixed parameter (1,350 mmol/dm³ for POPE-POPG and 1,234 mmol/dm³ for POPE-POPG-TOCL) during the fitting. All three (D_t^{SAT}, D_t^{MID}, D_t^{SOL}) dependencies were fitted (Figure 3) simultaneously with Function 3 using Multi-Data Fit Mode in Origin software (Version 2019b. OriginLab Corporation, Northampton, MA, USA). The global fit fitted the individual linear dependencies and their slopes (R_e) and calculated one shared partition coefficient (K_p) for all three dependencies.

RESULTS AND DISCUSSION

Solubilisation of POPE-POPG and POPE-POPG-TOCL ULLs induced by non-ionic surfactant DDAO was studied at five different lipid concentrations. Decrease of the lipid particle sizes, which is typical for the solubilisation process, was examined using nephelometry. We can see examples of the experiments in Figure 1. The inset of Figure 1 shows raw solubilisation data for POPE-POPG-TOCL membranes at three lipid concentrations. We can see that the method is sensitive not only for the changes in the size of the scattering particles, but for their concentration as well. The main part of Figure 1 shows a solubilisation experiment comparison of the two types of membrane we investigated, at the same lipid concentration 0.1 mmol/dm³. Intensity of the scattered light was normalised (to the highest detected intensity) for better comparison. All dependencies follow the three-stage process described earlier. All dependencies were fitted with bilinear functions (Equation 1) and reverse sigmoid function (Equation 2) to obtain critical concentrations D_t^{SAT}, D_t^{MID}, D_t^{SOL}. An example of the fitting functions can be seen in Figure 2 (critical concentrations are indicated by arrows).

All acquired D_t^{SAT}, D_t^{MID}, D_t^{SOL} values are plotted as a function of concentration of the lipid in Figure 3. We can see their values increase linearly with increasing concentration of lipid for both types of membrane. The only exception is the saturation concentration D_t^{SAT} for POPE-POPG membranes. The reason is that for POPE-POPG membranes, the intensity of scattered light in the first phase of solubilisation was increasing, as opposed to staying approximately the same, as was the case for POPE-POPG-TOCL membranes (an example can be seen in Figure 1). Surfactant-induced increase in the particle size has been reported in literature (Kragh-Hansen et al., 1998). The mentioned study shows that DDAO induced a fusion of small ULLs to larger vesicles before the transition into micelles. The

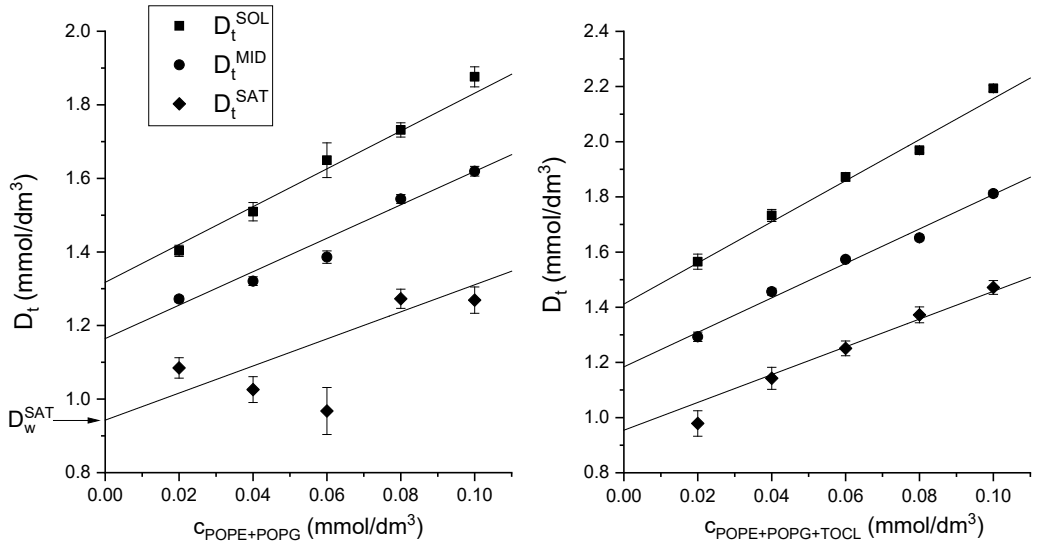

Figure 3. Linear dependencies of critical DDAO concentrations on the concentration of POPE-POPG (left) and POPE-POPG-TOCL (right). The figure shows the global fit used to calculate the effective molar ratios (R_e) and the partition coefficients (K_p). D_w^{SAT} represents the concentration of DDAO surfactant in the water phase at the stage of complete saturation of the lipid bilayers by DDAO.

ULLs interacting with DDAO were composed of sarcoplasmic reticulum lipid extract (lipid composition was not specified), and the buffer in use contained 0.1 mmol/dm^3 $CaCl_2$. Binding of Ca^{2+} ions to the membrane are known as an important factor involved in the membrane fusion (Martens & McMahon, 2008). Our buffer did not contain such ions, and the ULLs lipid composition was different as well. The reason for such increase in intensity needs to be studied further. The increase in the intensity made the fitting of D_t^{SAT} less reliable, as we can see the error bars (Figure 3) are greater than for any other parameter. Nevertheless, this parameter was not excluded from further analysis, because doing so have not provided significantly different results. All three critical concentrations were fitted with the global function (Equation 3, Figure 3) as described earlier. Instrumental weighing was applied during the fitting, because it uses the square of the reciprocal of the error values, so points with smaller error values have more weight. Results of the fitting are shown in Table 1.

D_W represents the concentration of surfactant in the water phase at particular stage of the solubilisation process. D_W values were obtained by extrapolation of the global function to zero lipid concentration (see Figure 3, where D_w^{SAT} is depicted as an example). D_W values (D_w^{SAT}, D_w^{MID}, D_w^{SOL}) were obtained as a y-coordinates of the intersection points of the global function with the y-axis. The critical micellar concentration of DDAO at 27°C in its non-ionic form (at pH >7) is 2.1 mmol/dm^3 (Herrmann, 1962). All our calculated values of D_W are smaller than this value, which means that DDAO molecules did not form micelles during the solubilisation experiment. Therefore, we propose that the solubilisation process in this study took place by the transbilayer mechanism (Kragh-Hansen et al., 1998).

The effective molar ratio (R_e) of the amount of DDAO integrated into the bilayer to the amount of lipid is a constant, independent of the concentration of lipid and specific for surfactant–lipid mixture. The R_e (we will be using values for D_t^{MID} concentration for comparisons) values were 4.6 ± 0.3 for POPE-POPG and 6.3 ± 0.3 for POPE-POPG-TOCL. We have determined the partition coefficient of DDAO in bilayers consisting of POPE-POPG K_p = 5,300 ± 400 and for the POPE-POPG-TOCL K_p = 6,500 ± 500.

Regarding the difference between POPE-POPG and the cardiolipin-containing model membrane, the latter was more stable against the DDAO-induced solubilisation. As we can see in Table 1, the R_e values were higher at all three evaluated critical concentrations. The calculated partition coefficient was higher as well. Assuming it is caused purely by the presence of cardiolipin would be premature. Domain formation in bacteria membranes can also play an important role. These domains, reported to be enriched in cardiolipin, have been suggested to play an important role in regulatory functions of the cell (Epand & Epand, 2009 and references therein). Many studies with bacterial model membranes tend to neglect the importance of the presence of cardiolipin in the model membranes. Further investigation is needed, because it appears cardiolipin is an important part of bacterial membrane, even though its function is not yet completely known. We would like to continue the research of cardiolipin-containing model membranes in the future, for example using fluorescence microscopy with the help of cardiolipin specific dye 10-N-nonyl acridine orange.

The partition coefficients and R_e values calculated in the present study are greater than have been reported for the interaction of DDAO with mammalian model

Table 1. Global fit (Equation 3) results of POPE-POPG and POPE-POPG-TOCL static light scattering data.

Critical DDAO concentration	POPE-POPG		POPE-POPG-TOCL	
	R_e	D_W [mmol/dm³]	R_e	D_W [mmol/dm³]
D_t^{SAT}	3.7 ± 0.2	0.9 ± 0.1	5.0 ± 0.3	1.0 ± 0.1
D_t^{MID}	4.6 ± 0.3	1.2 ± 0.2	6.3 ± 0.3	1.2 ± 0.2
D_t^{SOL}	5.1 ± 0.3	1.3 ± 0.2	7.5 ± 0.4	1.4 ± 0.2
K_p	5,300 ± 400		6,500 ± 500	

R_e is the effective ratio of the amount of DDAO integrated into the lipid bilayer to the amount of lipid. D_W is the concentration of surfactant in the water phase. K_p is molar partition coefficient of DDAO between the bilayer and water phase.

membranes. For example, in our recent article (Želinská et al., 2020), we have researched the interaction of DDAO with dioleoylphosphatidylcholine (DOPC) and cholesterol (CHOL)-enriched DOPC liposomes (33 mol% of CHOL). The R_e values for the D_t^{MID} concentration were 2.2 ± 0.3 in the case of DOPC ULLs and 1.8 ± 0.3 for DOPC-CHOL type of membrane. Also, the calculated partition coefficients were reported smaller: 2,300 ± 400 (for DOPC) and 2,100 ± 600 (for DOPC-CHOL).

Other studies reported smaller molar partition coefficients for mammalian model membranes as well. For example, Hrubšová et al. (2003) calculated K_p = 500 ± 200 in a system egg yolk phosphatidylcholine (EYPC) ULLs/water. R_e for the D_t^{MID} concentration was 0.6 ± 0.2. MLLs of EYPC were reported to have a molar partition coefficient of DDAO equal to 1,200 ± 400 (Karlovská et al., 2004a). In these two studies, only a dependence of D_t^{MID} on the lipid concentration was used for the calculations.

Our data and calculations show us that the partitioning of DDAO between the aqueous phase and the bacterial model membranes is higher than it is in the case of mammalian model membranes, and yet, the bacterial ULLs needed more DDAO to become solubilised. Because the hydrophobic part of the studied phospholipids is very similar, we suggest that the reason for such big differences might be caused by the polar parts of the phospholipids. In comparison with PCs, the polar part of PEs has smaller diameter (the choline group in PCs is bigger than the ammonium group) and binds smaller amount of water molecules. The ammonium group is able to form hydrogen bonds with phosphate and oxygen atoms of adjacent molecules. A molecular dynamics simulation (Murzyn et al., 2005) of POPE-POPG (in the proportion 3:1) with Na^+ ions (to neutralise the negative charge of POPG) has shown that POPE molecules interact readily with POPG and other POPE molecules with hydrogen bonds and water bridges. These bonds strengthen interlipid contacts in the bilayer. These physico-chemical properties of PCs and PEs–PGs-containing membranes might be the reason for our findings, but further analysis is needed. Therefore, in the future, we would like to widen this research to monitoring the effect of DDAO on fluidity of the membrane and the process of pore formation using fluorescent probes.

ACKNOWLEDGEMENT

This work has been supported by the VEGA grants 1/0228/17 and 1/0223/20, JINR topical themes 04-4-1142-2021/2025 and APVV project 17-0239.

References

[1] Belička, M., Klacsová, M., Karlovská, J., Westh, P., Devínsky, F., & Balgavý, P. Molecular and component volumes of N,N-dimethyl-N-alkylamine N-oxides in DOPC bilayers. *Chem Phys Lipids*. 2014a;180:1–6.

[2] Belička, M., Kučerka, N., Uhríková, D., et al. Effects of N,N-dimethyl-N-alkylamine-N-oxides on DOPC bilayers in unilamellar vesicles: Small-angle neutron scattering study. *Eur Biophys J*. 2014b;43(4–5):179–189.

[3] Búcsi, A., Karlovská, J., Chovan, M., Devínsky, F., & Uhríková, D. Determination of pK a of N-alkyl-N,N-dimethylamine-N-oxides using 1H NMR and 13C NMR spectroscopy. *Chemical Papers*. 2014;68(6):842–846.

[4] Bukovský, M., Mlynarčík, D., & Ondráčková, V. Immunomodulatory activity of amphiphilic antimicrobials on mouse macrophages. *Int J Immunopharmacol*. 1996;18(6–7):423–426.

[5] Chen, Y.-F. Phase behaviour of cardiolipin [dissertation]. Cornell University; 2012.

[6] Devínsky, F., Kopecká-Leitmanová, A., Šeršeň, F., & Balgavý, P. Cut-off effect in antimicrobial activity and in membrane perturbation efficiency of the homologous series of N,N-dimethylalkylamine oxides. *The Journal of Pharmacy and Pharmacology*. 1990;42(11):790–794.

[7] Epand, R. M., & Epand, R. F. Lipid domains in bacterial membranes and the action of antimicrobial agents. *Biochim Biophys Acta Biomembr*. 2009;1788(1):289–294.

[8] Gallová, J., Želinská, K., & Balgavý, P. Partial volumes of cholesterol and monounsaturated diacylphosphatidylcholines in mixed bilayers. *European Pharmaceutical Journal*. 2017; 1:1–3.

[9] Herrmann, K. W. Non-Ionic—Cationic Micellar Properties of

Dimethyldodecylamine Oxide. *The Journal of Physical Chemistry*. 1962;66(4):295–300.

[10] Hrubšová, A., Karlovská, J., Devínsky, F., Lacko, I., & Balgavý, P. Solubilization of unilamellar egg yolk phosphatidylcholine liposomes by N-alkyl-N,N-dimethylamine N-oxides. *Česká a slovenská farmacie*. 2003;52(6):299–305.

[11] Huláková, S., Fulier, B., Gallová, J., & Balgavý, P. Effect of N-dodecyl-N,N-dimethylamine N-oxide on unilamellar liposomes. *Acta Fac Pharm Univ Comen*. 2013;60(2):7–13.

[12] Huláková, S., Gallová, J., & Devínsky, F. Cholesterol protects phosphatidylcholine liposomes from N,N-dimethyl-1-dodecanamine N-oxide influence. *Acta Chim Slov*. 2015;62(2):420–427.

[13] Karlovská, J., Devínsky, F., Lacko, I., Gallová, J., & Balgavý, P. Solubilization of multilamellar liposomes by N-dodecyl-N,N-dimethylamine N-oxide. *Acta Fac Pharm Univ Comen*. 2004a;51:119–128.

[14] Karlovská, J., Lohner, K., Degovics, G., Lacko, I., Devínsky, F., & Balgavý, P. Effects of non-ionic surfactants N-alkyl-N,N-dimethylamine-N-oxides on the structure of a phospholipid bilayer: Small-angle X-ray diffraction study. *Chem Phys Lipids*. 2004b;129(1):31–41.

[15] Kragh-Hansen, U., le Maire, M., & Møller, J. V. The mechanism of detergent solubilization of liposomes and protein-containing membranes. *Biophysical Journal*. 1998;75(6):2932–2946.

[16] Lichtenberg, D., Ahyayauch, H., Alonso, A., & Goni, F. M. Detergent solubilization of lipid bilayers: A balance of driving forces. *Trends Biochem Sci*. 2013a;38(2):85–93.

[17] Lichtenberg, D., Ahyayauch, H., & Goni, F. M. The mechanism of detergent solubilization of lipid bilayers. *Biophysical Journal*. 2013b;105(2):289–299.

[18] Lopes, S. C., Neves, C. S., Eaton, P., & Gameiro, P. Cardiolipin, a key component to mimic the E. coli bacterial membrane in model systems revealed by dynamic light scattering and steady-state fluorescence anisotropy. *Anal Bioanal Chem*. 2010;398(3):1357–1366.

[19] Lopes, S. C., Neves, C. S., Eaton, P., & Gameiro, P. Improved model systems for bacterial membranes from differing species: The importance of varying composition in PE/PG/cardiolipin ternary mixtures. *Mol Membr Biol*. 2012;29(6):207–217.

[20] MacDonald, R. C., MacDonald, R. I., Menco, B. P. M., Takeshita, K., Subbarao, N. K., & Hu, L. R. Small-volume extrusion apparatus for preparation of large, unilamellar vesicles. *Biochim Biophys Acta Biomembr*. 1991;1061(2):297–303.

[21] Martens, S., & McMahon, H. T. Mechanisms of membrane fusion: Disparate players and common principles. *Nat Rev Mol Cell Biol*. 2008;9(7):543–556.

[22] Meister, A., Finger, S., Hause, G., & Blume, A. Morphological changes of bacterial model membrane vesicles. *Eur J Lipid Sci Technol*. 2014;116(9):1228–1233.

[23] Memoli, A., Annesini, M. C., & Petralito, S. Surfactant-induced leakage from liposomes: A comparison among different lecithin vesicles. *Int J Pharm*. 1999; 184(2):227–235.

[24] Murín, A., Devínsky, F., Koleková, A., & Lacko, I. Relation between chemical-structure and biological-activity of N-alkyl dimethylaminoxides series and some other related-compounds. *Biológia*. 1990;45:521–531.

[25] Murzyn, K., Róg, T., & Pasenkiewicz-Gierula, M. Phosphatidylethanolamine-phosphatidylglycerol bilayer as a model of the inner bacterial membrane. *Biophysical Journal*. 2005;88(2):1091–1103.

[26] Olson, F., Hunt, C. A., Szoka, F. C., Vail, W. J., & Papahadjopoulos, D. Preparation of liposomes of defined size distribution by extrusion through polycarbonate membranes. *Biochim Biophys Acta Biomembr*. 1979;557(1):9–23.

[27] Pontali, E., Matteelli, A., & Migliori, G. B. Drug-resistant tuberculosis. *Curr Opin Pulm Med*. 2013; 19(3):266–272.

[28] Pozo Navas, B., Lohner, K., Deutsch, G., et al. Composition dependence of vesicle morphology and mixing properties in a bacterial model membrane system. *Biochim Biophys Acta Biomembr*. 2005; 1716 (1):40–48.

[29] Ruiz, J., Goni, F. M., & Alonso, A.. Surfactant-induced release of liposomal contents. A survey of methods and results. *Biochim Biophys Acta Biomembr*. 1988; 937:127–134.

[30] Schlame, M., Ren, M., Xu, Y., Greenberg, M. L., & Haller, I. Molecular symmetry in mitochondrial cardiolipins. *Chem Phys Lipids*. 2005;138(1–2):38–49.

[31] Šeršeň, F., Gabunia, G., Krejčírová, E., & Kráľová, K. The relationship between lipophilicity of N-alkyl-N,N-dimethylamine oxides and their effects on the thylakoid membranes of chloroplasts. *Photosynthetica*. 1992;26:205–212.

[32] Singh, S. K., Bajpai, M., & Tyagi, V. K. Amine Oxides: A Review. *J Oleo Sci*. 2006;55(3):99–119.

[33] Uhríková, D., Kučerka, N., Islamov, A., Gordeliy, V., & Balgavý, P. Small-angle neutron scattering study of N-dodecyl-N,N-dimethylamine N-oxide induced solubilization of dioleoylphosphatidylcholine bilayers in liposomes. *Gen Physiol Biophys*. 2001; 20 (2):183–189.

[34] Xu, Z.-Q., Flavin, M. T., & Flavin, J. Combating multidrug-resistant Gram-negative bacterial infections. *Expert Opin Investig Drugs*. 2014; 23 (2):163–182.

[35] Želinská, K., Gallová, J., Huláková, S., Uhríková, D., & Ivankov, O. Solubilisation of model membrane by DDAO surfactant – partitioning, permeabilisation and liposome-micelle transition. *Gen Physiol Biophys*. 2020; 39:107–122.

sciendo

Eur. Pharm. J. 2021, 68(1), 24-29.
ISSN 1338-6786 (online) and ISSN 2453-6725 (print version),
DOI: 10.2478/afpuc-2020-0021

EUROPEAN PHARMACEUTICAL JOURNAL

Characterization of bioactive substances MHGF-68 on tumour cell lines with LiveFlow In Vitro Technology

Original Paper

Hodoši R.[1], Nováková E.[1], Macková K.[2], Molitorisová M.[3], Šupolíková M.[1,3]✉

[1]Comenius University, Faculty of Natural Sciences, Department of Microbiology and Virology, Ilkovičova 6, Mlynská dolina, 842 15, Bratislava 4, Slovak republic
[2]Slovak Academy of Sciences, Center of Biosciences, Dúbravská cesta 9, 845 05 Bratislava, Slovak republic
[3]Comenius University in Bratislava, Faculty of Pharmacy, Department of Galenic Pharmacy, Odbojárov 10 832 32 Bratislava 3, Slovak Republic

Received 11 November, 2020, accepted 22 March, 2021

Abstract As part of experimental research, growth factor-like substances associated with MHV-68, named MHGF-68, were discovered in our laboratory. MHGF-68 activity was manifested by the ability to alter cell morphology, that is, normal phenotype to transformed, resp. suppresses the transformed phenotype of tumour cells. The aim of the experiments was to monitor the effect of MHGF-68 on the change of the cell actin cytoskeleton in the tumour cell line Hepa1c1c7, as well as the normal cell line NIH3T3, and compare conventional stationary cultivation and dynamic cultivation conditions using a LiveFlow system (In Vitro Technologies). LiveFlow is an advanced system to test the impact of different compounds on the cell cultures, which allows simulation of *in vivo* conditions thanks to continuous flow of cultivation medium. MHGF-68 was prepared with the infection of BHK-21 cells with MHV-68 virus under non-permissive conditions (41°C). After dynamic cultivation with MHGF-68, we observed changes in morphology on Hepa1c1c7 cells. In cells cultured in a dynamic environment, we observed more pronounced changes in cell morphology in comparison with cells cultured statically. We observed no changes in the cytoskeletal structures in the NIH 3T3 cell line affected by MHGF-68 in both types of cultivation. The advantage of LiveFlow in comparison to *in vivo* testing is that the experiments performed in this system are less time and money consuming. Dynamic cultivation in the LiveFlow system is suitable for optimizing experiments before testing substances *in vivo*.

Keywords *MHV-68 – bioactive substances MHGF-68 – cytoskeletal structure – LiveFlow system – tumour cell line*

INTRODUCTION

In vitro cultures are a tool for preliminary investigation cell behaviour. They allow to control most of the experimental variables and permit quantitative analysis. In comparison to *in vivo*, *in vitro* models are highly controllable, with a reduction in time and cost (Table 1). Common model for *in vitro* studies is the cell monolayer cultured in static conditions. Ideally, an *in vitro* model should come as close as possible to the *in vivo* situation (Giusti et al., 2014). LiveFlow is an advanced system to test the impact of different compounds on the cell cultures, which allows simulation of *in vivo* conditions thanks to continuous flow of cultivation medium; with the possibility of exact regulation flow speed, IVTech technology is based on compact, user-friendly and transparent cell culture chambers (LiveBox) with shape and dimensions similar to the 24-well plate wells. The main advantage of LiveFlow is the possibility to simulate different tissues and view them in real time, maintaining the same protocols used in traditional cell culture experiments. In this study, we treated cells with MHGF-68 and observed the effect on the cell morphology after cultivation with stationary conditions and after dynamic cultivation resembling *in vivo* conditions with a LiveFlow system (In Vitro Technologies). MHGF-68 compounds are bioactive compounds that resemble cellular growth factors and were isolated in our laboratory in 2015 (Šupolíková et al., 2015). There are already known herpesviruses and poxviruses which have genes encoding secretory proteins with structural similarity to cellular growth factors (Konvalina et al., 2002). The first growth factors related

* *E-mail: miroslava.supolikova@uniba.sk*

Table 1. Comparison of IVTech, in vitro and in vivo testing.

In vitro	In vivo	IVTech (advanced cell culture systems)
Lack of human complexity	Ethically controversial	Human organ environment simulation
Lack of side effects tests	Time ineffective	Multi-organ models
Lack of geometrical complexity	Expensive (2–30 times more than in vitro)	3D and dynamic cell cultures
Cells cultivated in static conditions	No high-throughput monitoring	Real time monitoring

to herpesviruses were obtained from the alphaherpesviruses, specifically pseudorabies virus (PRGF) and herpes simplex virus (HSV) type 1 and type 2 (HSGF-1 and HSGF-2) (Golais et al., 1990; Golais et al., 1992). MHGF-68 compounds were obtained by the cultivation of BHK-21 cells infected with murine herpesvirus-68 (MHV-68) under non-permissive conditions for viral replication (cultivation at 41°C). The viral origin of MHFG-68 was confirmed with a panel of monoclonal antibodies directed against viral glycoprotein B (Šupolíková et al., 2015). These substances are able to change the cell morphology from normal to transformed phenotype and vice versa (Šupolíková et al., 2018). Basic chemical separation of MHGF-68 substances on FPLC column with Sephadex G15 in the absence of salts resulted in loss of transformation activity, while the ability to suppress transformation remained conserved. On the other hand, both effects were conserved when separated on the same column but washed with phosphate buffered saline (PBS). MHGF-68 substances were separated on two biologically active components $MHGF_A$ and $MHGF_B$ after separation on the different column (RP-HPLC C18) using methanol–water phase. Function of these components is to change the normal cell phenotype to transformed phenotype (Šupolíková et al., 2015).

In our experiments, we have confirmed that MHGF-68 has a two-component character and its Mr is < 1000. We used MALDI technique, which is also suitable for checking the samples during the purification procedure for checking the mass of the protein/peptide content after fractionation after RP-HPLC, FPLC respectively (Olejníková *et al*., unpublished data). HPCL-MS showed that every fraction offers different types and different amount of ions during the ionization, which means that the fractions consist of different types of (bio)chemical substances. Chemometrical techniques showed that there are (bio)chemical substances responsible for biological activity. Detailed structure of those compounds needs further study and subsequent experimental work (Vojs Staňová, personal communication). Based on preliminary, the results of the solid-phase extraction (SPE) experiments show that MHGF-68 biologically active substances contain in its molecule a phenolic structure, as evidenced by this that the substances are ionized only at high pH = 9 and pH = 11. This fact is also confirmed by the fact that these substances are not captured on the C8 column, but they are captured on a functional group column propylamine, which behaves as a weak annex. At the same time, these substances, despite ionization, are partially captured on phenyl and cyanide column (Vojs Staňová et al., 2015). The aim of the present study was to compare the effect of MHGF-68 on selected cell lines in conditions of stationary *in vitro* cultivation and dynamic *in vitro* cultivation in LiveFlow apparatus.

MATERIALS AND METHODS

MHGF-68

MHGF-68 compounds were obtained by the cultivation of BHK-21 cells (baby hamster kidney) infected with murine herpesvirus-68 (MHV-68). Monolayers of BHK-21 cells were cultivated in Dulbecco's modified Eagle's medium (DMEM) enriched with 10% fetal bovine serum (FBS), 1% penicillin/streptomycin, 1% L-glutamine and 0.1% gentamicin. Subsequently, cells were infected with MHV-68 with multiplicity of infection (MOI) 0.01 and incubated for 24 hours in 41°C. Afterwards, cells were transferred to 37°C and cultivated for another 24 hours. After cultivations, media from these cells were pooled, lyophilized and stored in +4°C until other experiments were performed (Šupolíková et al., 2015). The fraction of MHGF-68 used in experiments was acquired by FPLC separation on Sephadex G15 column, eluted by redistilled water, so the transformation suppressing activity remained. Experimental conditions: 5 ml of medium obtained from infected cells MHV-68 was loaded onto an HPLC analyser (Shimadzu, Kyoto, Japan) with column of dimensions 950 x 20 mm containing sorbent Sephadex G15 Fine (Pharmacia, Lund, Sweden). Deionized was used as the mobile phase water or saline (pH 7.2). Flow mobile phase was 0.8 ml/min. Fractions were collected based on the signal from the UV detector at the wave detectors lengths 220 and 254 nm (Vojs Staňová et al., 2015).

Cells

Experiments were performed on adherent fibroblast cell lines Hepa1c1c7 and NIH3T3. Cell line Hepa1c1c7 (ATCC® CRL-2026™) is a stabilized tumour cell line isolated from murine hepatocellular carcinoma, whereas cell line NIH3T3 is a normal cell line derived from murine embryonal cells (ATCC® CRL1658™). Cells were cultivated in DMEM enriched with 7%

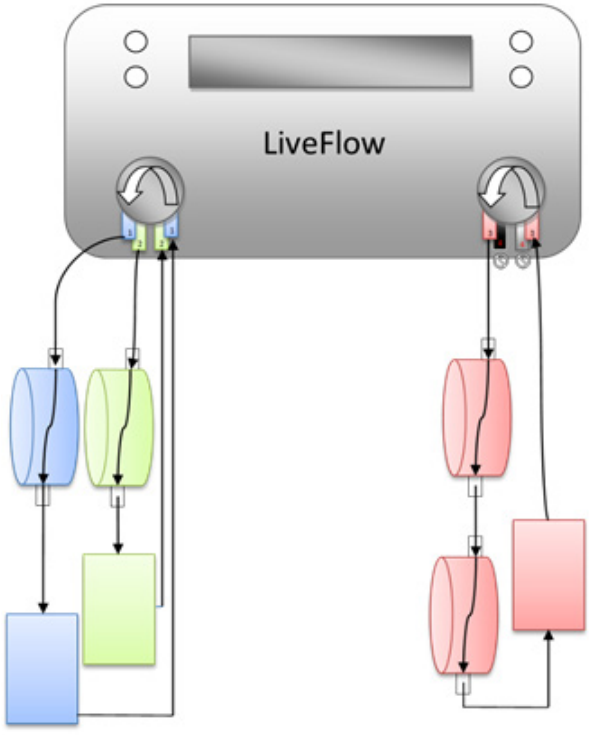

Figure 1. LiveFlow system scheme . Blue and green – LiveBox with samples, parallel circuits of medium, Red – controls, series circuit of medium.

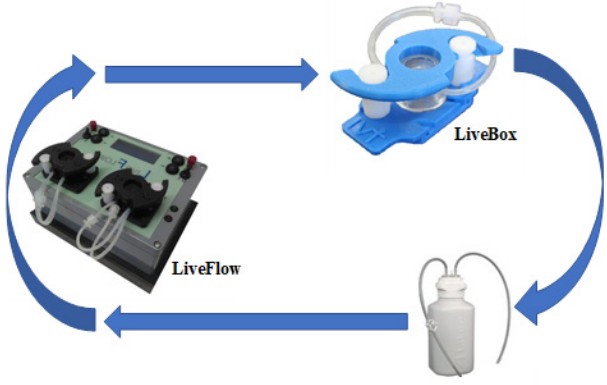

Figure 2. Scheme of dynamic cultivation using LiveFlow (IVTech). LiveBox with adherent cell line on the glass slide inside, reservoir with cultivation medium and LiveFlow ensuring continual flow of the medium.

FBS, 1% PSA (antibiotics: 100 U/ml penicillin/streptomycin, 100 µg/ml amphotericin) and 1% L-glutamine, and they were incubated in 37°C with 5% CO_2.

Cell cultivation in dynamic environment with the use of LiveFlow system

Sterile circular glass cover slides (20 mm in diameter) were placed in 6-well plates (1 slide per well). 1 x 10^5 cells were seeded onto glass slides in volume of 0.25 ml per slide. After a 20-minute-long incubation, 2 ml of DMEM was added to each well. After a 24-hour-long cultivation, glass slides were placed into LiveFlow system, as shown in Figure 1, and the cultivation medium with MHGF-68 (diluted 1:100) was added. In every experiment, control untreated cells (without MHGF-68) were used. Volume of circulating medium was 7.5 ml per LiveBox (1 slide). Cells were cultivated 24, 48 and 72 hours with continuous flow of medium at a speed of 180 µl per minute (Figure 2). Incubation was performed at 37°C, 5% CO_2. For information: LiveFlow system is commercially manufactured by In Vitro Technologies (in short IVTech) and distributed by Scintilla spol. s r.o.

Cell cultivation in static conditions

Sterile circular glass cover slides (20 mm in diameter) were placed in 6-well plates (1 slide per well). 1 x 10^5 cells were seeded onto glass slides in volume of 0.25 ml per slide. After a 20-minute-long incubation, 2 ml of DMEM was added to each well. After a 24-hour-long cultivation, the medium was exchanged with a medium with MHGF-68 (diluted 1:100). In every experiment, control untreated cells (without MHGF-68) were used. Cells were cultivated for 24, 48 and 72 hours at 37°C, 5% CO_2.

Immunofluorescence assay

After incubation, the cells were fixed with 4% paraformaldehyde solution and permeabilized with 0.01% Triton X-100 (PBS solution). Alexa Fluor 555 conjugated with Phalloidin was used to visualize actin filaments. To visualize cell nuclei, DAPI stain was used. Prepared slides were observed using Leica TCS SP8 AOBS (Leica Microsystems, Germany) confocal microscope with HC PL APO CS2 63x/1.40 OIL lens.

RESULTS AND DISCUSSION

The cytoskeleton plays an important role in the regulation of various cellular processes associated with transformation, such as proliferation, contact inhibition, and cell growth in thin agar or apoptosis. In general, loss of actin filaments is considered a marker of oncogenicity (Pawlak and Helfman, 2001; Etienne-Manneville, 2004; Shutova and Alexandrova, 2010). In this study, morphological changes in cellular actin cytoskeleton after treatment with bioactive substances MHGF-68 were observed. These changes were significantly more pronounced on Hepa1c1c7 cells, especially after dynamic cultivation in LiveFlow system. After dynamic cultivation in LiveFlow, the shape of untreated (control) cells was rhomboidal (Figure 3A, B, C). Actin cytoskeleton of untreated cells was diffusive, probably depolymerized, with small aggregations of actin molecules with filamentous actin near cell margin (Figure 3C). Cells treated with MHGF-68 after 24 hours of cultivation had enlarged nuclei and changed

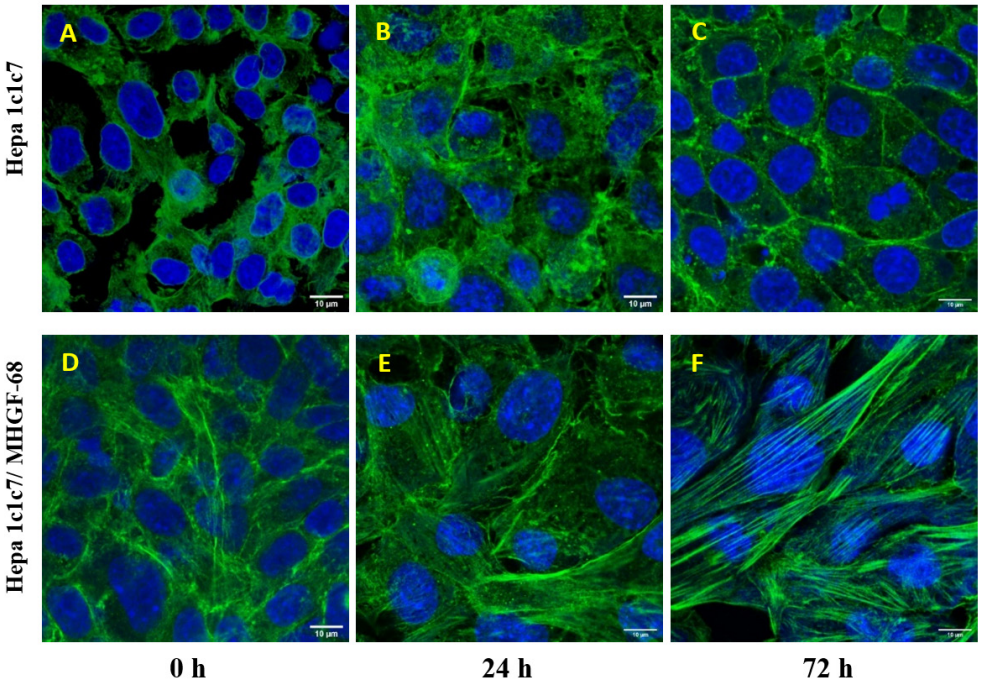

Figure 3. Distribution of actin filaments in Hepa1c1c7 cells incubated with MHGF-68 after dynamic cultivation.
Hepa1c1c7 cells were incubated with MHGF-68. After 0, 24 and 72 h, the cells were fixed and labeled with Alexa Fluor 555 phalloidin. Nuclei were stained with DAPI. The intracelular distribution of actin filamets (green) and nuclei (blue) were imaged by confocal laser scanning fluorescence microscopy (Leica TCS SP8 AOBS) with HC PL APO CS2 63x/1.40 OIL lens.
A *Hepa1c1c7 untreated, 0 h cultivation* **B** *Hepa1c1c7 untreated, 24 h cultivation* **C** *Hepa1c1c7 untreated, 72 h cultivation* **D** *Hepa1c1c7 + MHGF-68, 0 h cultivation* **E** *Hepa1c1c7 + MHGF-68, 24 h cultivation* **F** *Hepa1c1c7 + MHGF-68, 72 h cultivation*

shape (Figure 3E). After 72 hours, cells gained spindle-like shape (Figure 3F). On the contrary, highly organized actin filaments and high granulation of cytoplasm were found in whole-cell volume of cells incubated with MHGF-68 (Figure 3D). Any significant changes in NIH 3T3 cells were not detected. In comparison with dynamic cultivation, cytoskeleton structure of Hepa1c1c7 cells after static cultivation was different. Highly organized actin filaments were not present in the whole volume of cells, but were largely arranged along the edges of the cells (Figure 4E, F). After 72 hours of static cultivation, signs of spindle-shaped cell formation were observed (Figure 4F). On the normal NIH 3T3 cell line cultured with MHGF-68, we did not observe any changes in the cell cytoskeleton during the dynamic culture (data not shown). Comparison of 72 hours static and dynamic cultivation of Hepa1c1c7 with MHGF-68 showed that during stationary cultivation, changes were less visible (Figure 5). In the case of untreated cells, the formation of highly organized actin filaments and the enlargement of nuclei were observed only after dynamic cultivation in LiveFlow (Figure 5D).

Our results from monitoring the effect of MHGF-68 on cell proliferation, metabolic activity and viability of the cells were confirmed by xCELLigence analyser too (Šupolíková et al., unpublished data). We found that the effect of the MHGF-68 fractions was relatively short-lived and decreased with longer time of cultivation. Since the chemical structure of MHGF-68 fractions is not yet known, the described biological activities require further studies.

CONCLUSION

Changes of cell size and shape and distribution of actin filaments were observed during both types of cultivation in normal and tumour cell line. Comparison of stationary and dynamic cultivation showed that the effect of MHGF-68 on cytoskeletal structures is more significant during dynamic cultivation. Regarding quantitative determination of the activity of bioactive compounds MHGF-68, it is more suitable to use stationary cultivation. We confirmed by MTT assay that the effect of MHGF-68 in a static cultivation showed a significant inhibitory effect on the proliferation and viability of NIH 3T3 and Hepa1c1c7 cells and that the effect in the dynamic cultivation did not have a significant effect on the proliferation and viability of Hepa1c1c7 cells (data not shown). However, dynamic cultivation in LiveFlow system is suitable for the optimization of experiments before *in vivo* tests on laboratory animals, as it simulates conditions in live organisms by continuous flow of culture medium.

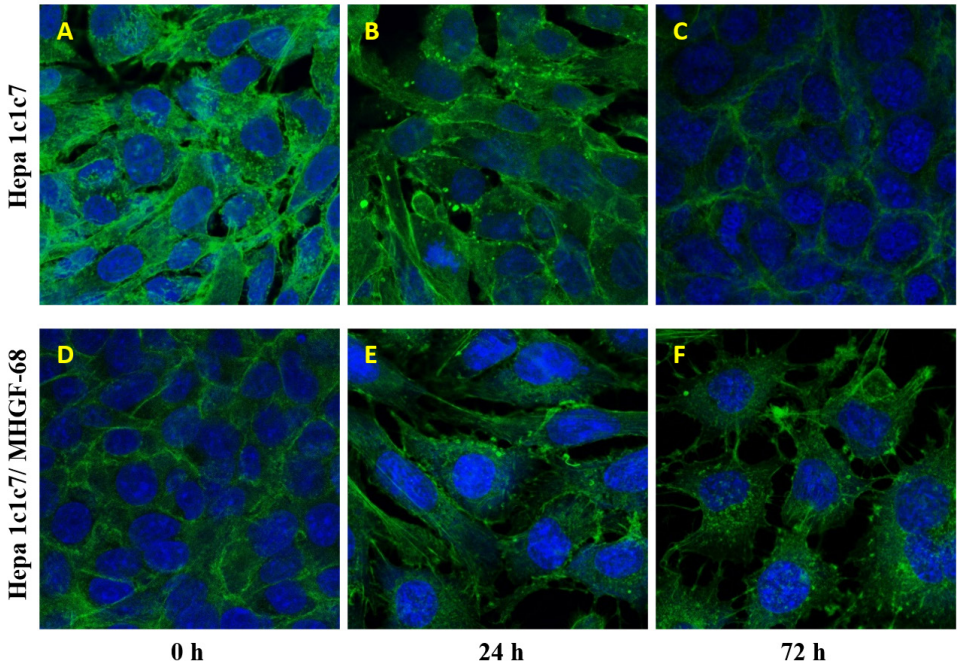

Figure 4: Distribution of actin filaments in Hepa1c1c7 cells incubated with MHGF-68 after static cultivation. Hepa1c1c7 cells were incubated with MHGF-68. After 0, 24 and 72 h, the cells were fixed and labeled with Alexa Fluor 555 phalloidin. Nuclei were stained with DAPI. The intracelular distribution of actin filamets (green) and nuclei (blue) were imaged by confocal laser scanning fluorescence microscopy (Leica TCS SP8 AOBS) with HC PL APO CS2 63x/1.40 OIL lens. **A** *Hepa1c1c7 untreated, 0 h cultivation* **B** *Hepa1c1c7 untreated, 24 h cultivation* **C** *Hepa1c1c7 untreated, 72 h cultivation* **D** *Hepa1c1c7 + MHGF-68, 0 h cultivation* **E** *Hepa1c1c7 + MHGF-68, 24 h cultivation* **F** *Hepa1c1c7 + MHGF-68, 72 h cultivation*

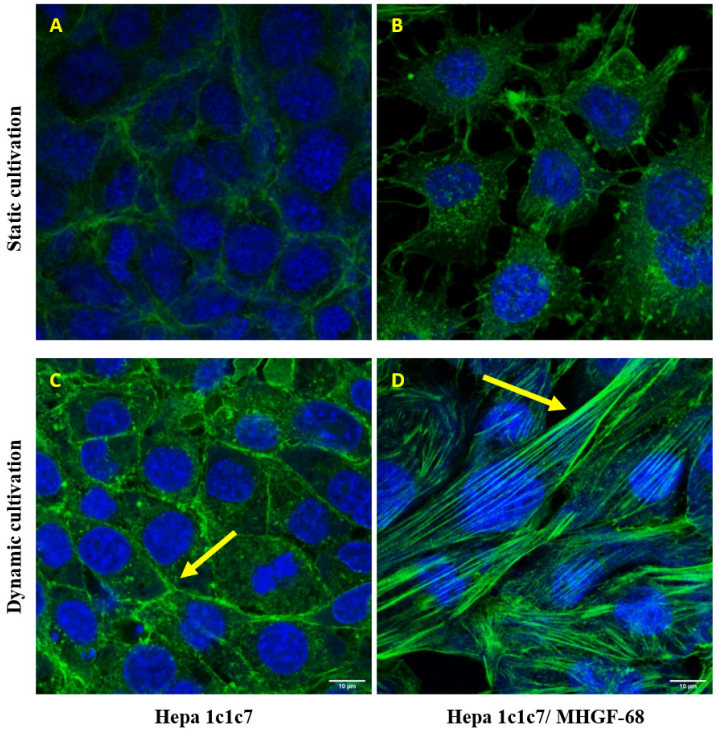

Figure 5. Distribution of actin filaments in Hepa1c1c7 cells incubated 72 h with MHGF-68 after static and dynamic cultivation. Hepa1c1c7 cells were incubated with MHGF-68. After 72 h, the cells were fixed and labeled with Alexa Fluor 555 phalloidin. Nuclei were stained with DAPI. The intracelular distribution of actin filamets (green) and nuclei (blue) were imaged by confocal laser scanning fluorescence microscopy (Leica TCS SP8 AOBS) with HC PL APO CS2 63x/1.40 OIL lens.
A *Hepa1c1c7 untreated, static cultivation* **B** *Hepa1c1c7 + MHGF-68, static cultivation* **C** *Hepa1c1c7 untreated, dynamic cultivation* **D** *Hepa1c1c7 + MHGF-68, dynamic cultivation*

ACKNOWLEDGEMENTS

This research was carried out with financial support from VEGA 1/0061/18, APVV-0621-12 and OPVaV-2015/3.1/01-SORO.

References

[1] Etienne-Manneville S. Actin and microtubules in cell motility: which one is control? Traffic. 2004; 5: 470–477.
[2] Giusti S, Sbrana T, La Marca M, Di Patria V, Martinucci V, Tirella A, Domenici C, Ahluwalia A. A novel dual-flow bioreactor simulates increased fluorescein permeability in epithelial tissue barriers. Biotechnol J. 2014; 9: 1175–1184.
[3] Golais F, Košťál M, Csabayová M, Leško J. The glycoprotein B gene and its syn3 locus of herpes simplex virus type 1 are involved in the synthesis of virus-associated growth factor (HSGF-1). Acta Virol. 1992; 36: 505–515.
[4] Golais F, Leško J, Hillerova A, Sabo A, Kolcunova A. A putative virus-encoded growth factor in a crude extract of pseudorabies virus infected and transformed cells. Biologisches Zentralblatt 1990; 109: 481–487.
[5] Konvalina I, Gašperík J, Golais F. A novel class of growth factors related to herpesviruses. Acta Veterinaria Brno 2002; 71: 29–36.
[6] Pawlak G, Helfman DM. Cytoskeletal changes in cell transformation and tumorigenesis. Curr Opin Genet Dev.2001; 11: 41–47.
[7] Shutova MS, Alexandrova AY. Normal and transformed fibroblast spreading: role of microfilament polymerization and actin-myosin contractility. Cell Tissue Biol.2010; 4: 25–35.
[8] Šupolíková M, Labudová M, Nováková E, Vojs Staňová A, Šišovský V, Golais F. The effect of Murine Herpesvirus 68 (MHV-68) Related Growth Factor 68 (MHGF-68) on the Tumor progression in Athymic Nude Mice Am. J. Biomed. Life Sci. 2018; 6(6): 127–131.
[9] Šupolíková M, Vojs Staňová A, Kúdelová M, Marák J, Zelník V, Golais F. Cells transformed by murine herpesvirus 68 (MHV-68) release compounds with transforming and transformed phenotype suppressing activity resembling growth factors. Acta Virol. 2015; 59(4): 418–422.
[10] Vojs Staňová A, Šupolíková M, Koiš P, Golais F, Marák J. Analýza a identifikácia biologicky aktívnych látok indukovaných myším herpetickým vírusom (Analysis and identification of biologically active substances induced by murine herpes virus). Zdravotnícke listy 2015; 3(4): 110–114.

sciendo

Eur. Pharm. J. 2021, 68(1), 30-39.
ISSN 1338-6786 (online) and ISSN 2453-6725 (print version),
DOI: 10.2478/afpuc-2020-0020

EUROPEAN PHARMACEUTICAL JOURNAL

Nephroprotective Effect of Coenzyme Q10 alone and in Combination with N-acetylcysteine in Diabetic Nephropathy

Original Paper

Mahajan Manojkumar S., Upaganlawar Aman B., Upasani Chandrashekar D.*

Shri Neminath Jain Brahmacharyashram Trust's
Shreeman Sureshdada Jain College of Pharmacy
Nashik, Maharashtra, India

Received 3 November, 2020, accepted 29 March, 2021

Abstract **Aim:** Oxidative stress due to chronic hyperglycaemia is a key factor in the development and progression of various microvascular complications including diabetic nephropathy (DN) and associated renal injury. Treatment with antioxidants is one of the strategies to protect the kidney from oxidative tissue damage to improve renal physiology during DN. The investigation, therefore, was designed to assess the nephroprotective effect of coenzyme Q10 (CoQ10) and N-acetylcysteine (NAC), either alone or in combination in streptozotocin (STZ)-nicotinamide (NAD) induced diabetic nephropathy (DN) in rats.
Methods: T2DM induced by STZ (55 mg/kg, i.p.)-NAD (110 mg/kg, i.p.) in Sprague-Dawley rats (220–250 g) was confirmed by the elevated blood glucose level and glycated haemoglobin. DN was assessed by renal function tests. The diabetic rats were treated with CoQ10 (10 mg/kg, p.o.) and/or NAC (300 mg/kg, p.o.) for 8 weeks after confirmation of DN. Oxidative tissue damage due to STZ-NAD was estimated by malondialdehyde (MDA), superoxide dismutase (SOD) and catalase (CAT), reduced glutathione (GSH), myeloperoxidase (MPO) and nitric oxide (NO) in the renal homogenate.
Results: Data showed significant alteration in serum and urinary creatinine, total protein, albumin, serum urea, blood urea nitrogen (BUN) and uric acid in diabetic animals as compared to the control rats. CoQ10 and/or NAC effectively alleviated the disturbances in renal function. Diabetic rats showed increased MDA, decreased SOD and CAT activities and decreased GSH along with a significant increase in MPO activity and nitrite content. Treatment with the aforementioned antioxidants and their combination ameliorated the kidney damage as indicated by the reduced OS with improved renal function.
Conclusion: The investigation suggests that the chronic hyperglycaemia-induced OS leads to the development and progression of DN. The combined treatment with CoQ10 and NAC has shown a remarkable nephroprotective effect suggesting that combined antioxidant therapy with CoQ10 and NAC may be useful in the attenuation of DN.

Keywords *Diabetic nephropathy – oxidative stress – streptozotocin – coenzyme Q10 – N-acetylcysteine*

INTRODUCTION

Diabetes mellitus (DM) is a group of heterogeneous disorders characterized by hyperglycaemia linked to insulin deficiency or decreased tissue sensitivity (Maitra, 2015; Masharani, 2008). The two types of DM are type 1 DM (T1DM) and type 2 DM (T2DM).

T2DM or non-insulin-dependent diabetes mellitus (NIDDM), a multifactorial disorder develops as a result of insulin resistance with relative insulin deficiency and is most common among adults. T2DM features a strong genetic component in addition to the acquired pathogenic causes associated with secretion and resistance to insulin (Kohei, 2010).

Premature deaths due to DM are associated with macro and microvascular complications. The primary microvascular complications of DM are diabetic nephropathy (DN), diabetic neuropathy and diabetic retinopathy (Pal et al., 2014; Geraldes et al., 2009).

DN is the foremost cause of chronic kidney disease (CKD) and end-stage renal disease (ESRD). It is a progressive and irreversible loss of renal function involving glomerular hyperfiltration, incipient nephropathy, microalbuminuria, overt proteinuria and ESRD (Mogensen et al., 1983). DN induces renal structural changes like an accumulation of extracellular matrix and glomerular mesangial expansion, interstitial fibrosis and basement membrane thickening (Vora & Ibrahim, 2003).

Hyperglycaemia plays a crucial role in the development of DN. It has been shown that persistent hyperglycaemia in DM can induce OS by several mechanisms that involve, glucose auto-

* *E-mail: cdupasani@gmail.com*

oxidation, activation and acceleration of polyol pathway, protein glycation through non-enzymatic means and reduced antioxidant defense. Hyperglycaemia is believed to act by activation of Protein kinase C (PKC) pathway, generation of reactive oxygen species (ROS) and over-expression of transforming growth factor-β (TGF-β) (Schena & Gesualdo, 2005; Brownlee, 2001).

The normal kidney owing to its high metabolic activity generates substantial OS that is stabilized by an antioxidant defense system. Uncontrolled blood glucose level shifts this equilibrium to a pro-oxidant state resulting in tissue injury and vascular anomalies It has been shown that the mechanisms involved in the development of the DN induce considerable OS by one or other means (Vasavada & Agarwal, 2005).

At present, none of the therapies used for DN have proved efficacious due to the involvement of diverse etiologic factors in the progression of DN. Therefore, it is difficult to select the best possible treatment approach and therapeutic agent. Consequently, effective and novel therapeutic strategies are required in the treatment of DN. Studies have demonstrated the beneficial effects of antioxidant therapies in DN (Mahajan et al., 2019).

CoQ10 (ubiquinone) is an endogenous, vitamin-like lipophilic substance serving as a natural antioxidant. CoQ10 plays a key role in the mitochondrial electron transport chain and scavenges free radicals to protect the β cells from the harmful effects of OS by its antioxidant properties (Hodgson et al., 2002; Rosenfeldt et al., 2007). Studies have also shown that CoQ10 is effective for glycaemic control among individuals with T2DM and reduces HbA_{1c} levels (Maheshwari et al., 2014). NAC is a glutathione precursor and a powerful antioxidant. NAC has been shown to impart protection to the β-cells against cellular damage. NAC attenuates hyperglycaemia and improves glucose intolerance. This action of NAC is linked to glucose-induced insulin release (Haber et al., 2003; Ahmad et al., 2012; Shimizu et al., 2005).

So far, no earlier studies have reported the synergistic effect of CoQ10 and NAC in the treatment of DN. Hence, we have selected these antioxidants and an effort was taken to study their combined effect in nephroprotection against experimentally induced DN. Therefore, the current research was aimed to explore the nephroprotective effect of CoQ10 and NAC alone and in combination in STZ-NAD-induced DN.

METHODS

Drugs and Chemicals

CoQ10 was obtained as a gift sample from Zydus Cadila, Ahmedabad, India. NAC was purchased from Loba Chemie (Mumbai, India). STZ and NAD were purchased from Sigma-Aldrich (USA). Spectrophotometric kits for determination of superoxide dismutase (SOD), catalase (CAT), and myeloperoxidase (MPO) activity and malondialdehyde (MDA), reduced glutathione (GSH) and nitric oxide (NO) content were acquired from Elabscience Biotechnology Inc. (Houston, USA). Kits for estimation of total protein and albumin were obtained from Arkray Healthcare Pvt. Ltd. (Mumbai, India). Determination of serum and urinary creatinine, serum urea, BUN and uric acid was carried by using the biochemical kits purchased from Tulip Diagnostics Pvt. Ltd. (Mumbai, India). All the other chemicals and reagents used in the study were of analytical grade.

Animals

Forty healthy male Sprague-Dawley rats (SD, 8 weeks, 220–250 g) were obtained from the National Institute of Bioscience, Pune. Rats were acclimated for 1 week before the commencement of the study. Animals were housed under a controlled environment of temperature (18–22°C) and light (12 hr light/dark cycle, lights on 07:00–19:00). All the rats were provided *ad libitum* access to water and standard food. All the experimental procedures in this study were carried out following the guidelines issued by the Committee for the Purpose of Control and Supervision of Experiments on Animals (CPCSEA) for the care and use of animals. The Institutional Animal Ethics Committee (IAEC) approved the protocol of the study bearing the reference number SSDJ/IAEC/2016/02.

Induction of Diabetic Nephropathy

T2DM was induced in overnight fasted male SD rats using STZ (55 mg/kg) as a single intraperitoneal (i.p.) injection. STZ was dissolved in freshly prepared cold citrate buffer (pH 4.5) and administered immediately. STZ was injected 15 min. after the administration of nicotinamide (110 mg/kg, i.p.) dissolved in normal saline (Ghasemi et al., 2014; Badole et al., 2013). Hyperglycaemia was determined at 72 h and then at the end of the first week post-treatment with STZ-NAD using a glucometer (AlereG1, Korea). Blood glucose level was estimated in the samples collected from the end part of tails. Animals showing elevated blood glucose level greater than 250 mg/dL were served as diabetic and were included in the nephropathy studies.

Experimental Design

Rats were divided into the following five groups with six animals each.

Group I: Normal rats (control, negative control without any treatment)

Group II: Diabetic control rats (STZ-NAD DN, positive control without any treatment)

Group III: Diabetic rats + CoQ10 (10 mg/kg/day) suspended in 1% aqueous solution of Tween 80 and designated as CoQ10 group (Garjani et al., 2011; Maheshwari et al., 2014)

Group IV: Diabetic rats + NAC (300 mg/kg/day) dissolved in distilled water and designated as NAC group (Lee et al., 2016; Odetti et al., 2003)
Group V: Diabetic rats + CoQ10 and NAC (CoQ10 + NAC group) CoQ10 and NAC were administered orally to rats using an intragastric tube daily for a period of 8 weeks.
Treatment of Diabetic rats from groups III, IV and V was initiated at the beginning of the 5th week and continued till the end of the 12th week of the study duration.
At the end of the experimental period, and twenty-four hours after the last antioxidant dose, the rats were placed individually in the metabolic cages for 24 hours to collect urine samples. The urine samples were centrifuged and stored in amber-coloured vials. After that, blood samples from retro-orbital plexus were collected from the rats under pentobarbitone sodium anaesthesia. Whole blood collected in commercially available ethylene diamine tetra-acetic acid (EDTA) tubes was used for the estimation of HbA1c. Serum was separated by allowing the collected blood to clot in tubes without EDTA and was used for the estimation of renal parameters. Both urine and serum samples used for biochemical assessment were stored at -20°C.
HbA_{1C} was estimated from whole blood samples. Total protein, albumin and creatinine were estimated in serum and urine samples. Urea, BUN and uric acid were determined from serum with the help of biochemical kits using Prietest Touch Biochemistry Analyzer, Robonik India Pvt. Ltd. (Mumbai, India).
Creatinine clearance (Ccr, mL/min) was determined from the following formula: (urine creatinine [mg/dL] × 24 h urine volume [mL])/(serum creatinine [mg/dL]×1440 [min]). Urinary albumin excretion rate (UAER, µg/min) was calculated by using the formula: Albumin [mg/dL] ×volume of urine in timed collection [dL] ×1000)/1440 [min].
At the end, the rats were sacrificed by an overdose of pentobarbitone sodium (200 mg/kg, body weight, i.p.) and the kidneys were removed, washed with ice-cold saline, weighed and processed for tissue biochemical estimations.

Estimation of markers of Oxidative Stress

The dissected kidneys were placed in a Petri plates with ice-cold conditions. The tissues were sliced using a surgical scalpel in the presence of chilled 0.25 M sucrose. These were then blotted quickly using filter paper. These were minced and homogenized with 25 strokes of tight Teflon pestle of glass homogenizer at a speed of 10,000 × g at 0°C using the Remi cooling centrifuge. Either normal saline or phosphate-buffered saline (PBS) was used as the homogenization medium. 10% w/v tissue homogenate was prepared according to the protocol supplied by the manufacturer with the respective antioxidant enzyme assay kit. The total protein concentration in the homogenate was determined using a total protein assay kit (Bicinchonic acid method, E-BC-K075).

Statistical analysis

All the data were expressed as mean ± standard error of the mean (S. E. M.). One-way ANOVA was used to record inter-group variation followed by Tukey's multiple comparisons test as appropriate to test statistical significance using Graph Pad Prism version 5.0, GraphPad Software, Inc. The minimum significance level was set at $p < 0.05$ for all the tests.

RESULTS

Effect of CoQ10, NAC or their combination on body weight %

Significant ($p < 0.05$) difference in body weight % was observed when all the groups were compared (**Table 1**). Normal rats showed a significant ($p < 0.05$) increase in body weight % at the twelfth week in contrast to the STZ-NAD treated diabetic rats with a significant ($p < 0.05$) reduction in body weight % at the same period. Diabetic groups treated with CoQ10 and/or NAC prevented such a weight loss in comparison to the diabetic control group (Table 1). A significant ($p < 0.05$) effect of combined administration of CoQ10 and NAC on body weight % in diabetic rats was noted as compared to the diabetic animals receiving CoQ10 or NAC alone.

Effect of CoQ10, NAC or their combination on the kidney to body weight ratio

As shown in Table 1, induction of T2DM with STZ-NAD in the rats significantly ($p < 0.05$) increased the kidney to body weight ratio than in the normal rats. Diabetic rats treated with CoQ10, NAC or their combination (CoQ10 + NAC) for eight weeks (5th–12th week) significantly ($p < 0.05$) prevented the increase in kidney to body weight ratio as compared to the diabetic control rats. On the other hand, the combined administration of CoQ10 and NAC significantly ($p < 0.05$) abrogated the elevation in kidney to body weight ratio as compared to the diabetic control group and the diabetic rats receiving either CoQ10 or NAC alone.

Effect of CoQ10, NAC or their combination on blood glucose level and HbA_{1C}

As given in Table 2, 72 h post STZ-NAD injection (week 0) showed a significant ($p < 0.05$) increase in blood glucose level of all the treatment groups as compared to the normal rats. Oral administration of CoQ10 showed a significant ($p < 0.05$) decrease in blood glucose levels relative to the diabetic animals. A significant ($p < 0.05$) decrease in blood glucose level was observed in the diabetic animals treated with NAC as compared to the diabetic control group. It was also noted that NAC didn't affect the elevated blood glucose level in comparison to the observations with NAC treated diabetic rats at week 0 (Table 2). Treatment of the diabetic rats with combination of

Table 1. Effect of CoQ10, NAC or their combination on body weight% and kidney to body weight ratio (mg/g).

Groups	Body weight %		Kidney to Body Weight Ratio (mg/g)
	Initial at Week 0	Final at Week 12	
Control	100.0 ± 0.368	145.2 ± 0.865*	3.807 ± 0.041
STZ-NAD DN	100.0 ±1.389	87.5 ± 0.958a*	7.504 ± 0.193 a
CoQ10 (10 mg/kg)	100.0 ±0.763	105.2 ± 1.122ab*	5.490 ± 0.199ab
NAC (300 mg/kg)	100.0 ±1.128	106.5 ± 0.467ab*	5.201 ± 0.072ab
CoQ10 + NAC	100.0 ±1.039	112.0 ± 1.217abcd*	4.530 ± 0.126abcd

Values are expressed as mean ± SEM; n = 6. One-way ANOVA followed by Tukey's multiple comparison test. [a]p < 0.05 as compared to the normal control group, [b]p < 0.05 as compared to the diabetic control group, [c]p < 0.05 as compared to diabetic CoQ10 alone treated group and [d]p < 0.05 as compared to diabetic NAC alone treated group, [*]p < 0.05 as compared with the same group at 0 week.

Table 2. Effect of CoQ10, NAC or their combination on blood glucose level (mg/dL) and HbA_{1C}.

Groups	Blood Glucose (mg/dL)		HbA_{1C} (%)
	Initial at Week 0	Final at Week 12	
Control	91.83 ± 2.937	91.0 ± 3.13	4.733 ± 0.084
STZ-NAD DN	499.0 ± 17.27a	534.0 ± 24.28a	9.05 ± 0.283 a
CoQ10 (10 mg/kg)	473.2 ± 17.35a	413.5 ± 5.812ab*	6.15 ± 0.080ab
NAC (300 mg/kg)	480.0 ± 15.73a	451.7 ± 11.8ab	6.4 ± 0.085ab
CoQ10 + NAC	477.7 ± 15.34a	351.5 ± 12.03abcd*	5.4 ± 0.171abcd

Values are expressed as mean ± SEM; n = 6. One-way ANOVA followed by Tukey's multiple comparison test. [a]p < 0.05 as compared to the normal control group, [b]p < 0.05 as compared to the diabetic control group, [c]p < 0.05 as compared to diabetic CoQ10 alone treated group and [d]p < 0.05 as compared to diabetic NAC alone treated group, [*]p < 0.05 as compared with the same group at 0 week.

CoQ10 and NAC resulted in significant ($p < 0.05$) attenuation of hyperglycaemia as compared to the other diabetic groups with or without treatment included in the study.

HbA_{1C} was significantly ($p < 0.05$) elevated in the diabetic control rats than the normal rats (Table 2). Treatment with CoQ10 resulted in a significant ($p < 0.05$) change in HbA_{1C} as compared to the diabetic control rats. NAC treatment significantly ($p < 0.05$) decreased HbA_{1C} than the diabetic rats. The combination treatment decreased HbA_{1C} level significantly ($p < 0.05$) as compared to the diabetic groups treated with CoQ10 or NAC alone (Table 2).

Effect of CoQ10, NAC or their combination on serum total protein, albumin, creatinine and creatinine clearance

A significant ($p < 0.05$) decline in renal function was observed in the diabetic control rats than the normal rats (Table 3). Diabetic rats treated with CoQ10, NAC or their combination significantly ($p < 0.05$) improved the renal function than the diabetic control group. The creatinine clearance in the diabetic rats receiving the aforementioned treatments was improved significantly ($p < 0.05$) as compared to the diabetic control group. The combination treatment had a more beneficial effect on the restoration of renal function **(Table 3)**.

Effect of CoQ10, NAC or their combination on serum urea, BUN and uric acid

As illustrated in Figure 1, the diabetic rats treated with CoQ10, NAC or CoQ10+NAC resulted in a significant ($p < 0.05$) decrease in serum urea (Fig. 1a), BUN (Fig. 1b) and uric acid levels (Fig. 1c). More beneficial effect of the combination treatment in diabetic rats was noted in terms of significant ($p < 0.05$) difference in these parameters than the diabetic groups treated with CoQ10 or NAC alone.

Values are expressed as mean ± SEM; $n = 6$. One-way ANOVA followed by Tukey's multiple comparison test. [a]$p < 0.05$ as compared to the normal control group, [b]$p < 0.05$ as compared to the diabetic control group, [c]$p < 0.05$ as compared to diabetic CoQ10 alone treated group and [d]$p < 0.05$ as compared to diabetic NAC alone treated group.

Effect of CoQ10, NAC or their combination on urine volume, urinary protein and albumin excretion

In the diabetic control group, 24 h urine volume (Fig. 2a) increased significantly ($p < 0.05$) than the normal rats. Diabetic groups treated with CoQ10, NAC or their combination showed a significant ($p < 0.05$) decrease in the urine output as compared to the diabetic control group without any

Table 3. Effect of CoQ10, NAC or their combination on serum total protein, albumin, creatinine and creatinine clearance.

Groups	Total Protein (g/dL)	Albumin (g/dL)	Creatinine (mg/dL)	Creatinine clearance (mL/min)
Control	7.55 ± 0.071	3.65 ± 0.042	0.426 ± 0.032	1.134 ± 0.088
STZ-NAD DN	4.88 ± 0.094[a]	1.86 ± 0.114 [a]	2.7 ± 0.182 [a]	0.269 ± 0.030[ab]
CoQ10 (10 mg/kg)	6.21 ± 0.149[ab]	2.95 ± 0.117[ab]	1.51 ± 0.110[ab]	0.631 ± 0.039[ab]
NAC (300 mg/kg)	5.93 ± 0.195[ab]	2.56 ± 0.133[ab]	1.55 ± 0.105[ab]	0.608 ± 0.045[ab]
CoQ10 + NAC	6.9 ± 0.063[abcd]	3.05 ± 0.067[abd]	1.05 ± 0.058[abcd]	0.907 ± 0.039[abcd]

Values are expressed as mean ± SEM; n = 6. One-way ANOVA followed by Tukey's multiple comparison test. [a]p < 0.05 as compared to the normal control group, [b]p < 0.05 as compared to the diabetic control group, [c]p < 0.05 as compared to diabetic CoQ10 alone treated group and [d]p < 0.05 as compared to diabetic NAC alone treated group.

treatment.

There was a significant ($p < 0.05$) elevation in the urinary protein (Fig. 2b) and UAER (Fig. 2c) of the diabetic rats than the normal rats. The treatment of diabetic groups with CoQ10, NAC or their combination significantly ($p < 0.05$) reduced the appearance of proteins in the urine and UAER as compared to the diabetic control group.

It was noted that co-administration of CoQ10 and NAC to the diabetic rats led to a more significant effect in reducing UAER Values are expressed as mean ± SEM; $n = 6$. One-way ANOVA followed by Tukey's multiple comparison test. [a]$p < 0.05$ as compared to the normal control group, [b]$p < 0.05$ as compared to the diabetic control group, [c]$p < 0.05$ as compared to diabetic CoQ10 alone treated group and [d]$p < 0.05$ as compared to diabetic NAC alone treated group.

Effect of CoQ10, NAC or their combination on renal oxidative stress and anti-oxidant markers

Diabetic control rats showed significant ($p < 0.05$) increase in the MDA. Treatment of diabetic rats using the combination of CoQ10 and NAC after induction of DN exhibited significant ($p < 0.05$) reduction in MDA than the diabetic rats treated orally with CoQ10 or NAC alone (Fig. 3a).

The activities of SOD and CAT enzymes in the kidney of diabetic control rats were significantly ($p < 0.05$) decreased. The oral administration of CoQ10, NAC or CoQ10 + NAC to the diabetic rats significantly ($p < 0.05$) restored the activities SOD and CAT (Fig. 3b & c). The GSH level was significantly ($p < 0.05$) decreased in STZ-NAD treated rats, as compared to the normal rats. Intragastric administration of CoQ10, NAC or CoQ10 + NAC to the diabetic rats showed significant increase ($p < 0.05$) in the GSH (Fig. 3d).

Values are expressed as mean ± SEM; $n = 6$. One-way ANOVA followed by Tukey's multiple comparison test. [a]$p < 0.05$ as compared to the normal control group, [b]$p < 0.05$ as compared to the diabetic control group, [c]$p < 0.05$ as compared to diabetic CoQ10 alone treated group and [d]$p < 0.05$ as compared to diabetic NAC alone treated group.

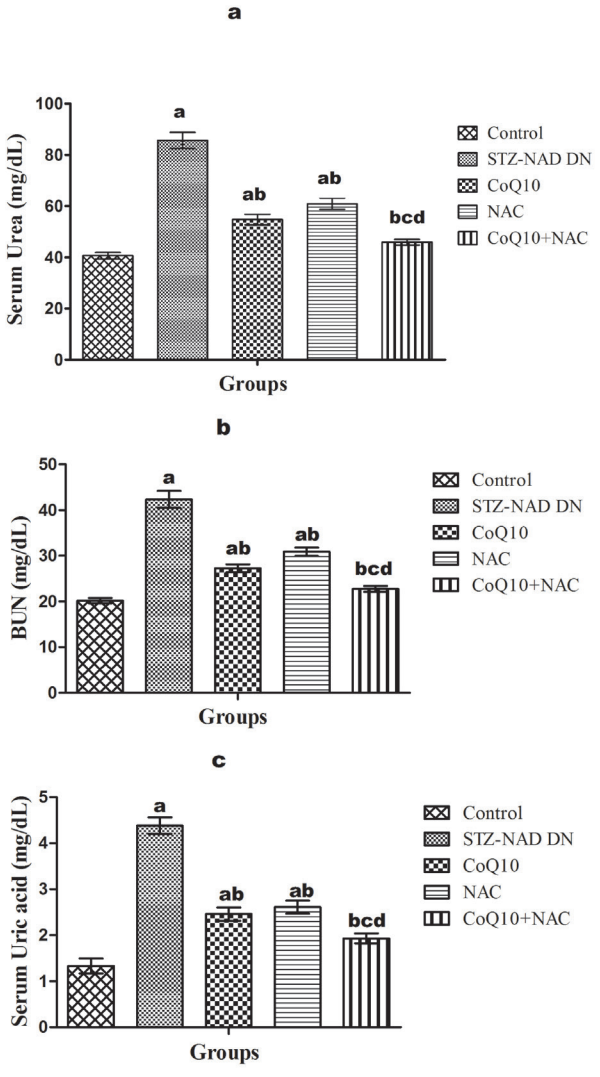

Figure 1. Effect of CoQ10, NAC or their combination on a) serum urea, b) BUN and c) uric acid.

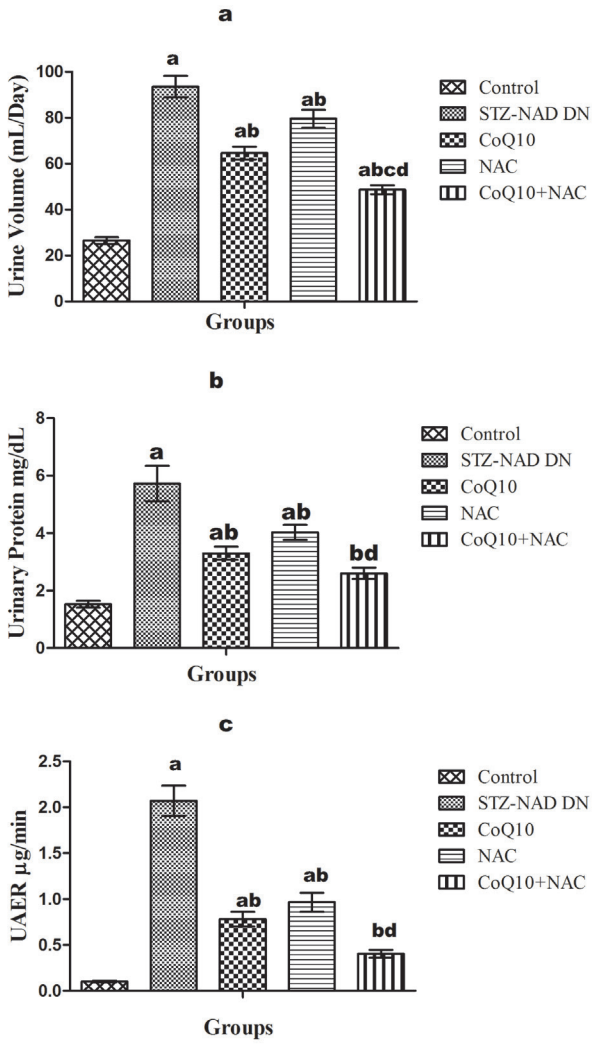

Figure 2. Effect of CoQ10, NAC or their combination on a) urine volume (mL/Day), b) urinary protein (mg/dL) and c) UAER (µg/min).

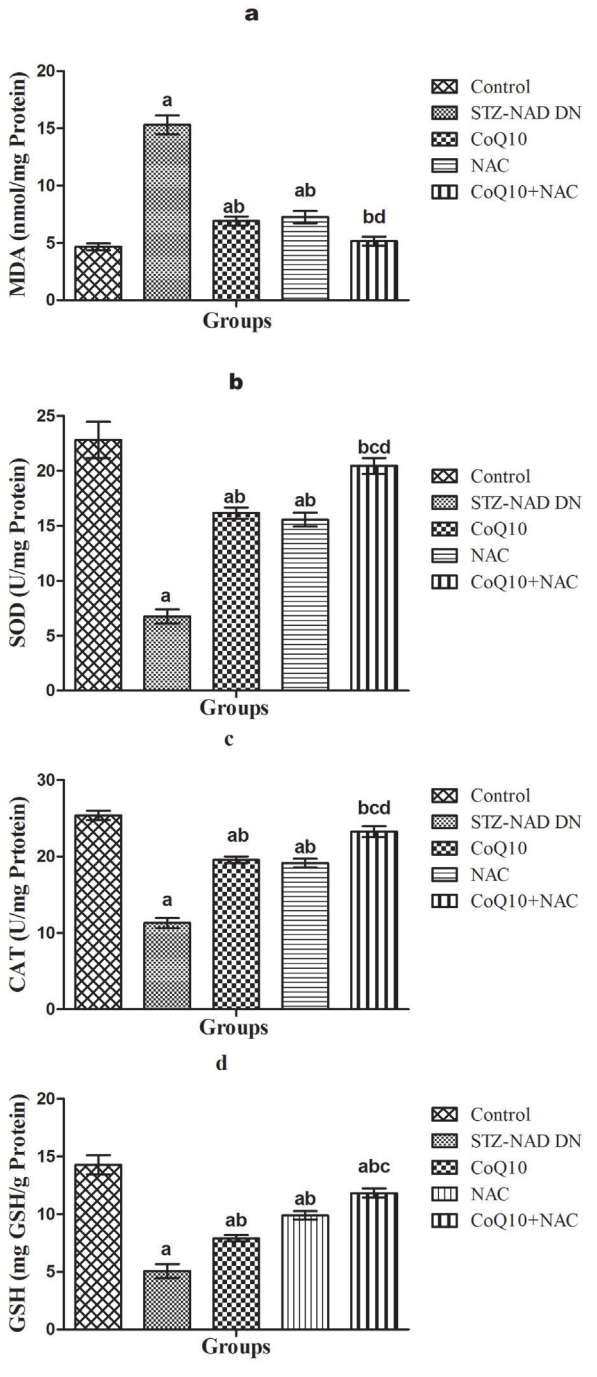

Figure 3. Effect of CoQ10, NAC or their combination on renal OS and anti-oxidant markers a) MDA, b) SOD, c) CAT and d) GSH.

Effect of CoQ10, NAC or their combination on MPO activity and NO content in renal tissue

As given in Table 4, MPO activity and nitrite content were significantly ($p < 0.05$) increased in the kidney of diabetic control rats as compared to the normal rats. CoQ10, NAC or their combination significantly ($p < 0.05$) reversed the MPO activity and nitrite. More significant ($p < 0.05$) decrease in these parameters was noted with the combined treatment of CoQ10 and NAC to the diabetic rats.

DISCUSSION

The aim of the present study was to investigate the effect of CoQ10 and NAC alone and in combination on STZ-NAD induced rat model of DN. In the current investigation, STZ-NAD administration to rats resulted in classical features of DM, like hyperglycaemia, retarded growth, polyuria, proteinuria, structural and functional abnormalities in the kidney along with the increased OS. These observations concerned with DN were consistent with previous findings (Garjani et al., 2011; Maheshwari et al., 2014). STZ-NAD induced renal damage was revealed from increased MDA level, reduced SOD and CAT activities and decreased GSH content in renal tissue. Also, renal MPO activity and nitrite content were

Table 4. Effect of CoQ10, NAC or their combination on MPO activity and NO in renal tissue.

Groups	MPO (U/g Tissue)	NO (µmol/g Tissue)
Control	8.00 ± 0.718	4.38 ± 0.567
STZ-NAD DN	27.28 ± 0.871[a]	12.45 ± 0.776[a]
CoQ10 (10 mg/kg)	16.63 ± 0.639[ab]	6.36 ± 0.355[b]
NAC (300 mg/kg)	17.27 ± 0.556[ab]	7.23 ± 0.480[ab]
CoQ10 + NAC	13.07 ± 0.582[abcd]	4.68 ± 0.425[bd]

Values are expressed as mean ± SEM; n = 6. One-way ANOVA followed by Tukey's multiple comparison test. [a]p < 0.05 as compared to the normal control group, [b]p < 0.05 as compared to the diabetic control group, [c]p < 0.05 as compared to diabetic CoQ10 alone treated group and [d]p < 0.05 as compared to diabetic NAC alone treated group.

increased significantly in the rats with DN. On the other hand, the treatment of rats with DN by the antioxidants CoQ10 or NAC improved the renal parameters with restriction of hyperglycaemia and restoration of anti-oxidant enzymes. Especially when the combined treatment was given, more beneficial outcomes were observed.

DN is rapidly becoming the major cause of the ESRD globally. Chronic hyperglycaemia is known to play a key role in all the diabetic complications including DN. Also, persistent hyperglycaemia is linked to the early and sustained OS generation during DM. OS and uncontrolled hyperglycaemia together play a decisive role in the pathogenesis of tubuloglomerular abnormalities (Mahajan et al., 2019).

Thus, one of the different strategies to alleviate DM or its complications is by using antioxidants. Various endogenous or exogenous antioxidants were found useful in diabetic complication including DN due to their ability to scavenge the free radicals and modulate various signalling pathways to restore the renal function. Antioxidants like vitamin E and C, CoQ10, NAC, α-lipoic acid, taurine and others are found effective against oxidative cell damage (Ahmadi et al., 2013; Jemai et al., 2009). Therefore, antioxidants could be used effectively as a complementary therapy in OS induced complications like DN. Recent animal and human studies have shown the beneficial effects of CoQ10 on elevated HbA_{1C}, urea, and creatinine in DM (Maheshwari et al., 2017; Zhang et al., 2019). Studies with NAC revealed its effectiveness against renal impairment associated with diabetes as indicated by a reduced urinary protein and urinary thiobarbituric acid reactive substances (Shimizu et al., 2005; Lee et al., 2016).

In the current research, a significant decline in body weight % in diabetic rats was noted. This reduction in body weight could be due to the excessive degradation of tissue proteins and increased muscle wasting. It was also evident that insulin deficiency contributes to the decreased protein synthesis and low serum total protein levels in diabetic rats (Rajkumar & Govindarajulu, 1991).

The results of the study showed that in diabetic rats treated with CoQ10, NAC or their combination, body weight % improved significantly probably due to the protective effect of these antioxidants in controlling muscle wasting, enhanced glucose uptake, reduced insulin resistance and inhibition of gluconeogenesis (Rajkumar et al., 1999; Amin et al., 2014; Midaoui et al., 2008).

The kidney to body weight ratio of the diabetic rats increased significantly due to renal hypertrophy, which is the key feature in initial alteration by DM. It was previously shown that over-utilization of glucose, glycogen accumulation, and increased lipogenesis in the renal tissue during DM lead to kidney hypertrophy (Teoh et al., 2010; Mogensen, 1999). Treatment of diabetic rats with CoQ10, NAC or their combination effectively attenuated kidney hypertrophy.

Persistent hyperglycaemia has direct linkages the development of DN. Elevated blood glucose affects the endogenous antioxidant defense system and aggravates the development of DN through intracellular ROS, lipid peroxidation and leakage of urinary protein (Algenstaedt et al., 2003). In the current investigation, persistent hyperglycaemia was developed in diabetic rats until week 12 of the study period. Also, all the diabetic animals showed increased HbA_{1c}. Diabetic animals treated with CoQ10, NAC or their combination for 8 weeks restricted hyperglycaemia and HbA_{1c}.

Studies showed that patients with T2DM often have a deficiency of CoQ10 as marked by considerably lower levels of CoQ10 in plasma in comparison to healthy individuals, which in turn impair body's defense against hyperglycaemia induced OS (Ates et al., 2013; Hasegawa et al., 2005; Sourris et al., 2012; Mezawa et al., 2012). Mezawa et al showed the beneficial effects of CoQ10 in increasing insulin production and/or insulin secretion. Additionally, CoQ10 might attenuate OS in mitochondria and improve the functioning of β-cell along with enhanced insulin sensitivity (Anwar et al., 2014). Consequently, exogenous administration of CoQ10 could potentially attenuate mitochondrial dysfunction induced by OS, thus improving glycaemic control in T2DM (Alam et al., 2014).

Several clinical and experimental studies revealed the beneficial effects of NAC against insulin resistance and associated complications. In most of these studies, NAC reduced hyperglycaemia maybe by improving insulin sensitivity and enhancing peripheral glucose uptake by its antioxidant properties (Ammon et al., 1992; Ho et al., 1999). In this study, oral administration of NAC (300 mg/kg, p.o.) to the diabetic rats restricted hyperglycaemia than the diabetic control group but didn't reduce blood glucose levels in comparison to the observations from similar group at week 0. Thus, the combined treatment employed herein may have a synergistic effect of CoQ10 and NAC in reducing hyperglycaemia and HbA_{1c}.

It was shown that in DM, excessive excretion of total protein and albumin in urine leading to their reduced serum levels

contributed to the pathogenesis of DN (Roy et al., 2010). CoQ10, NAC or their combination treatment restored serum total protein and albumin by preventing their urinary excretion. The combination treatment with CoQ10 and NAC in diabetic rats was found more effective than CoQ10 or NAC alone in restoration of serum total proteins and albumin.

The most common characteristics in the development of DN are the elevated serum creatinine (SCr) and declined creatinine clearance (Ccr) (Dabla, 2010). The present study showed the significant elevation in the SCr, and decline in CCr in diabetic groups than normal rats pointing to the declined renal function and development of DN. However, diabetic rats that received CoQ10 (10 mg/kg), NAC (300 mg/kg) or their combination decreased SCr and improved CCr, particularly in the animals treated with the combination of the antioxidants.

In addition to the chronic hyperglycaemia, polyuria is another feature of DM arising from osmotic diuresis. The significant increment in the urine output (mL/day) noted in this study may be due to glucosuria associated osmotic diuresis. In this study, severe renal impairment in the diabetic rats was identified by substantial rise in the urinary total proteins and UAER. Decreased serum albumin and increased UAER in diabetic complications were linked to the rapid progression of renal disease.

Earlier reports demonstrated that DM induced renal dysfunction is associated with a gradual reduction in serum albumin level. Albuminuria, resulting from damage to the glycosaminoglycans in the basement membrane and increased pore size may be linked to the decreased serum albumin (Mora-Fernández et al., 2014; Haraldsson & Sörensson, 2004). Consequently, the reduction of proteinuria could be beneficial for improving renal function and to prevent the progression of DN towards ESRD (Oktem et al., 2006). Combined oral administration of CoQ10 and NAC to the diabetic rats was found effective in reversing the urinary protein loss declining UAER.

OS is the key element in the development and progression of DN and associated renal injury. Diabetic state is believed to induce OS by an imbalance between the normal antioxidant defense and elevated ROS production. It has been shown that antioxidant treatment in DN improves renal function by directly acting against oxidative tissue damage (Mahajan et al., 2019). Moreover, exogenous administration of antioxidants restricts the progression of DN by effective inhibition of ROS and scavenging the preformed intracellular ROS (Agrawal & Sadhukhan, 2015).

We noted impaired oxidative stability in diabetic rats as indicated by the elevated MDA level and reduced activity of antioxidant enzymes SOD and CAT. It is believed that during DM hyperglycaemia-induced OS increases lipid peroxidation (Idris et al., 2001). MDA, the product of lipid peroxidation is responsible for the cellular injury. As an aldehyde, MDA links sugar and protein to form glycated proteins. Such structural and functional abnormalities in proteins might be responsible for diabetic complications. Thus, increased levels of HbA_{1c} may have some linkages with increased lipid peroxidation (Krhač & Lovrenčić, 2019). There was a considerable decrease in lipid peroxidation and an elevation in SOD, CAT activity, along with increased GSH content in the renal tissue of rats treated orally with a combination of CoQ10 and NAC.

Studies correlated MPO and DM with a positive relationship between the raised MPO activity and the pathogenesis of DN (Rovira-Llopis et al., 2013). The MPO-hydrogen, a peroxide-chloride system, leads to a variety of chlorinated protein and lipid adducts that may cause dysfunction in the different compartments of the kidney (Prabhakar, 2004). In the present study, oral combination therapy of diabetic rats with CoQ10 and NAC significantly reduced renal MPO activity in the renal tissue than the CoQ10 and NAC alone treated rats.

NO is implicated in pathogenesis of DN since it modulates renal structure and function. In diabetes, abnormal NO production is linked to the progression of the kidney damage. Studies showed that most of the cytotoxicity attributed to NO is due to peroxynitrite, produced from the reaction between NO and the superoxide anion (Stamler et al., 1992; Kisic et al., 2016). In the present study, there was a significant elevation in nitrite content in the renal tissue of diabetic rats as compared to the normal rats. However, the diabetic rats treated with a combination of CoQ10 and NAC effectively reduced renal nitrite levels.

In conclusion, the results presented in this study provide valuable information supporting that treatment with antioxidants might prevent or delay the renal damage associated with DN. Oral administration of antioxidants, that is, CoQ10 and NAC possesses a significant nephroprotective effect against STZ-NAD induced DN. A combination therapy with CoQ10 and NAC is more promising as it improves renal function and reduces OS in the rats subjected to DN. Nephroprotective effect shown by the combination treatment in this study may be attributed to hypoglycaemic and antioxidant properties of these compounds that attenuated OS and enhanced renal function in diabetic rats. Finally, it was concluded that the combined administration of CoQ10 with NAC might attenuate or delay the progression of DN.

ABBREVIATIONS

AGEs: Advanced glycation end products
ANOVA: Analysis of variance
ATP: Adenosine triphosphate
BUN: Blood urea nitrogen
CAT: Catalase
CoQ10: Coenzyme Q10
DM: Diabetes mellitus
DN: Diabetic nephropathy
GLUT2: Glucose transporter 2
GSH: Reduced glutathione
h: Hour

HbA_{1c}: Glycated haemoglobin
i.p.: Intraperitoneal
MDA: Malondialdehyde
MPO: Myeloperoxidase
NAC: N-acetylcysteine
NAD: Nicotinamide
NIDDM: Non-insulin-dependent diabetes mellitus
NO: Nitric oxide
OS: Oxidative stress
p.o.: Per oral
PKC: Protein kinase C
ROS: Reactive oxygen species
SEM: Standard error of the mean
SOD: Superoxide dismutase
STZ: streptozotocin
T2DM: Type-2 diabetes mellitus

References

[1] Agarwal N, Sadhukhan P. Therapeutic Insights against Oxidative Stress Induced Diabetic Nephropathy: A Review. J Autoimmune Disord. 2015; 1: 1–17.

[2] Ahmad A, Mondello S, Di Paola R et al. Protective effect of apocynin, a NADPH-oxidase inhibitor, against contrast-induced nephropathy in the diabetic rats: A comparison with n-acetylcysteine. Eur J Pharmacol. 2012; 674: 397–406.

[3] Ahmadi A, Mazooji N, Roozbeh J, Mazloom Z, Hasanzade J. Effect of alpha-lipoic acid and vitamin E supplementation on oxidative stress, inflammation, and malnutrition in hemodialysis patients. Iran J Kidney Dis. 2013; 7: 461–467.

[4] Ahmadvand H. Effects of coenzyme Q10 on hemoglobin A1C, serum urea and creatinine in alloxan-induced Type 1 diabetic rats. Iran J Pharmacol Ther. 2012; 11: 64–67.

[5] Alam M, Rahman M. Mitochondrial dysfunction in obesity: Potential benefit and mechanism of co-enzyme Q10 supplementation in metabolic syndrome. J Diabetes Metab Disord. 2014; 13: 1–11.

[6] Algenstaedt P, Schaefer C, Biermann T, et al. Microvascular Alterations in Diabetic Mice Correlate with Level of Hyperglycemia. Diabetes. 2003; 52: 542–549.

[7] Amin M, Asaad G, Abdel Salam R, El-Abhar H, Arbid M. Novel CoQ10 Antidiabetic Mechanisms Underlie Its Positive Effect: Modulation of Insulin and Adiponectine Receptors, Tyrosine Kinase, PI3K, Glucose Transporters, sRAGE and Visfatin in Insulin Resistant/Diabetic Rats. PLoS One. 2014; 9: e89169.

[8] Ammon HP, Muller PH, Eggstein M, Wintermantel C, Aigner B, Safayhi H, et al. Increase in glucose consumption by acetylcysteine during hyperglycemic clamp. A study with healthy volunteers. Arzneimittelforsch. 1992; 42: 642–645.

[9] Anwar M, Abd El-Moniem M, Megahed H, EL-Toukhy S, Mohammed N, Youness E. Effect of Coenzyme Q10 Supplementation on Markers of Oxidative Stress in Streptozotocin Induced Diabetic Rats. *Journal of Applied Pharmaceutical Science*. 2014; 4: 9–15.

[10] Ates O, Bilen H, Keles S, Alp H, Keles M, et al. Plasma coenzyme Q10 levels in type 2 diabetic patients with retinopathy. Int J Ophthalmol. 2013; 6: 675–679.

[11] Badole SL, Bagul PP, Mahamuni SP et al. Oral L-glutamine increases active GLP-1 (7-36) amide secretion and improves glycemic control in streptozotocin-nicotinamide induced diabetic rats. ChemBiol Interact. 2013; 203: 530–541.

[12] Brownlee M. Biochemistry and molecular cell biology of diabetic complications. Nature. 2001; 414: 813–20.

[13] Dabla PK. Renal function in diabetic nephropathy. World J Diabetes. 2010; 1: 48–56.

[14] Garjani A, Andalib S, Biabani S, Soraya H, Doustar Y, et al. Combined atorvastatin and coenzyme Q10 improve the left ventricular function in isoproterenol-induced heart failure in rat. Eur J Pharmacol. 2011; 666: 135–141.

[15] Geraldes P, Hiraoka-Yamamoto J, Matsumoto M, Clermont A, Leitges M, et al. Activation of PKC-delta and SHP-1 by hyperglycemia causes vascular cell apoptosis and diabetic retinopathy. Nat Med. 2009; 15: 1298–1306.

[16] Ghasemi A, Khalifi S, Jedi S. Streptozotocin-nicotinamide induced rat model of type 2 diabetes. Acta Physiol Hung. 2014; 101: 408–420.

[17] Haber CA, Lam TK, Yu Z et al. N-acetylcysteine and taurine prevent hyperglycemia-induced insulin resistance in vivo: possible role of oxidative stress. Am J Physiol Endocrinol Metab. 2003; 285: E744–E753.

[18] Haraldsson B, Sörensson J. Why do we not all have proteinuria? An update of our current understanding of the glomerular barrier. News Physiol Sci. 2004; 19: 7–10.

[19] Hasegawa G, Yamamoto Y, Zhi J, Tanino Y, Yamasaki M, et al. Daily profile of plasma %CoQ10 level, a biomarker of oxidative stress, in patients with diabetes manifesting postprandial hyperglycaemia. Acta Diabetol. 2005; 42: 179–181.

[20] Ho E, Chen G, Bray TM. Supplementation of N-acetylcysteine inhibits NF-kappaB activation and protects against alloxan-induced diabetes in CD-1 mice. FASEB J. 1999; 13: 1845–1854.

[21] Hodgson JM, Watts GF, Playford DA, Burke V, Croft KD. Coenzyme Q10 improves blood pressure and glycaemic control: A controlled trial in subjects with type 2 diabetes. Eur J Clin Nutr. 2002; 56: 1137–1142.

[22] Idris I, Gray S, Donnelly R. Protein kinase C activation: isozyme-specific effects on metabolism and cardiovascular complications in diabetes. Diabetologia. 2001; 44: 659–673.

[23] Jemai H, El Feki A, Sayadi S. Antidiabetic and antioxidant effects of hydroxytyrosol and oleuropein from olive leaves in alloxan-diabetic rats. J Agric Food Chem. 2009; 57: 8798–8804.

[24] Kisic B, Miric D, Dragojevic I, Rasic J, Popovic L. Role of Myeloperoxidase in Patients with Chronic Kidney Disease. Oxid Med Cell Longev. 2016; 1–10.

[25] Kohei KA. Pathophysiology of type 2 diabetes and its treatment policy. JMAJ. 2010; 53: 41-46.

[26] Krhač M, Lovrenčić MV. Update on biomarkers of glycemic control. World J Diabetes. 2019; 10: 1–15.

[27] Lee ES, Kim HM, Kang JS, Lee EY, et al. Oleanolic acid and N-acetylcysteine ameliorate diabetic nephropathy through reduction of oxidative stress and endoplasmic reticulum stress in a type 2 diabetic rat model. Nephrol Dial Transplant. 2016; 3: 391–400.

[28] Mahajan MS, Gulecha VS, Upaganlawar AB, Upasani CD. Antioxidant Defense in Diabetic Nephropathy In: Uddin S & Upaganlawar AB: Oxidative Stress and Antioxidant Defense: Biomedical value in Health and Diseases, 1st ed. New York: Nova; 2019.

[29] Maheshwari R, Balaraman R, Sen AK, Shukla D, Seth A. Effect of concomitant administration of coenzyme Q10 with sitagliptin on experimentally induced diabetic nephropathy in rats. Renal Failure. 2017; 39: 130–139.

[30] Maheshwari RA, Balaraman R, Sen AK, Seth AK. Effect of coenzyme Q10 alone and its combination with metformin on streptozotocin-nicotinamide-induced diabetic nephropathy in rats. Indian J Pharmacol. 2014; 46: 627–32.

[31] Maitra A. The Endocrine System. in: Kumar V, Abbas A, Fausto N, Aster J. Robbins and Cotran Pathologic Basis of Disease. 9th ed. Philadelphia: Elsevier Saunders; 2015.

[32] Masharani, U. Diabetes Mellitus and hypoglycemia. In: McPhee SJ, Papadakis MA, Tierney LM. Current medical diagnosis and treatment, 47th ed. New York: McGraw-Hill; 2008.

[33] Mezawa M, Takemoto M, Onishi S, Ishibashi R, Ishikawa T, Yamaga, M, et al. The reduced form of coenzyme Q10 improves glycemic control in patients with type 2 diabetes: an open label pilot study. Biofactors. 2012; 38: 416–421.

[34] Midaoui A, Ismael M, Lu H, Fantus I, de Champlain J, Couture R. Comparative effects of N-acetyl-L-cysteineand ramipril on arterial hypertension, insulin resistance, andoxidative stress in chronically glucose-fed rats. Can J Physiol Pharmacol. 2008; 86: 752–60

[35] Mogensen CE. Microalbuminuria, blood pressure and diabetic renal disease. Origin and development of ideas. Diabetologia. 1999; 42: 263–285.

[36] Mogensen CE, Christensen CK, Vittinghus E. The stages in diabetic renal disease. With emphasis on the stage of incipient diabetic nephropathy. Diabetes. 1983; 32: 64–78.

[37] Mora-Fernández C, Domínguez-Pimentel V, de Fuentes MM, et al. Diabetic kidney disease: from physiology to therapeutics. J Physiol. 2014; 592: 3997–4012.

[38] Odetti P, Pesce C, Traverso N, Menini S, Maineri EP, et al. Comparative trial of N-acetyl-cysteine, taurine, and oxerutin on skin and kidney damage in long-term experimental diabetes. Diabetes. 2003; 52: 499–505.

[39] Oktem F, Ozguner F, Yilmaz HR, et al. Melatonin reduces urinary excretion of N-acetyl-beta–D-glucosaminidase, albumin and renal oxidative markers in diabetic rats. Clin Exp Pharmacol Physiol. 2006; 33: 95–101.

[40] Pal PB, Sinha K, Sil PC. Mangiferin attenuates diabetic nephropathy by inhibiting oxidative stress mediated signaling cascade, TNFα related and mitochondrial dependent apoptotic pathways in streptozotocin-induced diabetic rats. PLoS One. 2014; 9: e107220.

[41] Prabhakar SS. Role of nitric oxide in diabetic nephropathy. Semin Nephrol. 2004; 24: 333–344.

[42] Rajkumar L, Govindarajulu P. Increased degradation of dermal collagen in diabetic rats. Indian J Exp Bio. 1991; 29: 1081–1083.

[43] Rajkumar V, Ragatzki P, Sima A, Levy J. Enhanced platelet aggregation, high homocysteine level, and microvascular disease in diabetic muscle infaractions. Endocrine. 1999; 11: 57–60.

[44] Rosenfeldt FL, Haas SJ, Krum H. Coenzyme Q10 in the treatment of hypertension: a meta-analysis of the clinical trials. J Hum Hypertens. 2007; 21: 297–306.

[45] Rovira-Llopis S, Rocha M, Victor M et al. Is myeloperoxidase a key component in the ROS-induced vascular damage related to nephropathy in type 2 diabetes?" ARS. 2013; 19: 1452–1458.

[46] Roy S, Trudeau K, Roy S, Behl Y, Dhar S, Chronopoulos A. New insights into hyperglycemia-induced molecular changes in microvascular cells. J Dent Res. 2010; 89: 116–128.

[47] Schena FP and Gesualdo L. Pathogenetic mechanisms of diabetic nephropathy. J. Am. Soc. Nephrol. 2010; 16: 30–33.

[48] Shimizu MH, Coimbra TM, de Araujo M et al. N-acetylcysteine attenuates the progression of chronic renal failure.Kidney Int. 2005; 68: 2208–2217.

[49] Sourris K, Harcourt B, Tang P, Morley A, Huynh K, et al. Ubiquinone (coenzyme Q10) prevents renal mitochondrial dysfunction in an experimental model of type 2 diabetes. Free Radic Biol Med. 2012; 52: 716–723.

[50] Stamler JS, Singel DJ, Loscalzo J. Biochemistry of nitric oxide and its redox-activated forms. Science. 1992; 258: 1898–902.

[51] Teoh SL, Abdulatiff A, Das S. Histological changes in the kidneys of experimental diabetic rats fed with Momordicalcharantia (bitter gourd) extract. Rom J MorpholEmbryol. 2010; 51: 91–5.

[52] Vasavada N and Agarwal R. Role of Oxidative Stress in Diabetic Nephropathy. Adv Chronic Kidney Dis. 2005; 12: 146–154.

[53] Vora JP and Ibrahim HAA. Clinical manifestations and natural history of diabetic nephropathy. In: Johnson R and Feehally J: Comprehensive clinical nephrology, 2nd ed. Edinburgh: Mosby; 2003.

[54] Zhang X, Shi Z, Liu Q, Quan H, Cheng X. Effects of coenzyme Q10 intervention on diabetic kidney disease. Medicine. 2019; 98: 1–18.

sciendo

Eur. Pharm. J. 2021, 68(1), 40-45.
ISSN 1338-6786 (online) and ISSN 2453-6725 (print version),
DOI: 10.2478/afpuc-2020-0023

EUROPEAN PHARMACEUTICAL JOURNAL

Evaluation of variability of silymarin complex in Silybi mariani fructus harvested during two production years

Original Paper

Habán M.[1,2]✉, Zvercová D.[2], Adamjaková M.[1]

[1]Comenius University in Bratislava, Faculty of Pharmacy, Department of Pharmacognosy and Botany
[2]Slovak University of Agriculture in Nitra, Faculty of Agrobiology and Food Resources, Department of Sustainable Agriculture and Herbology

Received 24 January, 2021, accepted 28 April, 2021

Abstract Milk thistle [*Silybum marianum* (L.) Gaertn.], a member of *Asteraceae* family, is one of the most cultivated medicinal plants widespread throughout the world. The pharmacological drug is a ripe fruit without pappus – Silybi mariani fructus – containing flavonolignans and generating silymarin complex. In folk medicine, it is used for the treatment of liver disorders, kidney problems, rheumatism as well as gastronomic disturbances, cardiac and neurotic disorders, and fever. The components of silymarin complex are useful in cancer prevention and treatment. The aim of the study was to determine the amount of silymarin complex contained in the fruit of the harvest of two consecutive years and how much they differ from one another. Representative samples of fruit were collected in 2015 and 2016 and distributed by a company Agrofos (Slovakia). Regarding the analytical method, we used a high-performance liquid chromatography (HPLC); the method was approved by the European Pharmacopoeia 10. The statistical significance was on the level $P < 0.05$. The total content of silymarin complex was 15.28 ± 0.06 g.kg^{-1} (in 2015) and 16.65 ± 0.09 g.kg^{-1} (in 2016). In both studied years, the highest representation of silybin B was observed (7.04 ± 0.07 g.kg^{-1} versus 5.92 ± 0.08 g.kg^{-1}). The differences between the individual fractions of the silymarin complex were statistically significant. There was also a significant difference of 9% in the total silymarin content between 2015 and 2016. In conclusion, we can state that both samples of Silybi mariani fructus meet the requirements of the European Pharmacopoeia.

Keywords *Silybum marianum – silymarin complex – HPLC*

INTRODUCTION

Milk thistle [*Silybum marianum* (L.) Gaertn.] belongs to the *Asteraceae* family. This plant, originated in the Mediterranean region, is widespread throughout the world and has been grown throughout Europe, Africa, China, India and Australia for centuries (Polyak et al., 2013). Ražná et al. (2015) stated that it is one of the most cultivated medicinal plants on the Slovak market. It was cultivated on more than 1000 hectares in 2014 and 2015. The pharmacological drug forms ripe fruit without pappus, known as Silybi mariani fructus (Nagy et al., 2015). The fruits are achenes, dark brown to black colour, mostly flattened and oval. The length of the fruit ranges from 5 to 7 mm, width from 2 to 3 mm and thickness is about 1.5 mm (Abenavoli et al., 2010). During the harvest, the entire flower heads are cut, even with inflorescence, just before the fruit ripens. Obtained fruits are rich in flavonoids, which are concentrated in the pericarp and seed (Andrzejewska et al., 2011; Giuliani et al., 2018). These biologically active phytochemicals, flavonolignans (silybin A and silybin B, isosilybin A and isosilybin B, silydianin, silychristin, isosilychristin and others) and flavonoid taxifolin are collectively known as silymarin (Pendry et al., 2017). The silymarin complex forms 60%–80% of the extract of Silybi mariani fructus. The silymarin content most often ranges from 1% to 3% of dry matter, but can exceed 8% (Karkanis et al., 2011; Lucini et al., 2015). When isolated from fruit, a multi-stage purification takes place, including extraction with ethyl acetate. This is an achieved enrichment of pharmacologically active flavonoids, while neutral or undesirable components are removed (Jedlinszki et al., 2016). Silymarin and its flavonolignans are commercially available in various formulations containing fruit extracts such as liquid

* E-mail: haban@fpharm.uniba.sk, miroslav.haban@uniag.sk
ORCID: 0000-0002-8013-0088.

extracts, capsules and tablets as well as in combination with synthetic chemical drugs or other herbal materials (Elateeq et al., 2020). Silybi mariani fructus are used as a medicine for hemorrhoids and heart disorders (Ghorbani, 2005), while roots and stems are used as a medicine for blood pressure and fever (Mirdeilami et al., 2011). The plant has a long history as a medicinal plant in folk medicine used for the treatment of liver disorders, kidney problems, rheumatism, gastronomic disturbances, cardiac disorders and fever (Marmouzi et al., 2021). Qin et al. (2017) found out that the silymarin also shows antioxidant and anti-diabetic activities. It was shown to be a putative neuroprotective agent against many neurological diseases including Alzheimer's and Parkinson's diseases and cerebral ischaemia (Borah et al., 2013). In addition, silymarin possesses antioxidant, anti-inflammatory and anti-fibrotic properties. It stimulates the biosynthesis of proteins, increases lactation and possesses immune-modulation activity (Abenavoli et al., 2010). Silymarin also shows in vitro efficacy as a cancer chemopreventive agent by arresting human prostate carcinoma proliferation in cancer cell cultures (Tyagi et al., 2002) and in human cancer models (Singh et al., 2002). Silybin, one of the constituents of silymarin, was included in the list of molecules useful in a broad-spectrum integrative approach for cancer prevention and treatment (Block et al., 2015). The anticancer efficacy of silybin is exerted through its ability to affect cancer cell proliferation and metabolism, inflammation and angiogenesis (Deep & Agarwal, 2010). Silibinin clearly demonstrates the inhibition of multiple cancer cell signalling pathways, including a growth inhibition, inhibition of angiogenesis, chemosensitization and the inhibition of invasion and metastasis. The cumulative evidence implicates that silibinin is a potential agent for a cancer chemoprevention and chemotherapy (Li et al., 2010). Several studies have reported a beneficial effect of silymarin in different experimental models of acute and chronic inflammation, for example, in rats with formalin-induced paw oedema (Alhadidi et al., 2009). The findings by Li et al. (2016) demonstrate that silymarin is able to attenuate the airway inflammation induced by a cigarette smoke extract in human bronchial epithelial cells. Ripe seeds contain a large amount of oil (approximately 200–300 $g.kg^{-1}$). Although it contains a relatively high amount of fatty acids (linoleic, linolenic, oleic and arachidic acid), it is a by-product of the industrial production of silymarin and must be removed from seeds before the extraction. Relatively large amounts of strongly lipophilic organic solvents, most often hexane or petroleum ether, are used for degreasing. The oil from milk thistle is used in foods and pharmaceutical industries, but due to ineffective reasons of exploitation and lack of cost-effective technologies, it is relatively rare on the market (Abouzid et al., 2016; Mei et al., 2013). The total yield of milk thistle and silymarin varies depending on environmental conditions, genotypes, sowing and harvest dates as well as gaps between rows and different farming practices (Karkanis et al., 2011).

METHODS

For this experiment, we used representative samples of fruit collected in 2015 and 2016 and distributed by the company Agrofos (Slovakia). The samples were analysed according to the guidelines of the European Pharmacopoeia (Ph. Eur. 10), which were partially modified by the methodological procedure. High-performance liquid chromatography method (HPLC) was applied to evaluate the silymarin complex of Silybi mariani fructus, using Agilent 1200 Infinity system. The research was carried out at the Department of Sustainable Agriculture and Herbology of Slovak University of Agriculture in Nitra.

The samples were ground in a grinder and 5 g was placed in the apparatus for continual extraction. We added 100 ml of petroleum ether and let it heat in a water bath for 8 hours. We added 100 ml of methanol to the sample and placed it in the apparatus where it was extracted in a water bath for another 5 hours. After the evaporation of the methanol extract, the sample was concentrated to a volume of about 30 ml. The extraction flask and filter were washed with methanol, and the extract was filled in up to 50 ml. Consequently, we prepared the reference solution by dissolving the dried thistle extract and by diluting the sample to 100 ml with the same solvent.

The following were the HPLC conditions: column with length l = 0.125 m and with diameter = 4 mm; stationary phase – 5 µm silica gel end-capping octadecylsilyl; mobile phase – a mixture of phosphoric acid, methanol and water (0.5:35:65), and a mixture of phosphoric acid, methanol and water (0.5:50:50) with the flow 0.8 $ml.min^{-1}$. The detection was carried out by spectrophotometer at 288 nm and injection volume 10 µl.

Concerning the identification of silymarin complex fractions, we used the record from the chromatogram of the dried milk thistle's extract and from the chromatogram of the reference solution to correctly identify the area and height of the peaks for silychristin, silydianin, silybin A, silybin B and isosilybin A + B (Fig. 1). The peak areas of the respective diastereomers were calculated by the percentage of the total peak area of a known concentration of the isomeric flavonolignan mixture. To obtain the results, we calculated the specific weights of flavonolignans presenting the proportional relations between the individual peak areas and their corresponding applied quantity.

The statistical evaluation of data was carried out by using the program STATISTICA CZ version 10 and ANOVA main effects by means of Fisher's LSD test at the statistical significance level $\alpha = 0.05$.

RESULTS

Concerning the experimental part of presented study, two parallel analyses and measurements were performed in four repetitions. There were 6 major flavonolignans (silychristin,

silydianin, silybin A, silybin B, isosilybin A and isosilybin B) in the silymarin complex of the analysed samples. Individual components of the silymarin complex were identified by the size of the peaks detected by HPLC analysis (Fig. 2) and converted to g.kg^{-1}. The results are reported as mean ± standard deviation (SD) and median. In each observed year, the differences between the representations of individual components of the silymarin complex were statistically significant ($P < 0.05$). In a sample of Silybi mariani fructus collected in 2015 (Table 1), the value of silybin B was twice as high as the value of silybin A. The common value of isosilybin A and isosilybin B was the second most abundant silymarin fraction. This was followed by silydianin with the smallest average value in the set of silymarin components; the lowest measured value of this component being 0.88 g.kg^{-1} and the highest 0.96 g.kg^{-1}. Analogous results were achieved in 2016 (Table 2), when the highest proportion of silybin B component was achieved. Compared to the previous year, it was lower by 1.12 g.kg^{-1}. The amount of silychristin in 2016 ranged from 4.40 g.kg^{-1} to 3.79 g.kg^{-1}. The average value of silybin A was lower by 0.10 g.kg^{-1} compared to 2015, while the common value of isosilybin A + B fractions increased by 0.89 g.kg^{-1}. This year was also recorded the lowest value of the silydianin component. Its amount ranged from 1.56 g.kg^{-1} to 1.94 g.kg^{-1}. Between 2015 and 2016, the period monitored in terms of qualitative production of Silybi mariani fructus for the determination of silymarin, there was a significant difference ($P < 0.05$) in observed values. The results showed that after counting all silymarin components, the silymarin complex was 1.37 g.kg^{-1} higher in 2016 than in 2015. This represents a difference of 9%. After evaluating the ratio of individual fractions, we can state that we did not work with samples of fruit of different chemotypes.

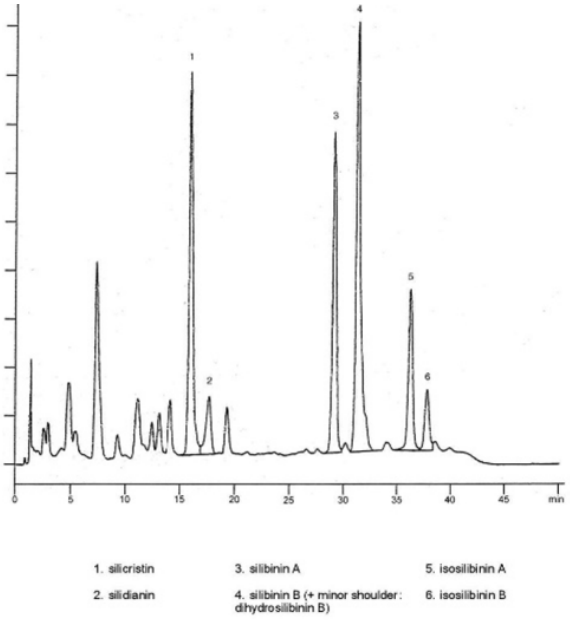

Figure 1. Chromatogram of Silybi mariani fructus according to the European Pharmacopoeia 10.

DISCUSION

In a scientific study carried out by Wianovska and Wiśniewski (2015), a pressurized liquid extraction to prepare samples was used. This isolated the silymarin mixture in a one-step extraction process and, therefore, reduced the extraction time and volumes of solvents used. Using this method, the total content of the silymarin complex was 22.7 g.kg^{-1} (2.27%). Compared to values in presented study, there was a difference of 0.74% concerning fruit collected in 2015 and the difference of 0.6% regarding the fruit collected

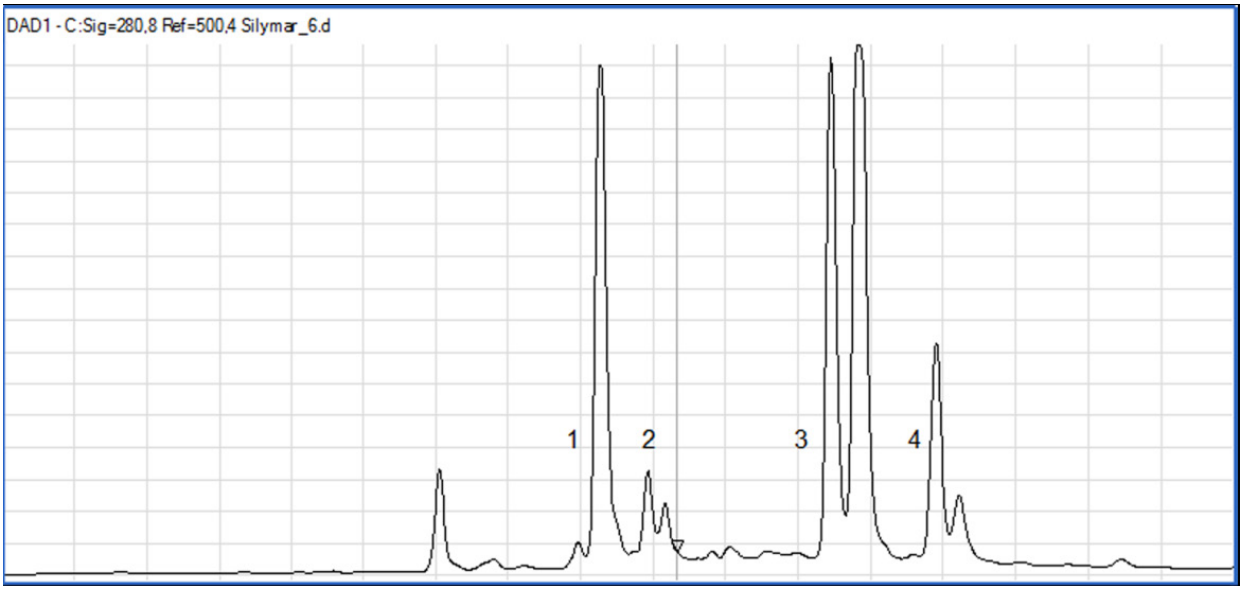

Figre 2. Chromatogram of Silybi mariani fructus (2015). 1 - silychristin, 2 - silydianin, 3 - silybin A, B, 4 - isosilybin A, B.

Table 1. Fractions of silymarin complex (g.kg^{-1}) in Silybi mariani fructus, 2015 (n = 4).

Silymarin components	Mean ± SD	Median
Silychristin	3.18 ± 0.06^{a}	3.18
Silydianin	0.91 ± 0.01^{b}	0.90
Silybin A	3.06 ± 0.06^{c}	3.07
Silybin B	7.04 ± 0.07^{d}	7.07
Isosilybin A + B	1.09 ± 0.05^{e}	1.10
Summary	15.28 ± 0.06^{A}	15.27

Different indices after the numerical values indicate significant differences at the level of P < 0.05. The indices $^{a, b, c, d, e}$ represent a statistically significant difference between the individual components of the silymarin complex and ^{A} indicates a significant difference in content of silymarin compared to the content in 2016.

Table 2. Fractions of silymarin complex (g.kg^{-1}) in Silybi mariani fructus, 2016 (n = 4).

Silymarin components	Mean ± SD	Median
Silychristin	4.03 ± 0.24^{a}	3.97
Silydianin	1.76 ± 0.14^{b}	1.78
Silybin A	2.96 ± 0.15^{a}	2.99
Silybin B	5.92 ± 0.08^{c}	5.92
Isosilybin A + B	1.98 ± 0.05^{d}	2.00
Summary	16.65 ± 0.09^{B}	16.66

Different indices after the numerical values indicate significant differences at the level of P < 0.05. The indices $^{a, b, c, d}$ represent a statistically significant difference between the individual components of the silymarin complex, and ^{B} indicates a significant difference in content of silymarin compared to the content in 2015.

in 2016. However, the whole process of analysis is time-consuming. Nevertheless, calibration models are currently being developed for highly efficient and fast determination methods to substitute the HPLC method (Ashie et al., 2021). A promising alternative is a near-infrared (NIR) spectroscopy, a fast and non-destructive method for the analysis of samples without the need of sample pretreatment (Vagnerova et al., 2016). This NIR technique gives information about structural and physical qualities of materials based on the radiation transmittance or reflectance at wavelengths in various ranges (Rodriguez-Saona et al., 2000). The proposed method offers a promising approach to the determination of the quality and quantity of active ingredients for its rapid and non-polluting properties and low costs (Ashie et al., 2021). Using NIR technique, Vagnerova et al. (2016) found out that the varieties of milk thistle (Silyb and Mirel) have different ratio of the main silymarin complex components. They also proved that the calibration model of studied varieties can be used to identify an unknown sample. This model is able to classify these varieties. Drouet et al. (2019) used ultrasound extraction to determine the content of the silymarin complex, which was at least 1.80 g.kg^{-1}, and a liquid extraction to quantify the flavonolignans. They observed that silybin B presented the highest representation (7.52–1.29 g.kg^{-1}), followed by silydianin (4.21–0.40 g.kg^{-1}), isosilybin A (2.49–0.45 g.kg^{-1}), silychristin (1.52–0.01 g.kg^{-1}) and silybin A (1.09–0.01 g.kg^{-1}). In another study, Ghafor et al. (2014) analysed the amount of flavonolignans and determined that the highest content within the silymarin complex was reached by silybin A. In all our measurements, we recorded the predominance of silybin B. Wallace et al. (2005) compared the yield of silymarin in the extraction with ethanol boiling at 78.3 °C and ethanol heated to 60 °C. They found out that the average value of silymarin in the fruit in the extraction with boiling ethanol was 5.0 mg.g^{-1} = 5.0 g.kg^{-1}, while a 60 °C ethanol caused an increase in yield by 1.7 times. From this study, we can conclude that the preparation of mash or decoction of Silybi mariani fructus can degrade the whole silymarin complex and, at the same time, reduce the effects of the ingredients. The most studied substance from silymarin complex is silybin, which exists in the form of two stereoisomeric compounds: silybin A and silybin B. Poppe and Petersen (2016) presented in their study that the content of these components represents 10%–20% of the silymarin content, while isosilybin B represents only about 5% of its content. According to another study, using the same assay procedure as we used in our study, the silybin A content ranged from 0.44 g.kg^{-1} to 11.77 g.kg^{-1}, while the silychristin content varied from 2.05 g.kg^{-1} to 15.11 g.kg^{-1}. The average content of isosilybin A was 4.70 g.kg^{-1} and 3.67 g.kg^{-1} (Arampatzis et al., 2018). Khan et al. (2015) reported that the concentrations of various silymarin components strongly depend on growth conditions, and stress conditions have a strong impact on its biosynthesis. According to the European Pharmacopoeia, which sets the minimum content of silymarin in the dried drug to 1.5%, we can state that both samples meet the requirements of Pharmacopoeia (1.5% in 2015 and 1.7% in 2016).

ACKNOWLEDGEMENTS

We would like to thank Ing. Ľubomír Kobida for the consultation and chemical analysis. This study was elaborated thanks to the support of the Operational Programme of Integrated Infrastructure for the Project: Long-term Strategic Research of Prevention, Intervention and Mechanisms of Obesity and Its Comorbidities, IMTS: 313011V344, co-financed by the European Regional Development Fund, and project VEGA 1/0749/21.

References

[1] Abenavoli L, Capasso R, Milic N, Capasso F. Milk thistle in liver diseases: past, present, future. Phytotherapy Research 2010;24:1423-1432.

[2] Abouzid SF, Chen SN, Mcalpine JB, Friesen JB, Pauli GF. Silybum marianum pericarp yields enhanced silymarin products. J. Fitote. 2016;56:136-143.

[3] Alhadidi Q, Ahmed ZA, Numan IT, Hussain SAR. Dose-dependent anti-inflammatory effect of silymarin in experimental animal model of chronic inflammation. Afr. J. Pharm. Pharmacol. 2009;3:242-247.

[4] Andrzejewska J, Sadowska K, Mielcarek S. Effect of sowing date and rate on the yield and flavonolignan content of the fruits of milk thistle (Silybum marianum L. Gaertn.) grown on light soil in a moderate climate. J. Ind. Crop. 2011;33:462-468.

[5] Arampatzis AD, Karkanis CA, Tsiropoulos GN. Siymarin content and antioxidant activity of seeds of wild Silybum marianum populations growing in Greece. J AAB. 2018;174.

[6] Ashie A, Lei H, Han B, Xiong M, Yan H. Fast determination of free components in milk thistle extract with a hand-held NIR spectrometer and chemometrics tools. Infra Phys Tech. 2021;113:103629.

[7] Block KI, Gyllenhaal C, Lowe L, et al. Designing a broad-spectrum integrative approach for cancer prevention and treatment. Semin Cancer Biol. 2015;35:276-304.

[8] Borah A, Paul R, Choudhury S, et al. Neuroprotective potential of silymarin against CNS disorders: Insight into the pathways and molecular mechanisms of action. *CNS*. 2013;*19*:847-853.

[9] Deep G, Agarwal R. Antimetastatic efficacy of silibinin: molecular mechanisms and therapeutic potential against cancer. Cancer Metastasis Rev. *2010;29*:447-463.

[10] Drouet S, Leclerc AE, Garros L. A Green Ultrasound-Assisted Extraction Optimization of the Natural Antioxidant and Anti-Aging Flavonolignans from Milk Thistle Silybum marianum (L.) Gaertn. Fruits for Cosmetic Applications. Antioxidants. 2019;8:304.

[11] Elateeq AA, Sun Y, Nxumalo W, Gabr MMA. Biotechnological production of silymarin in Silybum marianum L.: A review. J. BCAB. 2020;29:101775.

[12] European Pharmacopoeia: 10th Edition. Strasbourg: EDQM Publications; 2020.

[13] Ghafor Y, Mohammad NN, Salh DM. Extraction and Determination of Chemical Ingredients from Stems of Silybum Marianum. CMR. 2014;6:26-32.

[14] Ghorbani A. Studies on pharmaceutical ethnobotany in the region of Turkmen Sahra, north of Iran: (Part 1): General results. J Ethpharm. 2005;102:58-68.

[15] Giuliani C, Tani C, Bini LM, Fico G, Colombo R, Martinelli T. Localization of phenolic compounds in the fruits of *Silybum marianum* characterized by different silymarin chemotype and altered colour. J. Fitote. 2018:210 -218.

[16] Jedlinszki N, Kálomista I, Galbács G, Csupor D. Silybum marianum (milk thistle) products in Wilson's disease: a treatment or a threat? J. Her. Med. 2016;6:157-159.

[17] Karkanis A, Bilalis D, Efthimiadou A. Cultivation of milk thistle (Silybum marianum L. Gaertn.), a medicinal weed. J Ind Crop. 2011;1:825-830.

[18] Khan AM, Abbasi HB, Shah AN, Yücesan B, Ali H. Analysis of metabolic variations throughout growth a nd development of adventitious roots in *Silybum marianum* L. (Milk thistle), a medicinal plant. PCTOC. 2015;123:501-510.

[19] Li D, Hu J, Wang T, et al. Silymarin attenuates cigarette smoke extract-induced inflammation via simultaneous inhibition of autophagy and ERK/p38 MAPK pathway in human bronchial epithelial cells. Sci rep. 2016;6.

[20] Li L, Zeng J, Gao Y, He D. Targeting silibinin in the antiproliferative pathway. Expert Opinion on Investigational Drugs. 2010;19:243-255.

[21] Lucini L, Pellizzonii M, Pellegrino R, Molinari GP, Colla G. Phytochemical constituents and *in vitro* radical scavenging activity of different *Aloe* species. J Food Chem. 2015;170:501-507.

[22] Marmouzi I, Bouyahaya A, Ezzat MS, Jemli EM, Kharbach M. The food plant Silybum marianum (L.) Gaertn.: Phytochemistry, Ethnopharmacology and clinical evidence. J Ethpharm. 2021;265:113303.

[23] Mei L, Wang L, Li Q, Yu J, Xu X. Comparison of acid degumming and enzymatic degumming process for Silybum marianum seed oil. J. Sci. Food Agric. 2013;93:2822-2828.

[24] Mirdeilami ZS, Barani H, Mazandarani M, Heshmati AG. Ethnopharmacological Survey of Medicinal Plantsin Maraveh Tappeh Region, Northoflran. J.P.P. 2011;2:325-336.

[25] Nagy M, Mučaji P, Grančai D. Farmakognózia. Biologicky aktívne rastlinné metabolity a ich zdroje. Bratislava: Herba; 2015.

[26] Pendry BA, Kemp V, Hughes MJ, et al. Silymarin content in *Silybum marianum* extracts as a biomarker for the quality of commercial tinctures. J Herb Med. 2017;10:31-36.

[27] Polyak JS, Ferenci P, Pawlotsky MJ. Hepatoprotective and Antiviral Functions of Silymarin Components in HCV Infection. PMC. 2014;57:1262-1271.

[28] Poppe L, Peretsen M. Variation in the flavonolignan composition of fruits from different Silybum marianum chemotypes and suspension cultures derived thereform. J Phyto. 2016;131:68-75.

[29] Qin N, Jia C, Xu J, Li D et al. New amides from seeds of *Silybum marianum* with potential antioxidant and antidiabetic activities. J. Fitot. 2017;119:83-89.

[30] Ražná K, Hlavačková L, Bežo M et al. Application of the RAPD and miRNA markers in the genotyping of *Silybum marianum* (L.) Gaertn. Acta fytotechn zootechn. 2015;18:83-89.

[31] Rodriguez-Saona EL, Fry SF, Calvey ME. Use of Fourier Transform Near-Infrared Reflectance Spectroscopy for Rapid Quantification of Castor Bean Meal in a Selection of Flour-Based Products. J. Agric. Food. Chem. 2000;48:5169-5177.

[32] Singh RP, Tyagi AK Zhao J, Agarwal R. Silymarin inhibits growth and causes regression of established skin tumors in SENCAR mice via modulation of mitogen-activated protein kinases and induction of apoptosis. Carcin. 2002;23:499-510.

[33] Tyagi A, Bhatia N, Condon MS, Bosland MC, Agarwal C, Agarwal R.

Antiproliferative and apoptotic effects of silibinin in rat prostate cancer cells. Pros. 2002;53:211-217.
[34] Vagnerova L, Bradacova M, Pluhackova H. The Determination of Contained Compounds in Milk Thistle (*Silybum marianum* L. (Gaertn.)). Mendel Net. 2016;23:168-172.
[35] Wallace SN, Carrier DJ, Clausen EC. Batch solvent extraction of flavanolignans from milk thistle (*Silybum marianum* L. Gaertner). Phytochem. Anal. 2005;16:7-16.
[36] Wianowska D, Wiśniewski M. Simplified Procedure of Silymarin Extraction from Silybum marianum L. Gaertner. J. Chrom. Sci. 2015;53:366-372.

sciendo

Eur. Pharm. J. 2021, 68(1), 46-53.
ISSN 1338-6786 (online) and ISSN 2453-6725 (print version),
DOI: 10.2478/afpuc-2020-0018

EUROPEAN PHARMACEUTICAL JOURNAL

Antimicrobial activity and cytotoxicity of transition metal carboxylates derived from agaric acid

Original Paper

Habala L.[1]✉, Pašková L.[2], Bilková A.[2], Bilka F.[2], Oboňová B.[1], Valentová J.[1]

[1]Department of Chemical Theory of Drugs, Faculty of Pharmacy, Comenius University in Bratislava, Kalinčiakova 8, 832 32 Bratislava, Slovakia
[2]Department of Cellular and Molecular Biology of Drugs, Faculty of Pharmacy, Comenius University in Bratislava, Kalinčiakova 8, 832 32 Bratislava, Slovakia

Received 13 November, 2020, accepted 1 March, 2021

Abstract Carboxylato-type transition metal complexes with agaric acid, a bioactive natural compound derived from citric acid, were prepared, and tested *in vitro* for their antimicrobial activity and cytotoxicity. The products as well as agaric acid itself are amphiphilic compounds containing a hydrophilic head (citric acid moiety) and a hydrophobic tail (non-polar alkyl chain). The putative composition of the carboxylates was assigned on grounds of elemental analysis, infrared (IR) and high-resolution mass spectra (HR-MS), as well as in analogy with known complexes containing the citrate moiety. The metal carboxylates showed interesting activity in several microbial strains, especially against *S. aureus* (vanadium complex; MIC = 0.05 mg/ml). They were also tested for their cytotoxic activity in hepatocytes, the highest activity having been found in the copper(II) and manganese(II) complexes. Further research based on these preliminary results is needed in order to evaluate the influence of parameters like stability of the metal complexes in solution on the bioactivity of the complexes.

Keywords *Bioinorganic chemistry – metallodrugs – agaric acid – anticancer – antimicrobial – amphiphilic compounds*

INTRODUCTION

Metallodrugs (metallopharmaceuticals) are pharmacologically active substances containing metal atoms, which are essential for their biological activity. They exhibit a number of bioactivities, such as anticancer (Galanski et al., 2003; Hanif and Hartinger, 2018; Johnson et al., 2021), antimicrobial (Regiel-Futyra et al., 2017; Lemire et al., 2013), antiviral (de Paiva et al., 2020), and enzyme inhibitory activities (Kilpin and Dyson, 2013; Habala et al., 2018; Lu and Zhu, 2014). Metallodrugs offer several advantageous features over purely organic compounds due to specific characteristics of coordination compounds. Their bioactivity is influenced by the type of central atom, its oxidation and coordination number, charge of the complex, coordination geometry, type and number of the ligands, and so forth (Ndagi et al., 2017; Frezza et al., 2010).

Agaric acid (agaricin, α-hexadecylcitric acid, 2-hydroxy-1,2,3-nonadecanetricarboxylic acid) is a natural compound related to citric acid, substituted at C-4 with a hexadecyl chain (Figure 1). Occasionally, however, the term agaric (agaricin) has been used to describe concentrated or dry extracts from the corresponding fungi, so the usage may be somewhat confusing. It occurs in various wood-decay fungi species. It was initially isolated from the fungus *Fomitopsis officinalis* but can be found in various other species as well, such as *Polyporus officinalis* and *Polyporus igniarius* (Stamets, 2006). *Fomitopsis officinalis* (synonyms: *Laricifomes officinalis*, *Agaricum officinale*) is known also under the common name agarikon. It occurs in temperate regions of the world, although it has recently become very rare in Europe and in Asia. It was first described in antiquity by the Greek physician Dioscorides. The fungus has been used for centuries in traditional medicine, especially in the treatment of tuberculosis and pneumonia (Stamets, 2006). It is sometimes named fly agaric due to its traditional use as insecticide against flies. The mushroom is considered poisonous, though the effects are not severe.

Agaricin has been used in traditional medicine in the form of extracts from *Fomitopsis officinalis* in varying degrees of purity. It has a pronounced anhidrotic effect and can be

* *E-mail: habala@fpharm.uniba.sk*

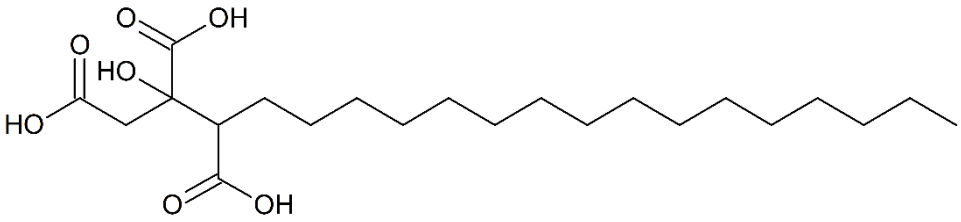

Figure 1. Chemical structure of agaric acid.

used in hyperhidrosis due to its parasympatholytic and anticholinergic activity. It has also been used topically as an anti-inflammatory agent and in the treatment of wounds. Its pharmacological utility was recognized early on, for example, the usefulness of 'white agaric' against excessive perspiration, as reported in 1831 in the journal Lancet (Burdach, 1831). Anticancer activity of agaric acid was mentioned in 1967 (Ciaccio et al., 1967). Despite its interesting pharmacological effects and long-time use in traditional medicine, the available data concerning its bioactivity is limited.

Agaric acid is a highly active inhibitor of fatty acid synthesis in mitochondria, acting by inhibition of the enzyme aconitase (Carrano and Malone, 1967). The mechanism of action is not fully understood but stems most likely from the analogy with citrate, for example, it inhibits citrate uptake in mitochondria (Chávez et al., 1978). Agaric acid is highly inhibitory against malic and α-glycerophosphate dehydrogenases at ~3.10^{-5} M and it also inhibits the growth of the nonpathogenic trypanosomatid *Crithidia fasciculata* used as a model for the pathogenic representatives of the *Trypanosoma* genus (Bacchi et al., 1969). Furthermore, it inhibits ADP-stimulated respiration. The compound functions as inducer of mitochondrial permeability transition, causing efflux of Ca^{2+}, collapse of transmembrane potential and mitochondrial swelling, probably by binding to mitochondrial ADP/ATP carrier (adenine nucleotide translocase, ANT) (García et al., 2005). The multiple negative charge of the citric moiety seems to be instrumental in this activity, along with the insertion of the alkyl chain into the hydrophobic phase of the membrane. Agaric acid is an amphiphilic-type compound as it contains a hydrophilic head (citric acid moiety) as well as a hydrophobic tail (non-polar alkyl chain). Amphiphilic compounds are a category of substances with specific biological activity. When equipped with suitable donor atoms, they can also act as ligands in metal complexes (Schattschneider et al., 2019). The hydrophobic moiety in the resulting complexes can interact with hydrophobic domains of DNA and proteins as well as with lipid membranes, whereas the central metal ion possesses Lewis acid character and thus can form coordination bonds with suitable donor atoms. Furthermore, it imparts redox properties on such complexes. Aggregation and self-assembly of metallosurfactants leads to metallomicelles.

At physiological pH, all three carboxylic groups of agaric acid can dissociate and are available for complexation, along with the hydroxyl group. However, almost no such metal complexes have been reported so far, except for the platinum complex of agaric acid and 1,2-cyclohexanediammine, whose preparation and anticancer activity in animal model was described (Bitha et al., 1986).

Agaric acid (denoted in this study as ligand L or as compound **8**) is a biologically active compound whose pharmacological potential remains largely unexplored. The aim of the presented study was to investigate the influence of complexation with various transition metals on the bioactivity of agaric acid. To this end, transition metal carboxylates of agaric acid with Cu, Ni, V, Co, La, Fe, and Mn were prepared. Here, we present the results of the *in vitro* measurements of their antimicrobial activities and of cytotoxicity in hepatocytes.

MATERIALS AND METHODS

General

The chemicals used in the syntheses were purchased from Sigma-Aldrich and are of analytical grade. They were used without further purification. Double distilled water was employed as reaction medium. Infrared (IR) spectra were measured with the help of the ATR (attenuated total reflectance) technique on a Nicolet 6700 FT-IR spectrometer from Thermo Scientific (Waltham, MA, USA) in the 600–4000 cm^{-1} range. Elemental analysis was conducted using a Flash2000 instrument from Thermo Scientific (Waltham, MA, USA). High-resolution mass spectra (HR-MS) were recorded on Thermo Scientific™ LTQ Orbitrap XLTM Hybrid Ion Trap-Orbitrap Mass Spectrometer (Thermo Scientific, Waltham, MA, USA). The instrument was used in full-scan mode (*m/z* range 100–700). The samples were dissolved in HPLC-grade methanol (conc. 2 ppm) and injected directly into the mass spectrometer. Electrospray (ESI) ion source was used to produce the ions. The conductivity measurements of solutions of the metal carboxylates were carried out in 1 mM dimethyl sulfoxide (DMSO) solutions by means of the conductivity benchtop meter inoLab Cond 7110 (Xylem Analytics, Weilheim, Germany).

General procedure for the synthesis of metal carboxylates

The metal complexes were prepared according to the modified procedures from (Abrahamson et al., 1994; Deng and

Zhou, 2009). Agaric acid (0.417 g, 1.0 mmol) was suspended in 70 ml of water. The mixture was stirred and heated almost to boiling temperature. Subsequently, a solution of NaOH (2.0 or 3.0 mmol, depending on the charge of the metal cation) in 30 ml of water was added. The heating was continued until complete dissolution of the solid. To the resulting clear colourless solution was added dropwise the aqueous solution of the respective metal salt (1 mmol). The following metal salts (as hydrates) were used: $CuCl_2 \cdot 2H_2O$, $MnCl_2 \cdot 2H_2O$, $NiCl_2 \cdot 6H_2O$, $CoCl_2 \cdot 6H_2O$, $FeCl_3 \cdot 6H_2O$, $La(NO_3)_3 \cdot 6H_2O$, $VOSO_4 \cdot 5H_2O$. After a short time, coloured precipitate started to form. The reaction mixture was stirred for 3 hours at room temperature. The resulting solid product was separated by filtration, washed successively with water and methanol, and dried in vacuum for several days to yield the product as variously coloured powders.

Antimicrobial activity testing

Antimicrobial activities of metal complexes and of the ligand were evaluated *in vitro* and expressed as the minimum inhibitory concentration (MIC). The standard broth dilution method (Lukáč et al., 2010) was employed in the determination. The following strains of Gram-positive, Gram-negative bacteria and a yeast pathogen were selected for the investigation: *Staphylococcus aureus* CNCTC Mau 29/58, *Escherichia coli* CNCTC 377/79 and *Candida albicans* CCM 8186, respectively. All the bacterial strains were obtained from Czech National Collection of Type Cultures (Prague, Czech Republic); yeast was purchased from Czech Collection of Microorganisms (Brno, Czech Republic).

Evaluation of cytotoxicity in HepG2 cells

HepG2 cells (ATCC HB-8065) were routinely cultured in a humidified atmosphere of 5% CO_2 at 37°C in Dulbecco's Modified Eagle Medium (DMEM) containing 10% Fetal Bovine Serum (FBS) and 0.2% (v/v) of penicillin/streptomycin solution. Complete medium was replaced every 2 to 3 days. The cultivation was carried out in 100 mm dishes. The cell count for a passage was 10 to 25. Cells were trypsinized to detach, then centrifuged, resuspended, seeded at 70% confluency and grown in 24-well culture plates for 24 h. Afterwards, the cells were incubated with rising inhibitor concentrations (0–75 µg/ml) for 24 h. Inhibitors were dissolved in DMSO. The concentration of vehiculum did not exceed 0.75% (v/v) (Miret et al., 2006). At the end of the incubation period, the cell proliferation was appraised using Janus Green B assay as described by Raspotnig *et al.* (Raspotnig et al., 1999). Briefly, the culture medium was detached from the cell layers by vacuum aspiration and the cell layers were fixed for 30 min in ethanol (50%), with subsequent vacuum aspiration of the fixative. Finally, the fixed cell layers were stained for 3 min with a 0.2% solution of Janus green B in Phosphate-Buffered Saline (PBS) (pH 7.1–7.2) at room temperature. After immediate removal of the stain using a vacuum aspirator, the whole plate was washed twice in cold tap water and eluted from cell layers by the addition of a 0.5 ml of 0.5 M HCl. The plate was analysed with a microplate reader (Biotec 3550-UV) against blanks of 0.5 M HCl at 595 nm. The cell count was determined using the calibration curve, which represents the dependency of A595 on HepG2 cell density. Each experiment was conducted threefold in duplicates.

RESULTS AND DISCUSSION

Synthesis and characterization of the metal complexes

All the metal carboxylates were prepared in good yields. The synthesis was accomplished in aqueous solution from the sodium salt of agaric acid prepared *in situ* and corresponding metal salts. The products were powders of various colours, stable in air. The solubility of the resulting metal carboxylates in common solvents was low in all cases. They were moderately soluble in DMSO and DMF (dimethyl formamide), and to some extent, also in alcohols, especially at elevated temperature. The complexes did not melt within the temperature range used. The syntheses are summarized in Table 1, along with the compositions of the metal carboxylates as obtained by elemental analysis and molar conductivities of their DMSO solutions.

The values of electric conductivity in the DMSO solutions (Table 1) suggest their non-ionic nature (Ali et al., 2013). The results of elemental analysis support the metal/ligand ratio 1:1, with varying number of water molecules present in the solid phase (2 or 3). The metal complexes were further investigated by infrared spectroscopy and high-resolution mass spectroscopy. The selected results of both types of spectroscopic measurements can be found in Table 2.

In the infrared spectra, bands corresponding to the vibrations of carboxyl groups (C=O) can be seen at 1539–1590 cm^{-1} (asymmetric stretching vibration) and 1394–1440 cm^{-1} (symmetric vibration). In the spectrum of pure agaric acid (the ligand), the band of the protonated carboxyl group appears at 1691 cm^{-1}. The relatively small difference $\nu_{as} - \nu_s$ (around 100–200 cm^{-1}) indicates the presence of coordinated carboxylate groups bonded to the metal in a covalent, bidentate fashion. The generally much higher intensity of the $\nu_{as}(COO^-)$ compared to the symmetric vibration band is a sign of coordinative (non-ionic) nature of the carboxylates (Palacios et al., 2004). The very low value of $\Delta\nu(COO^-)$ for iron(III) caboxylate (99 cm^{-1}) may be indicative for chelating bridging type of coordination in this complex. In the spectra of the carboxylates with bivalent metals, a residual carboxyl group (apparently protonated) can be seen at 1703–1705 cm^{-1}, whereas in the case of the trivalent metals (Fe, La) it is absent. The broad band around 3300 cm^{-1} can be ascribed to the stretching vibrations of the hydroxyl group of the citrate moiety and the water molecules. The intense signal caused

Table 1. The prepared metal carboxylates.

Comp. Nr.	Starting metal salt	Yield	Colour	Molar conductivity	Assumed composition	Elemental analysis theor.		Elemental analysis exp.	
		%		µS.mol-1.cm2		% C	% H	% C	%H
1	$CoCl_2 \cdot 6H_2O$	96	pink	9	$Co(L\text{-}2H)(2H_2O)$	51.84	8.31	51.70	8.55
2	$CuCl_2 \cdot 2H_2O$	75	light blue	3	$Cu(L\text{-}2H)(2H_2O)$	51.44	8.25	51.17	8.03
3	$NiCl_2 \cdot 6H_2O$	82	light-green	10	$Ni(L\text{-}2H)(3H_2O)$	50.17	8.43	50.19	8.46
4	$La(NO_3)_3 \cdot 6H_2O$	87	white	2	$La(L\text{-}3H)(2H_2O)$	44.90	7.02	44.91	7.19
5	$VOSO_4 \cdot 5H_2O$	84	grey-blue	11	$VO(L\text{-}2H)(3H_2O)$	49.34	8.28	49.30	8.03
6	$FeCl_3 \cdot 6H_2O$	86	light-brown	3	$Fe(L\text{-}3H)(3H_2O)$	50.46	8.28	50.50	7.95
7	$MnCl_2 \cdot 2H_2O$	95	brownish-white	5	$Mn(L\text{-}2H)(2H_2O)$	52.27	8.37	52.79	8.30

Table 2. Characteristic signals in IR and HR-MS spectra.

Substance	$\nu_{as}(COO^-)$ [a]	$\nu_s(COO^-)$ [b]	$\Delta\nu(COO^-)$ [c]	ν(C=O)	*m/z* theor. [d]	*m/z* found
1 (Co)	1590	1394	196	1704	472.1872	472.1875
2 (Cu)	1567	1417	150	1704	476.1836	476.1839
3 (Ni)	1575	1417	158	1704	471.1893	471.1899
4 (La)	1558	1403	155	---	(552.1603)	---
5 (V)	1563	1423	140	1705	480.1928	480.1932
6 (Fe)	1539	1440	99	---	468.1811	468.1816
7 (Mn)	1569	1409	160	1703	(468.1920)	---
8 (L)	---	---	---	1691	415.2696	415.2701

[a] $\nu_{as}(COO^-)$: asymmetric stretching vibration of the carboxyl; [b] $\nu_s(COO^-)$: symmetric stretching vibration of the carboxyl; [c] $\Delta\nu(COO^-) = \nu_{as}(COO^-) - \nu_s(COO^-)$; [d] the composition assigned to pseudomolecular ion was in all cases $[M(L\text{-}nH)]^-$, where n = 3–4, depending on the charge of the metal cation

by asymmetric vibrations of the COO^- groups overlaps with coordinated water deformation mode expected at approx. 1640 cm^{-1}. Strong and sharp absorption bands corresponding to $\nu(CH, CH_2)$ vibrations are found at approximately 2850 and 2900 cm^{-1}, those of $\delta(CH, CH_2)$ around 1230–1300 cm^{-1}. In the spectrum of the vanadium carboxylate, bands attributed to the vibrations of the V=O group can be seen as well: ν_s(V=O) = 988 cm^{-1}, ν_{as}(V=O) = 859 cm^{-1}. Generally, many signals in the spectra of metal carboxylates are shifted towards lower frequencies compared to those of free agaric acid, pointing to changes in vibrational status upon complexation to the respective metal.

The high-resolution mass spectrometry (HR-MS) with ESI ion source provides precise *m/z* values, enabling in this way the assignment of pseudomolecular ions for the compounds. The attempted ionization in positive mode did not produce molecular ions of the compounds, therefore, we had to resort to mass-spectrometric (MS) measurements in the negative mode. In most cases, we were able to find the pseudomolecular ion with the composition $[M(L\text{-}3H)]^-$ or $[M(L\text{-}4H)]^-$, except for the carboxylates of lanthanum and manganese. This can be attributed to the instability of these metal complexes in the mass spectrometer. The results support the metal/ligand ratio 1:1.

As an example, the HR-MS spectrum of the carboxylate of vanadyl is given in Figure 2. The signal of the pseudomolecular ion of the vanadium complex can be seen at *m/z* 480.1932. The free ligand (anion of agaric acid), originating from the dissociation of the complex, appears at *m/z* 415.2699.

Regarding the structures of analogous metal complexes with citric acid, it can be concluded that the structures of the prepared complexes might in some cases be dimeric or oligomeric, the great majority of them conforming to 1:1 metal/ligand ratio, for example, Zabiszak et al. (2018), Boghaei and Najafpour (2007), Huta et al. (2012), Field et al. (1974) and Zhou et al. (1999). The exact composition of these citrate complexes is often dependent on the pH of the reaction solution, for example, in the cobalt(II) complexes with citrate reported in Zhou et al. (2005). The coordination environment of cobalt in these complexes is

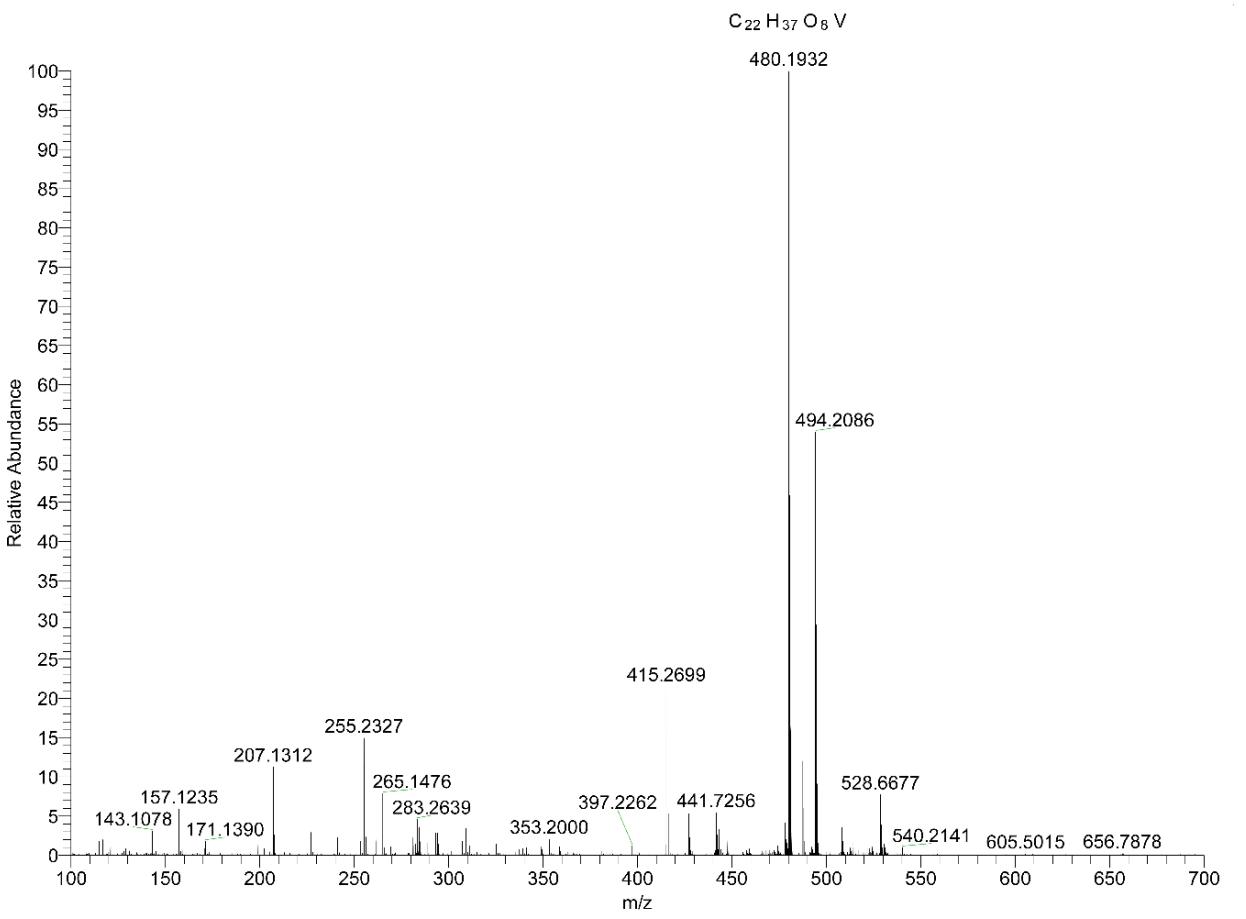

*Figure 2. HR-MS spectrum of the vanadium carboxylate (**5**).*

octahedral and the ligand is tridentate, binding through two carboxylates and the hydroxyl group. This type of coordination seems to be prevalent also in complexes with several other metals. With the copper(II) complex, a variety of structures seem possible as well (Boghaei and Najafpour, 2007; Drzewiecka et al., 2007; Mastropaolo et al., 1976). The presence of one or several charge-compensating counter-ions (like Na^+) is also possible, as in nickel(II) citrate (Baker et al., 1983) or in iron(III) citrate (Pierre and Gautier-Luneau, 2000; Vukosav et al., 2012). The ionic nature of any of the corresponding complexes with agaric acid can be fairly ruled out on the grounds of the results of electrical conductivity measurement (low values). The lanthanum complex with citric acid (Baggio and Perec, 2004) exhibits the composition $[La(Hcit)(H_2O)]_n$ and a polymeric structure, which could also fit well with the structure of the agaric acid analog, considering the $(\nu_{as} - \nu_s)$ value for the carboxylate in the IR spectra of the complex. Even if the analogy between complexes of citric and agaric acids might be useful, there are limits to this approach due to the steric requirements of the bulky alkyl substituent in agaric acid. To definitely establish the constitution and geometric arrangement of the metal carboxylates, further research is needed. The most straightforward method, X-ray single-crystal analysis, was not feasible as yet, due to difficulties with the preparation of single crystals of the complexes.

To sum up, the molar ratio metal/ligand 1:1 can be attributed to the prepared complexes. They are of non-ionic nature, most likely with hexacoordinate central atoms surrounded by the partly deprotonated agaric acid and several aqua ligands. They conform to the relative composition $M(L\text{-}mH)(H_2O)_n$ where $m, n = 2$ or 3.

Bioactivity

The prepared complexes along with the ligand were tested for their antimicrobial activity. Two bacterial strains (*S. aureus* and *E. coli*) and a yeast strain (*C. albicans*) were used. The results are summarized in Table 3. The best results were achieved with the vanadium carboxylate **5** in *S. aureus* (0.05 mg/ml). Interestingly, the activities of the same vanadium complex in *C. albicans* and *E. coli* were low. The results in other microbial strains were only inferior. Also, the antimicrobial activity of the copper complex, where the highest effect could be expected, was only mediocre. The activity of the ligand was in the same range as activity of the least active carboxylates.

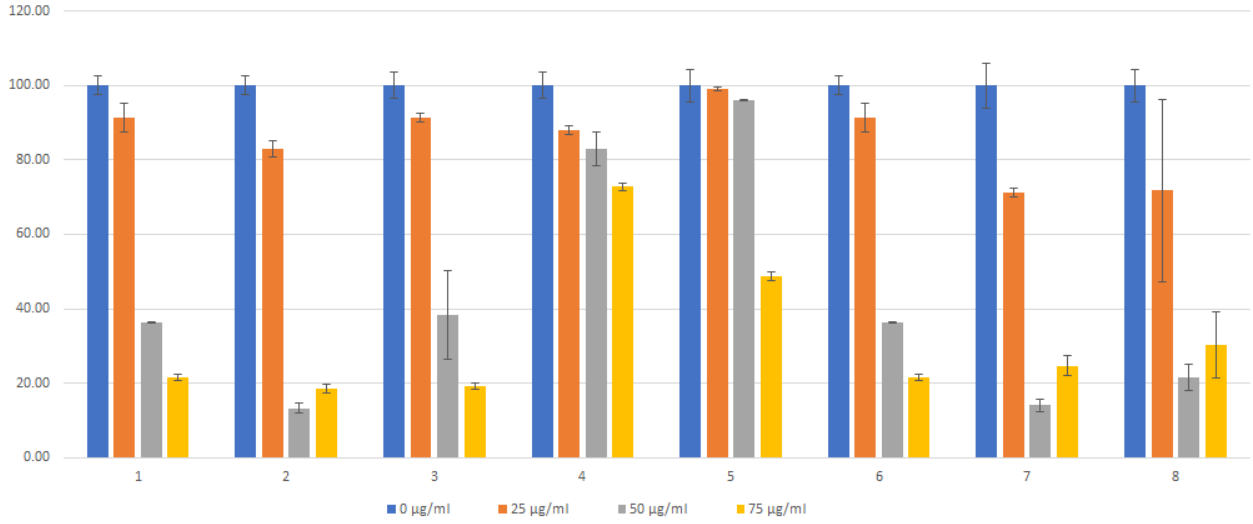

Figure 3. Cell viability for the investigated substances in the concentration range 0–75 µg/ml.

Table 3. Antimicrobial activity of metal carboxylates and the ligand (MIC = minimum inhibitory concentration).

Substance Nr.	Metal	MIC (mg/ml)		
		S. aureus	*E. coli*	*C. albicans*
1	Co	0.22	0.44	0.88
2	Cu	0.44	1.75	0.44
3	Ni	>3.5	1.75	0.88
4	La	1.75	1.75	1.75
5	V	0.05	3.5	0.88
6	Fe	3.5	0.88	0.44
7	Mn	3.5	3.5	0.44
8	(ligand)	1.75	3.5	0.88

The activities of the free metal ions can be appraised from the literature (Harrison et al., 2004; Nies, 1999)

To estimate the anticancer properties of the considered compounds, cytotoxicity in the human liver cancer cell line HepG2 was evaluated. HepG2 is an immortal cell line derived from hepatocellular carcinoma. It represents an *in vitro* model system for investigation of polarized human hepatocytes. The cell viability (percentage of cell survival) was determined in the concentration range 0–75 µg/ml (25 µg/ml step). The results are shown in Figure 3.

All the investigated complexes appear to be cytotoxic at the studied concentrations. The ligand itself (**8**) also exhibited comparatively high activity (21.5 % at 50 µg/ml). The activities of the free metal ions can be appraised from the literature (Borenfreund and Puerner, 1986).

The highest cytotoxicity was exercised at 50 µg/ml by the copper complex **2** and the manganese complex **7** (13.3 and 14.1 µg/ml, respectively). Interestingly, at 50 µg/ml the activities of all the complexes except these two were lower than the activity of the ligand but the picture changes at 75 µg/ml, where all the complexes except those of La and V score better than the pure ligand. Thus, the formation of metal carboxylates seems to improve upon the activity of the ligand (agaric acid), except in the case of the vanadium complex and even more so in the case of the lanthanum carboxylate. It is difficult to give a proper explanation for this synergic effect but binding of agaric acid to the metal might possibly facilitate the crossing of the cell membrane and thus accumulation of the metal in the cell. Similar improvement of cell membrane passage was observed in the amphiphilic Ru(II) complex reported in Siewert et al. (2017). Charged ruthenium species generally exhibit low cellular uptake (Alessio, 2016), yet this was radically improved upon incorporation of a C_{12} alkyl chain into the aforementioned ruthenium complex. Synergic effect of Cu(II)/Fe(III) complexation of non-ionic amphiphilic Schiff bases on antimicrobial activities was shown by Negm and Zaki (2008). It can be concluded that the donor atoms represent a highly hydrophilic area within the ligand, thus the lipophilicity of the complex molecule increases upon coordination to metal ions (decreasing the electron density of the moiety). This might lead to increased adsorption on the lipid-containing cell walls and affect the permeability of the membranes, resulting in more facile passage through the cell membrane of the microbes (Negm and Zaki, 2008; Schattschneider et al., 2019).

Another effect exercised by amphiphilic complexes could be improved protein binding, as demonstrated in the cobalt(III) complex carrying two phenanthroline ligands and a hydrophobic tetradecylamine ligand with a high affinity to human serum albumin (HSA) (Kumar et al., 2011). An amphiphilic complex of cobalt(III) carrying a dodecylamine ligand is able to intercalate with its long hydrophobic

chain between the base pairs in DNA, as indicated by cyclic voltammetry, spectroscopic methods and DNA viscosity measurements (Nagaraj and Arunachalam, 2014).

CONCLUSIONS

Agaric acid is a natural compound with manifold biological activities. In the course of this work, 7 new compounds, that is, carboxylates of agaric acid with transition metals were prepared. The complexes and the ligand (agaric acid) were tested for their *in vitro* antimicrobial activity against bacteria and yeast, as well as for their cytotoxicity in the hepatocytic cancer cell line HepG2.

Considerable antibacterial activity was found in the vanadium carboxylate, active against *S. aureus*. The majority of the complexes showed marked anticancer *in vitro* activity. The cytotoxicity was highest for the copper and manganese carboxylates.

The results are generally encouraging, especially considering that the expected molecular mass of the carboxylates might be quite high, and the complexes thus exhibit activity at low molar concentrations. The compounds are also interesting because of their amphiphilic nature. Hence, further investigation of these carboxylate complexes would be worthwhile, in particular into their structure and additional bioactivities. Of special interest is the evaluation of the behaviour of the complexes in solution, since they may undergo various changes upon dissolution, such as ligand dissociation and exchange. Based on the available analytical data, the complexes might be oligomeric or polymeric, thus their structure in aqueous solution can differ considerably from the solid-state structure.

ACKNOWLEDGMENTS

This publication was supported by the Scientific Grant Agency of the Slovak Republic, grant VEGA 1/0145/20, and Comenius University grant UK/324/2020.

CONFLICT OF INTEREST

The authors declare that they have no conflict of interest.

References

[1] Abrahamson HB, Rezvani AB, Brushmiller JG. Photochemical and spectroscopic studies of complexes of iron(II1) with citric acid and other carboxylic acids. Inorg Chim Acta. 1994;226:117–127.

[2] Alessio E. Thirty years of the drug candidate NAMI-A and the myths in the field of ruthenium anticancer compounds: a personal perspective. Eur J Inorg Chem. 2017;2017:1549–1560.

[3] Ali I, Wani WA, Saleem K. Empirical formulae to molecular structures of metal complexes by molar conductance. Synth React Inorg Met-Org Chem. 2013;43:1162–1170.

[4] Bacchi CJ, Ciaccio EI, Koren LE. Effects of some antitumor agents on growth and glycolytic enzymes of the flagellate *Crithidia*. J Bacteriol. 1969;98:23–28.

[5] Baggio R, Perec M. Isolation and characterization of a polymeric lanthanum citrate. Inorg Chem. 2004;43:6965–6968.

[6] Baker EN, Baker HM, Anderson BF, Reeves RD. Chelation of nickel(II) by citrate. The crystal structure of a nickel-citrate complex, $K_2[Ni(C_6H_5O_7)(H_2O)_2]_2$. Inorg Chim Acta. 1983;78:281–285.

[7] Bitha P, Child RG, Hlavka JJ, Lin Y. Platinum complexes of aliphatic tricarboxylic acid. EP0185225A1, Jun 25, 1986

[8] Boghaei DM, Najafpour MM. Crystal structure of $Gua_4[Cu_2(Cit)_2]$ {Gua = Guanidinium, Cit = Citrate = 2-hydroxo-1,2,3-tricarboxylatopropane}. Anal Sci. 2007;23:23–24.

[9] Borenfreund E.; Puerner JA. Cytotoxicity of metals, metal-metal and metal-chelator combinations assayed in vitro. Toxicology. 1986;39:121–134.

[10] Burdach M. Use of the white agaric in night perspirations. The Lancet. 1831;16:316.

[11] Carrano RA, Malone MH. Pharmacologic study of norcaperatic and agaricic acids. J Pharm Sci. 1967;56:1611–1614.

[12] Chávez E, Chávez R, Carrasco N. The effect of agaric acid on citrate transport in rat liver mitochondria. Life Sci. 1978;23:1423–1429.

[13] Ciaccio EI, Boxer GE, Devlin TM, Ford RT. Screening data from selected in vitro enzymatic systems I. Standard test compounds from the Cancer Chemotherapy Nation Service Center. Cancer Res. 1967;27:1033–1069.

[14] Ciaccio EI, Boxer GE, Devlin TM, Ford RT. Screening data from selected in vitro enzymatic systems II. Compounds specifically selected for the dehydrogenase inhibition screens. Cancer Res. 1967;27:1070–1104.

[15] de Paiva REF, Marçal Neto A, Santos IA, Jardim ACG, Corbi PP, Bergamini FRG. What is holding back the development of antiviral metallodrugs? A literature overview and implications for SARS-CoV-2 therapeutics and future viral outbreaks. Dalton Trans. 2020;49:16004–16033.

[16] Deng YF, Zhou ZH. Synthesis and crystal structure of a zinc citrate complex $[Zn(H_2cit)(H_2O)]_n$. J Coord Chem. 2009;62:1484–1491.

[17] Drzewiecka A, Koziol AE, Lowczak M, Lis T. Poly[tetraaquadi-μ_6-citrato-tetra-copper(II)]: a redetermination. Acta Cryst. 2007;E63:m2339–m2340.

[18] Field TB, McCourt JL, McBryde WAE. Composition and stability of iron and copper citrate complexes in aqueous solution. Can J Chem. 1974;52:3119–3124.

[19] Frezza M, Hindo S, Chen D, Davenport A, Schmitt S, Tomco D, Dou QP. Novel metals and metal complexes as platforms for cancer therapy. Curr Pharm Des. 2010;16:1813–1825.

[20] Galanski M, Arion VB, Jakupec MA, Keppler BK. Recent developments in the field of tumor-inhibiting metal complexes. Curr Pharm Des. 2003;9:2078–2089.

[21] García N, Zazueta C, Pavón N, Chávez E. Agaric acid induces mitochondrial permeability transition through its interaction with the adenine nucleotide translocase. Its dependence on membrane fluidity. Mitochondrion. 2005;5:272–281.
[22] Habala L, Devínsky F, Egger AE. Metal complexes as urease inhibitors. J Coord Chem. 2018;71:907–940.
[23] Hanif M, Hartinger CG. Anticancer metallodrugs: where is the next cisplatin? Future Med Chem. 2018;10:615–617.
[24] Harrison JJ, Ceri H, Stremick CA, Turner RJ. Biofilm susceptibility to metal toxicity. Environ Microbiol. 2004;6:1220–1227.
[25] Huta B, Lensboeur JJ, Lowe AJ, Zubieta J, Doyle RP. Metal-citrate complex uptake and CitMHS transporters: From coordination chemistry to possible vaccine development. Inorg Chim Acta. 2012;393:125–134.
[26] Johnson A, Northcote-Smith J, Suntharalingam K. Emerging metallopharmaceuticals for the treatment of cancer. Trends Chem. 2021;3:47–58.
[27] Kilpin KJ, Dyson PJ. Enzyme inhibition by metal complexes: concepts, strategies and applications. Chem Sci. 2013;4:1410–1419.
[28] Kumar RS, Paul P, Riyasdeen A, Wagniéres G, van den Bergh H, Akbarsha MA, Arunachalam S. Colloids Surf B Biointerfaces. 2011;86:35–44.
[29] Lemire JA, Harrison JJ, Turner RJ. Antimicrobial activity of metals: mechanisms, molecular targets and applications. Nat Rev Microbiol. 2013;11:371–384.
[30] Lu L, Zhu M. Protein tyrosine phosphatase inhibition by metals and metal complexes. Antioxid Redox Signal. 2014;20: 2210–2224.
[31] Lukáč M, Lacko I, Bukovský M, Kyselová Z, Karlovská J, Horváth B, Devínsky F. Synthesis and antimicrobial activity of a series of optically active quaternary ammonium salts derived from phenylalanine. Open Chem. 2010;8:194–201.
[32] Mastropaolo D, Powers DA, Potenza JA, Schugar HJ. Crystal structure and magnetic properties of copper citrate dihydrate, $Cu_2C_6H_4O_7{\cdot}2H_2O$. Inorg Chem. 1976;15:1444–1449.
[33] Miret S, De Groene EM, Klaffke W. Comparison of in vitro assays of cellular toxicity in the human hepatic cell line HepG2. J Biomol Screen. 2006;11:184–193.
[34] Nagaraj K, Arunachalam S. Synthesis, CMC determination, nucleic acid binding and cytotoxicity of a surfactant-cobalt(iii) complex: Effect of ionic liquid additive. New J Chem. 2014;38:366–375.
[35] Ndagi U, Mhlongo N, Soliman ME. Metal complexes in cancer therapy – an update from drug design perspective. Drug Des Devel Ther. 2017;11:599–616.
[36] Negm NA, Zaki MF. Structural and biological behaviors of some nonionic Schiff-base amphiphiles and their Cu(II) and Fe(III) metal complexes. Colloids Surf B Biointerfaces. 2008;64:179–183.
[37] Nies DH. Microbial heavy-metal resistance. Appl Microbiol Biotechnol. 1999;51:730–750.
[38] Palacios EG, Juárez-López G, Monhemius AJ. Infrared spectroscopy of metal carboxylates II. Analysis of Fe(III), Ni and Zn carboxylate solutions. Hydrometallurgy. 2004;72:139–148.
[39] Pierre JL, Gautier-Luneau I. Iron and citric acid: A fuzzy chemistry of ubiquitous biological relevance. BioMetals. 2000;13:91–96.
[40] Raspotnig G, Fauler G, Jantscher A, Windischhofer W, Schachl K, Leis HJ. Colorimetric determination of cell numbers by Janus green staining. Anal Biochem. 1999;275:74–83.
[41] Regiel-Futyra A, Dąbrowski JM, Mazuryk O, Śpiewak K, Kyzioł A, Pucelik B, Brindell M, Stochel G. Bioinorganic antimicrobial strategies in the resistance era. Coord Chem Rev. 2017;351:76–117.
[42] Schattschneider C, Kettenmann SD, Hinojosa S, Heinrich J, Kulak N. Biological activity of amphiphilic metal complexes. Coord Chem Rev. 2019;385:191–207.
[43] Siewert B, Langerman M, Hontani Y, Kennis JTM, van Rixel VHS, Limburg B, Siegler MA, Talens Saez V, Kieltyka RE, Bonnet S. Turning on the red phosphorescence of a [Ru(tpy)(bpy)(Cl)]Cl complex by amide substitution: self-aggregation, toxicity, and cellular localization of an emissive ruthenium-based amphiphile. Chem Commun. 2017;53:11126–11129.
[44] Stamets P. Antiviral activity from medicinal mushrooms. US 2006/0171958 Al, Aug 3, 2006
[45] Vukosav P, Mlakar M, Tomišić V. Revision of iron(III)–citrate speciation in aqueous solution. Voltammetric and spectrophotometric studies. Analyt Chim Acta. 2012;745:85–91.
[46] Zabiszak M, Nowak M, Taras-Goslinska K, Kaczmarek MT, Hnatejko Z, Jastrzab R. Carboxyl groups of citric acid in the process of complex formation with bivalent and trivalent metal ions in biological systems. J Inorg Biochem. 2018;182:37–47.
[47] Zhou ZH, Deng YF, Wan HL. Structural Diversities of Cobalt(II) Coordination Polymers with Citric Acid. Cryst Growth Des. 2005;5:1109–1117.
[48] Zhou ZH, Zhang H, Jiang YQ, Lin DH, Wan HL, Tsai KR. Complexation between vanadium(V) and citrate: spectroscopic and structural characterization of a dinuclear vanadium(V) complex. Trans Met Chem. 1999;24:605–609.

sciendo

Eur. Pharm. J. 2021, 68(1), 54-58.
ISSN 1338-6786 (online) and ISSN 2453-6725 (print version),
DOI: 10.2478/afpuc-2020-0024

EUROPEAN PHARMACEUTICAL JOURNAL

Iridoids From *Stachys Byzantina* K. Koch (Lamb's Ears) And *Stachys Germanica* L. (Downy Woundwort)

Original Paper

Háznagy-Radnai E.[1], Czigle Sz.[2,✉], Máthé I.[1]

[1]*Institute of Pharmacognosy, Faculty of Pharmacy, University of Szeged, Eötvös 6, H-6720 Szeged, Hungary*
[2]*Department of Pharmacognosy and Botany, Faculty of Pharmacy, Comenius University in Bratislava, Odbojárov 10, SK-832 32 Bratislava, Slovak Republic*
[3]*Institute of Ecology and Botany, Hungarian Academy of Sciences, Alkotmány u. 2-4., H-2163 Vácrátót, Hungary*

Received 16 March, 2021, accepted 6 May, 2021

Abstract Iridoids are a class of secondary metabolites found in a wide variety of plants. Iridoids are typically found in plants as glycosides, most often found to glucose. The genus *Stachys* L. is one of the largest genera of the Lamiaceae family, containing iridoids.
Aim: The aim of this study was the isolation and identification of iridoids from the aerial parts of *Stachys byzantina* K. Koch and *Stachys germanica* L.
Methods: For the isolation and identification of the iridoids, different chromatographic methods (NP-TLC, CPC and RP-HPLC) were used. The structures were established by one- and two-dimensional NMR and mass spectrometry, also.
Results: Iridoids (aucubin, harpagide, ajugoside and harpagoside) were isolated and identified by combination of different chromatographic methods from *S. byzantina* and *S. germanica*.
Conclusion: Stachys species may also be used as a potential source of iridoids.

Keywords *Stachys germanica – Stachys byzantina – iridoids – harpagide – aucubin – ajugoside – harpagoside*

INTRODUCTION

The family Lamiaceae consists of approximately 200 genera of 3500 species. The woundwort (*Stachys* L.) genus consists of 300 species. This is the third-largest relationship group of Labiate plants. It grows everywhere in the world with the exception of Australia, New Zealand and the Arctic regions. The number of species is particularly high in the Mediterranean region, Eastern Europe, Cape Province and Chile. Ten species live in Central Europe. The flowers of these annual or perennial herbs are light purple, dark pink, yellow or white. Some species grow in Hungary, too. *S. officinalis* L. is found in Europe, so in Hungary as well. *S. alpina* L. likes shady places, and it is found in fresh hornbeam-beech forests. *S. germanica* L. also grows in Hungary and Slovakia, and it is quite frequent in dry grasslands and pastures. *S. byzantina* L. is found as an ornamental plant, and *S. grandiflora* Stev. ex Willd. and *S. macrantha* K. Koch are found in botanical gardens. *S. sylvatica* L. can be found in hilly and mountainous zones along shrubs and forest paths, in moist, leafy forests, groves, scrubs and by forest springs. It lives on moist and wet clay and adobe soils which are rich in nutrients and have a neutral pH. *S. palustris* L. is widespread in the greater part of Europe, and it is common in Hungary, especially along marshes and bogs. *S. recta* L. is frequent on dry, stony grasses and steppe slopes. *S. annua* L. is found in most of Southern and Central Europe; it is native to Northern Europe; in Hungary, it is an ordinary plant. It can be found in ploughlands and stubble fields, mainly on hard soils (Tomou et al., 2020; Tutin et al., 1972).

Some members of the *Stachys* genus (extracts or their content material) have significant antibacterial, antifungal and antiphlogistic effects, and they can also be useful in anoxia, hepatitis and nephritis. It is proved by literature data that *Stachys* species have long been used in folk medicine for the treatment of genital tumours and cancerous ulcers (Skaltsa et al., 1999, 2001; Tomou et al., 2020).

* *E-mail: czigle@fpharm.uniba.sk*

Stachys species belong to the Lamioideae subfamily, and thus, they contain volatile oils in traces, but they have a great number of other secondary metabolic products, e.g. iridoids. As for their structure, their iridoids usually have 9 C atoms, with an OH group on C5 or C6. They typically contain a methyl or acetyl group on C8, giving C8 a quaternary character. For the most part, these iridoids cannot be detected in UV light, and therefore, a developing reagent is needed to make them visible. Their structure is relatively simple; at the same time, they are very sensitive to acids and enzymes, the presence of which leads to the decomposition of the compound (El-Naggar & Beal, 1980; Kobzar, 1986; Derkach et al., 1987; Jeker et al., 1989; Calis et al., 1991; Boros & Stermitz, 1990, 1991; Isamukhamedova & Pulatova, 1992; Kartev et al., 1994; Miyase et al., 1990; Munoz & Pena, 2001).

The aim of this study was the isolation and identification of iridoids from the aerial parts of *Stachys byzantina* (lamb's ears) and *Stachys germanica* (downy woundwort).

MATERIALS AND METHODS

Stachys germanica was collected at the Medicinal Plant Garden of the Faculty of Pharmacy, Comenius University in Bratislava. *Stachys byzantina* was gathered at Hungarian biotope and the Botanical Garden, Vácrátót, Hungary. Voucher specimens were deposited in the Institute of Pharmacognosy, University of Szeged, Hungary. The aerial parts of both species were collected at the flowering time, in June. The samples were conserved at -20°C until processing.

Solvents of analytical purity were purchased by Reanal (Budapest, Hungary), those of HPLC purity by Merck (Darmstadt, Germany).

Extraction and isolation of iridoids

S. byzantina and *S. germanica* were rubbed with $CaCO_3$ and extracted with methanol using ultrasonic shaker and Gerhardt shaker. The total methanolic extract was further purified on aluminium oxide (90 active neutral column 0.063–0.200 mm, Merck, Germany (70–230 mesh ASTM)). Extracts were concentrated under vacuum with a Rotavapor RE (Büchi, Germany) rotary evaporation system. This was dissolved in water, and a liquid-liquid distribution was performed with chloroform. Chlorophyll of all samples was removed by using a polyamide column chromatography.

Purification and isolation of chemical compounds

Silica gel 60 G (mean particle size 15 µm) (Merck, Germany) was used for vacuum-liquid chromatography (VLC). The concentrated extract was 6 g for *S. byzantina* and 8 g for *S. germanica*. After dissolution in water, VLC fractionation was carried out by using a water pump. Eluents were chloroform:methanol:water [70:10:1 and 10:70:1] and methanol:water [40:10 and 10:40].

The composition of the fractions was checked with thin-layer chromatography (TLC) in each case, and the solvent system was $CHCl_3$:MeOH:H_2O [25:10:1], as a mixture developed in this work, while the developer was the 1% concentrated hydrochloric acid solution of 4-(dimethylamino)benzaldehyde (105°C, 5 min).

The HPLC system (Shimadzu SPD 10 A/10 AV HPLC, Shimadzu Corporation, Japan) consisted of a gradient pump, analytical sampling valve, UV detector and integrator with software. Columns: BST SI-100 10 C-18 (250 mm, Ø 4 mm; Merck, Germany) and LiChrospher RP-18 (250 mm, Ø 5 µm; Merck, Germany), solvent system: method 1: water:acetonitrile [90:10]; method 2 – eluent: water:acetonitrile [98:2]; gradient program: isocratic; flow rate: 0.5 mL/min; injection volume: 20 µL; detector UV; column temperature: 23 °C. The fractions were concentrated under vacuum used a Rotavapor RE (Büchi, Germany) rotatory evaporation system.

Structural examination

The isolated iridoids were identified on the basis of their physical and spectroscopic properties. The basic information concerning the structure of compounds was provided by their NMR spectra.

Identification of isolated components

Melting points were measured with a melting point apparatus MP70 (Merck, Germany).

The UV spectra were recorded in MeOH and H_2O with Shimadzu UV 2101 PC spectrophotometer (Shimadzu Corporation, Japan).

^1H, ^{13}C and 2D (COSY, NOESY, HMBC and HMQC) NMR spectra were recorded in MeOH-*d*, H_2O-*d* and DMSO-*d* sample tubes at room temperature, with a Bruker Avance DRX 400 spectrometer (Bruker, Germany), at 400 MHz (^1H) and 100 MHz (^{13}C).

RESULTS AND DISCUSSION

Aerial parts of both *Stachys* species (*S. byzantina* and *S. germanica*) contained iridoids. Comparing the main iridoid component in the samples obtained from methanolic extract of drugs, harpagide was found in both *Stachys* samples. In addition to the iridoids in *S. byzantina*, ajugoside, aucubin and harpagide were identified by TLC (see Fig. 1), while those later two compounds were isolated and determined by RP-HPLC and NMR method aucubin and harpagide (see Tables 1 and 2). Harpagide and harpagoside (see Fig. 1) were detected in *S. germanica*. We could develop a method which can be used for the identification and detection of the iridoids of *Stachys* species.

In 1945, the Swedish botanist Erdtman subdivided this taxonomic family into two major subfamilies: the Lamioideae and the Nepetoideae. The Lamioideae subfamily

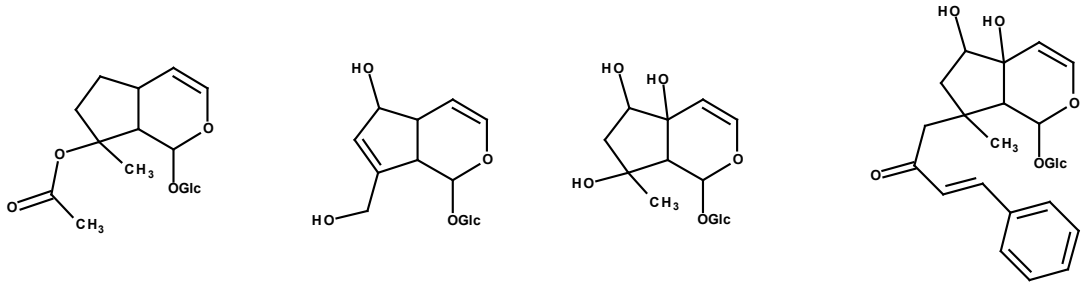

Figure 1. Isolated compounds.

Table 1. Physical and UV spectroscopic data on iridoids from S. byzantina and S. germanica.

Iridoids	M. P. [°C]	λ_{max} [nm]
Ajugoside	amorph. powder	206
Aucubin	179 – 183	210
Harpagide	amorph. powder	210
Harpagoside	amorph. powder	216

M. P., melting point.

is characterized by tricolpate and binucleate pollen, albuminous seeds, spatulate embryos, the presence of iridoid glycosides, lower content of essential oils and rosmarinic acid but higher content of phenylpropanoid glycosides, whereas the Nepetoideae have hexacolpate, trinucleate pollen, exalbuminous seeds, investing embryos, the presence of volatile terpenoids, mainly monoterpenes and high content of essential oil and rosmarinic acid. Both subfamilies contain caffeic acid and its derivatives (Erdtman, 1945; Cantino & Sanders, 1992).

The genus *Stachys* belongs to the subfamily Lamioideae. Iridoids are a class of secondary metabolites found in this genus. The first investigation of the iridoid content of in three species dates back to the beginning of the 1970s, when Adema detected iridoid glycoside in *S. palustris* and when Ukrainian researchers determined harpagide and 8-*O*-acetylharpagide in 17 *Stachys* species (Adema, 1968; Zinchenko, 1972). The main iridoid components in the *Stachys* species studied by Gritsenko et al. in 1977 were harpagide and 8-*O*-acetylharpagide. The presence of aucubin was also detected in some *Stachys* species (Gritsenko et al., 1977). Ajugol, ajugoside, harpagide and 8-*O*-acetylharpagide were detected in *S. atherocalyx*, *S. inflate* and *S. iberica* (Komissarenko et al., 1976, 1979). In 1980, the research team started an examination concerning 20 different *Stachys* species, which supplemented the previous results: beside harpagide and acetylharpagide as the main components, reptoside and diacetyl-reptoside were also found (Pakaln et al., 1980). In 1984, Lenherrr et al. performed the RP-HPLC analysis of 10 species belonging to the *S. recta* group, and melittoside, harpagide, acetylharpagide, ajugoside and ajugol were identified (Lenherrr, 1984). The data relating to the iridoids isolated until 1980 are summarized by El-Naggar & Beal (1980). El-Naggar's summary was followed by the work by Boros & Stermitz, which contains the summary of iridoids isolated between 1980 and 1990 (Boros & Stermitz, 1990, 1992). Russian researchers continued to investigate the chemical components of the *Stachys* species growing in Russia (Isamukhamedova & Pulakova, 1992; Kartev et al., 1994). Japanese researchers also conducted research into the iridoids *Stachys* species (Miyase et al., 1990). Monomelittoside, melittoside, 8-*O*-acetylharpagide, harpagide, ajugol, catalpol, 7-*O*-acetyl-8-epi-loganic acid, aucubin and 5-allosyloxy-aucubin were isolated by research made by Montenegrian, Greek, Hungarian and Italian scientists (Háznagy-Radnai et al., 2005, 2006, 2007; Munoz & Pena 2001; Kostos et al., 2001; Meremeti et al., 2004; Serrilli et al., 2005).

The isolated iridoid components of *Stachys* species found in Hungary are included in Table 3. Háznagy-Radnai et al., 2006, 2007 two iridoids, as harpagide and 8-*O*-acetylharpagide isolated in *S. byzantina and S. germanica*. Ajugoside and aucubin in both species right now.

CONCLUSIONS

The genus *Stachys* L. is one of the largest genera of the family Lamiaceae and subfamily Lamioideae containing iridoids. Iridoids (aucubin, harpagide, ajugoside and harpagoside) were isolated and identified by combination of different chromatographic methods (NP-TLC, CPC and RP-HPLC) from *S. byzantina* and *S. germanica*. The structures were established by one- and two-dimensional NMR and mass spectrometry. *Stachys* species may also be used as a potential source of iridoids.

Table 2. ^{1}H and ^{13}C NMR spectral data for isolated iridoids.

Aucubin (methanol):					
C/H	**DEPT**	**δ_C**	**δ_H**	**J(Hz)**	**HMBC(C→H)**
1	CH	96.1	4.94 d	(7.1)	H-1′, H-3′, H-9
3	CH	140.1	6.3 dd	(6.3, 1.8)	H-1, H-4
4	CH	104.1	5.08 dd	(6.3, 4.0)	H-3, H-5
5	CH	44.8	2.65 m		H-3, H-4, H-7, H-9
6	CH	81.3	4.43 m		H-4, H-5, H-7, H-9
7	CH	128.9	5.76 s		H-9, H-10
8	C	81.2			H-7, H-9
9	CH	46.5	2.89 t	(7.3)	H-1, H-7
10	CH_2	60.0	4.16 d	(15.4)	H-7
			4.34 d	(15.4)	
1′	CH	98.5	4.67 d	(7.8)	H-1, H-2′
2′	CH	73.5	3.22*		H-1′
3′	CH	76.6	3.37*		H-1′, H-2′, H-4′
4′	CH	70.2	3.28*		H-3′, H-5′, H-6′
5′	CH	76.9	3.26*		H-1′, H-4′, H-6′
6′	CH_2	61.2	3.64 dd	(12.2, 5.2)	H-5′
			3.85 d	(12.2)	
Harpagide (methanol):					
C/H	**DEPT**	**δ_C**	**δ_H**	**J(Hz)**	**HMBC(C→H)**
1	CH	92.0	5.74 s		H-1′, H-3, H-9
3	CH	141.3	6.31 d	(6.5)	H-1, H-4
4	CH	107.2	4.95 dd	(6.5, 1.5)	H-3, H-6, H-9
5	C	70.4			H-1, H-3, H-7, H-9
6	CH	77.0	3.70*		H-4, H-7, H-9
7	CH_2	45.8	1.80 dd	(13.8, 3.8)	H-10
			1.91 dd	(13.8, 4.8)	
8	C	81.2			H-7, H-9
9	CH	58.5	2.55 s		H-4, H-7, H-10
10	CH_2	23.6	1.25 s		H-7, H-9
1′	CH	98.1	4.58 d	(8.0)	H-1, H-2′
2′	CH	73.1	3.21 dd	(9.1, 8.0)	H-1′
3′	CH	76.4	3.38*		H-1′, H-2′
4′	CH	70.4	3.29*		H-3′
5′	CH	77.0	3.30*		H-4′, H-6′
6′	CH_2	61.4	3.66 dd	(11.8, 5.5)	H-5′
			3.90 d	(11.8)	

Table 3. The isolated iridoid components of Stachys species.

Species	**Iridoids**
S. alpina	harpagide, 8-*O*-acetylharpagide (Háznagy-Radnai, 2006, 2007)
S. annua	melittoside (Lenherr, 1984)
S. byzantina	harpagide, 8-*O*-acetylharpagide (Háznagy-Radnai, 2006, 2007)
S. germanica	harpagide, 8-*O*-acetylharpagide (Háznagy-Radnai, 2006, 2007)
S. grandiflora	harpagide, 8-*O*-acetylharpagide, melittoside (Háznagy-Radnai, 2006, 2007)
S. macrantha	harpagide, 8-*O*-acetylharpagide, ajugol, ajugoside, reptoside, allobetonicosid, macrathoside (Calis, 1991; Háznagy-Radnai, 2006, 2007)
S. officinalis	harpagide, 8-*O*-acetylharpagide, ajugol, ajugoside, reptoside, allobetonicosid, 6-*O*-acetylmioporoside (Kobzar, 1986; Derkach, 1987; Jeker, 1989; Háznagy-Radnai, 2006, 2007)
S. palustris	harpagide, 8-*O*-acetylharpagide, aucubin (Adema, 1968; Háznagy-Radnai, 2006, 2007)
S. recta	harpagide, 8-*O*-acetylharpagide, aucubin, ajugol, ajugoside, melittoside (Lenherr, 1984; Háznagy-Radnai, 2006, 2007)
S. sylvatica	harpagide, 8-*O*-acetylharpagide (Kukic, 2006; Háznagy-Radnai, 2006, 2007)

ACKNOWLEDGEMENTS

This work was supported by the Grant Agency of Ministry of Education, Science, Research and Sport of the Slovak (grants no. VEGA 2/0115/19 and VEGA 1/0359/18) and by the Slovak Research and Development Agency under the contract no. NKFI K 132044.

On the occasion of the 100th birth anniversary of our late teachers, nestors of Slovak Pharmacognosy, Prof. Dr. Ing. Jozef Tomko, DrSc. and Assoc.-Prof. Dr. PhMr. Jaroslav Kresánek, CSc.

CONFLICTS OF INTEREST

The authors declare no conflict of interest.

References

[1] Tomou EM, Barda Ch, Skaltsa HG. *Stachys*: a review of traditional uses, phytochemistry and bioactivity. Medicines. 2020;7(63):1-74.

[2] Tutin TG, Heywood VH, Burges NA et al. Flora Europaea, Volume 3. Cambridge: University Press; 1972.

[3] Skaltsa HD, Lazari DM, Chinou IB et al. Composition and antibacterial activity of the essential oils of *Stachys candida* and *S. chrysantha* from southern Greece. Planta Med. 1999;65:255-256.

[4] Skaltsa HD, Mavrmmati A, Constantinidis T. A chemotaxonomic investigation of volatile constituents in *Stachys* subsect. *Swainsonianeae* (Labiatae). Phytochemistry. 2001;572:235-244.

[5] El-Naggar LJ, Beal JL. Iridoids. A review. J Nat Prod. 1980;43:649-707.

[6] Kobzar AY. Phytochemical study of *Betonica officinalis*. I. Isolation of biologically active substances from the aerial parts of the plant. Khim Prir Soed. 1986;2:239.

[7] Derkach AI, Komissarenko NF; Pakalns D et al. Iridoids of some *Stachys* L. species. Rastit Resur. 1987;23:92-95.

[8] Jeker M, Sticher O, Calis I et al. Allobetonicoside and 6-*O*-acetylmioporoside from *Betonica officinalis* L. Helv Chim Acta. 1989;72:1787-1791.

[9] Calis I, Basaran AA, Saracoglu I, et al. Iridoid and phenylpropanoid glycosides from *Stachys macrantha*. Phytochemistry. 1992;3:167-169.

[10] Boros CA, Stermitz FR. Iridoids. An Updated Review I. J Nat Prod. 1990;53:1055-1147.

[11] Boros CA, Stermitz FR. Iridoids. An updated review. II. J Nat Prod. 1991;54:1172-1246.

[12] Isamukhamedova MP, Pulatova TP. Iridoids of *Stachys betonicae* flora. Khim Prir Soed. 1992;5:586-587.

[13] Kartev VG, Stepanichenko NN, Auelbekov SA. Chemical composition and pharmacological properties of plants of the genus *Stachys*. Khim Prir Soed. 1994;6:699-709.

[14] Miyase T, Ueno A, Kitani T et al. Studies on *Stachys sieboldii* Miq. I. Isolation and structures of new glycosides. Yakugaku Zasshi. 1990;110:652-657.

[15] Munoz O, Pena RC. Iridoids from *Stachys grandidentata* (Labiatae). J Biosciences. 2001;56:902-903.

[16] Erdtman G. Pollen morphology and plant taxonomy, 4. Labiatae. Verbanaceae and Aviceniaceae, Svensk Bot Tidskr. 1945;39:279-285.

[17] Cantino PD, Sanders RW. Subfamilial classification of Labiatae. Syst Bot. 1986;11:163-185.

[18] Adema F. Iridoid glucosides of species of *Lamium* and some related genera. Acta Bot Neerl. 1968;17:423-430.

[19] Zinchenko TV. *Stachys* and *Betonica* iridoids. Farm Zh (Kiev). 1972;27:86-87.

[20] Gritsenko EN, Kostyuchenko OI, Fefer IM et al. Iridoids of some genera of the Labiatae family. Mater S'ezda Farm B SSR. 1977;3 164-166.

[21] Komissarenko NF, Derkach AI, Sheremet IP et al. Harpagide and harpagide acetat of some species of the family Labiatae. Khim Prir Soed. 1976;1:109-110.

[22] Komissarenko NF, Derkach AI, Sheremet IP et al. iridoids of *Stachys inflata* and *Stachys iberica*. Khim Prir Soed. 1979;1:99-100.

[23] Pakaln DA, Komissarenko NF, Sheremet IP et al. Preliminary chemotaxonomic evalution of Caucasian species of the genus *Stachys*. Flory Ispol'z Ikh Nar Khoz. 1980;82-85.

[24] Lenherr A., Meier B, Sticher O. Modern HPLC as a tool for chemotaxonomical investigations: iridoid glucosides and acetylated flavonoids in the group of *Stachys recta*. Planta Med. 1984;50:403-409.

[25] Háznagy-Radnai E, Léber P, Tóth E et al. Iridoids of *Stachys* species growing in Hungary. JPC. 2005;18:314-318.

[26] Kostos M, Aligiannis N, Mitaku S et al. Chemistry of plants from Crete: stachyspinoside, a new flavonoid glycoside and iridoids from *Stachys spinosa*. Nat Prod Lett. 2001;15:377-388.

[27] Meremeti A, Karioti A, Skalska H, et al. Secondary metabolites from *Stachys ionica*. Biochem Syst Ecol. 2004;32:139-151.

[28] Serrilli AM, Ramunno A, Piccioni F et al. Flavonoids and iridoids from *Stachys corsica*. Nat Prod Res. 2005;19:561-565.

[29] Háznagy-Radnai E, Czigle Sz, Janicsák G et al. Iridoids of *Stachys* species growing in Hungary. JPC. 2006;19:187-190.

[30] Háznagy-Radnai E. Examination of the volatile and non-volatile components of Hungarian *Stachys* species [Annals 146 of Albert Szent-Györgyi Medical & Pharmaceutical Center – dissertation]. Szeged: JATE Press; 2007.

[31] Kukic J, Petrovic S, Pavlovic et al. Composition of essential oil of *Stachys alpina* L. ssp. *dinarica* Murb. Flavour Frag J. 2006;21:539-542.

sciendo

Eur. Pharm. J. 2021, 68(1), 59-62.
ISSN 1338-6786 (online) and ISSN 2453-6725 (print version),
DOI: 10.2478/afpuc-2021-0002

EUROPEAN PHARMACEUTICAL JOURNAL

Rapid and simple CZE-UV method for quality control of B1 and B6 vitamins in drugs and dietary supplements

Special Issue Article

Matuskova M.[1], Cizmarova I.[1], Chalova P.[1,2], Mikus P.[1,3], Piestansky J.[1,3]✉

[1]Department of Pharmaceutical Analysis and Nuclear Pharmacy, Faculty of Pharmacy, Comenius University in Bratislava, Odbojárov 10, SK-832 32 Bratislava, Slovak Republic
[2]Biomedical Research Center of the Slovak Academy of Sciences, Institute of Virology, Dubravska cesta 9, SK-845 05 Bratislava, Slovak Republic
[3]Toxicologic and Antidoping Center, Faculty of Pharmacy, Comenius University in Bratislava, Odbojárov 10, SK-832 32 Bratislava, Slovak Republic

Received 15 June, 2021, accepted 17 June, 2021

Abstract The application of hydrodynamically closed capillary zone electrophoresis combined with convenient ultraviolet (UV) detection allows fast, simple, environmentally friendly and cost-effective analysis of ions or ionisable molecules. This technique has been used to determine two selected B vitamins (thiamine, pyridoxine) in various drug formulations. The developed method was characterised by excellent validation parameters, such as linearity, precision, accuracy, limit of detection and limit of quantification. The total time of analysis was lower than 13.5 min. The results indicate that the method is suitable for implementation in routine quality control of selected B vitamins in pharmaceutical and food samples.

Keywords *capillary zone electrophoresis – hydrodynamically closed system – ultraviolet detection – thiamine – pyridoxine – quality control*

INTRODUCTION

Quality, safety and efficacy are the main drug attributes. The therapeutic effect depends on the exact amount of an active substance present in the medicine. Doses higher than therapeutic ones are often responsible for adverse and toxic effects. On the other hand, the use of lower doses cannot achieve the demanded benefit to human health. It is known that the active substances undergo decomposition processes due to the environmental effects. The quantity of the original drug can be reduced and the related degradation products can form. Typically, they have a negative impact on the drug quality and could represent a potential health risk. Therefore, measurement of the active substance in medicine is necessary to ensure its high quality.

Thiamine (THI) and pyridoxine (PYR) belong to a wide group of B vitamins. As active substances in drugs, they are indicated in nervous system diseases – for example, polyneuropathy, neuritis, herpes zoster, myalgia and states with B_1 and B_6 deficiency (Calderón-Ospina & Nava-Mesa, 2020). They are also offered as dietary supplements in order to provide them in sufficient amounts. THI and PYR can be administered in various dosage forms – injections, tablets, film-coated tablets, capsules or capsules with modified release.

Electrophoretic separation methods, especially capillary zone electrophoresis (CZE), seem to be useful in the analysis of active substances. CZE is simple to use, economical and ecological (consumption of low amount of sample and organic solvents) and is characterised by a high separation efficiency (Řemínek & Foret, 2021). These facts make it suitable for routine use in pharmaceutical analysis, which is demonstrated in some papers published by our laboratory group dealing with the analysis of antigripal drugs (Maráková et al., 2013), inflammatory bowel disease drugs (Maráková et al., 2017), vitamins (Maráková et al., 2014) or drugs used to treat tobacco use disorder (Piešťanský et al., 2013).

We have recently proposed a CZE method in a hydrodynamically closed separation system to determine THI and PYR in commercial beverages and food supplements (Matušková et al., 2020). Here, we used this method (with

* E-mail: piestansky@fpharm.uniba.sk

some minor modifications) to analyse THI and PYR content in various dosage forms and dietary supplements (Fig. 1a–c).

MATERIALS AND METHODS

Thiamine hydrochloride, pyridoxine hydrochloride and chemicals used for electrolyte system solution preparation (γ-aminobutyric acid [GABA], acetic acid [HAc], methylhydroxyethylcellulose [m-HEC]) were obtained from Sigma-Aldrich (Steinheim, Germany) and Serva (Heidelberg, Germany). Deionised water (18.2 MΩ cm) was used for the preparation of all solutions. The experiments were performed on EA 102 apparatus (Villa Labeco, Spisska Nova Ves, Slovakia) in a CZE single-column arrangement. A separation column was provided with a 300-μm internal diameter (i.d.) polytetrafluorethylene (PTFE) capillary tube of total length 90 mm and a contactless conductivity detector. The background electrolyte (BGE) was composed of 25 mM GABA + 50 mM HAc + 0.5% m-HEC (pH = 3.7). The samples were injected by a 200-nL internal sample loop of the injection valve of the analyser. All experiments were performed in a constant current mode. The driving current was 50 μA. An ultraviolet (UV) spectrophotometric absorbance detector (Knauer, Berlin, Germany) was connected to an on-column photometric detection cell via optical fibres. The detector was set at 260 nm.

Preparation of the sample for analysis depended on the pharmaceutical formulation. Here, three types of formulations were analysed – injections (Milgamma NA inject; Wörwag Pharma, Böblingen, Germany), film-coated tablets (B-komplex Sanofi; Zentiva, Prague, Czech Republic) and capsules (Diclovit, G.L. Pharma, Lannach, Austria). Preparation of injections was accompanied only by simple dilution with demineralised water at an appropriate concentration level. Pharmaceuticals formulated as film-coated tablets and capsules were crushed into a fine powder. An amount of the powder equivalent to the weight of one tablet (or capsule) was transferred to a 100-mL volumetric flask using demineralised water. The solution was sonicated for 30 min, filtrated using Whatman filter paper No.1 and diluted (if needed) with demineralised water. These solutions were then directly analysed using CZE as described above.

RESULTS AND DISCUSSION

At first, it was necessary to prove the proposed method for the demanded purpose. Therefore, we validated the modified CZE-UV method according to the ICH Q2(R1) guideline (ICH Harmonised Tripartite Guideline, 2005) recommendations. All resulting statistical data and performance parameters of the CZE-UV method are summarised in Table 1.

The method provided favourable parameters such as separation efficiency (N) and sample loadability, which resulted in sub-μg/mL limit of detection (LOD) and limit of quantification (LOQ) values. An illustrative electropherogram obtained from the analysis of THI and PYR standards at 0.25 μg/mL concentration level (LOQ of THI and concentration close to LOD of PYR) is presented in Fig. 1d. The enhanced sample loadability resulted from the use of wide-bore (300 μm i.d.) separation capillary tubes, which are typical for a hydrodynamically closed separation system. In comparison to our previous work (Matušková et al., 2020), the use of shorter separation column resulted in faster analysis of THI and PYR.

Excellent linearity of the calibration lines (concentration range 0.5–100 μg/mL) is indicated by the coefficient of determination (r^2) values. Acceptable repeatability was confirmed by the values of relative standard deviations (RSD) of migration time (RSD_{tm}), peak area (RSD_{area}), intercept *a* (RSD_a) and slope *b* (RSD_b) of the calibration lines. Critical factor of the validation procedure was the recovery parameter. The recovery experiment was performed by spiking the tested pharmaceutical dosage forms with THI and PYR standards at three concentration levels. Representative records, shown in Fig. 1e, illustrate the sample profile characteristics for THI and PYR in the original and spiked (at three concentration levels – 5, 10 and 25 μg/mL) commercial drug Diclovit.

Recovery values, calculated for the THI and PYR detection response in the standard (water) and tested drug matrices (injection solution, film-coated tablets, capsules; see Fig.

Table 1. Performance parameters of the CZE-UV method.

	Thiamine	Pyridoxine
t_m (min)	7.01	11.02
RSD_{tm} (%), n = 6	0.28	0.76
RSD_{area} (%), n = 6	2.28	8.60
a (mAU)	134.76	–39.09
RSD_a (%), n = 6	2.27	1.33
b (mAU/μg mL)	94.77	36.22
RSD_b (%), n = 6	0.49	0.29
r^2	0.9996	0.9990
Linear range (μg/mL)	0.5–100	1–100
LOD (μg/mL)	0.08	0.15
LOQ (μg/mL)	0.25	0.50
N	7900	6400
R	8.81	

LOD and LOQ were calculated as the signal (S) to noise (N) ratios to be 3 × S/N and 10 × S/N, respectively. Separation efficiency (N) was calculated according to the equation $N = 5.545*(t_m/w_{1/2})^2$, where t_m is the migration time and $w_{1/2}$ is the full width at half maximum of the peak. The calibration curve is expressed by the equation $y = b.x + a$. RSD_{tm} and RSD_{area} were calculated from the samples at LOQ concentration level. Resolution (R) was calculated according to the equation $R = 1.18*(t_2 – t_1)/(w_{1/2\,THI} + w_{1/2\,PYR})$, where t_2 is the migration time of PYR, t_1 is the migration time of THI, $w_{1/2\,THI}$ is the full width at half maximum of the THI peak and $w_{1/2\,PYR}$ is the full width at half maximum of the PYR peak.

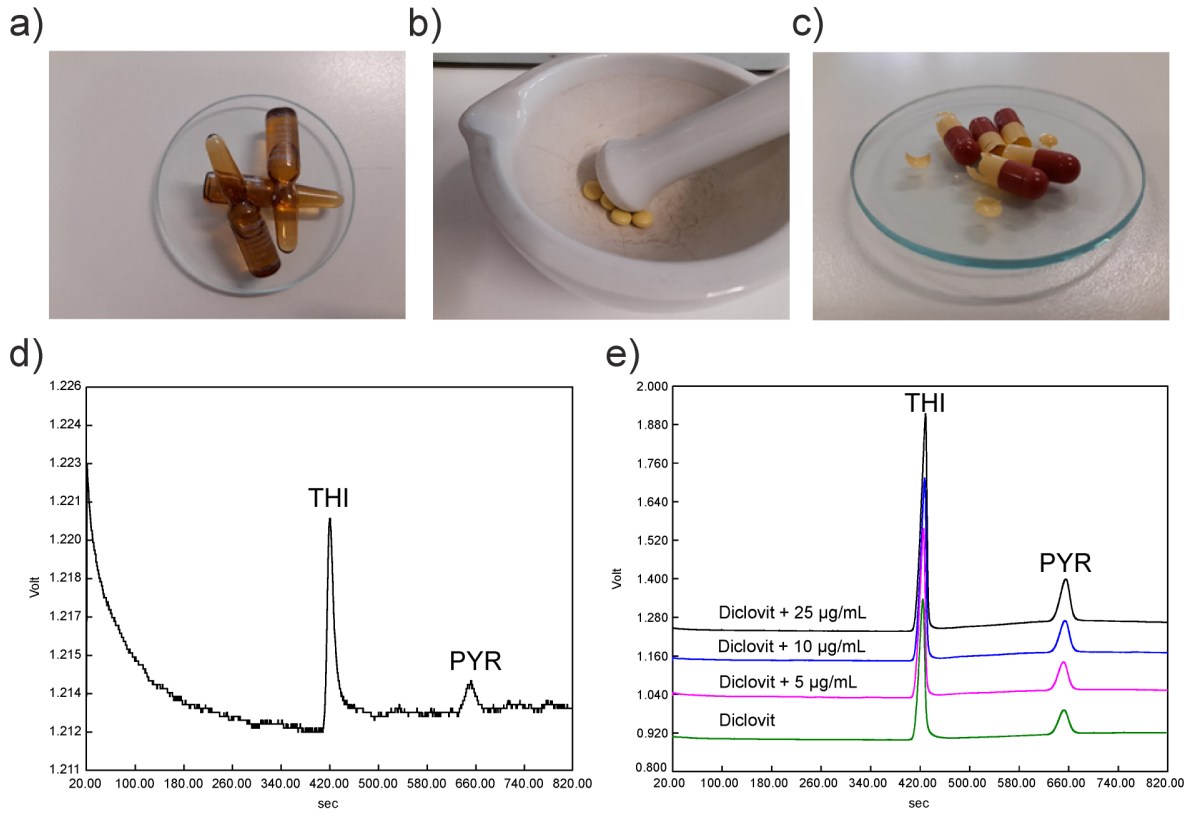

Figure 1. Analysis of THI and PYR in various pharmaceutical dosage forms – a) injection solutions Milgamma NA, b) film-coated tablets B-komplex Sanofi and c) capsules Diclovit. d) Illustrative electropherogram of THI and PYR at the concentration level 0.25 µg/mL. e) Illustrative electropherogram obtained from the CZE-UV analysis of non-spiked and spiked drug Diclovit. The spiked concentrations of THI and PYR were 5, 10 and 25 µg/mL. The injected volume was 200 nL.

1a–c), were in the range 95%–115% for THI and 90%–107% for PYR. This indicated acceptable effect of the matrix on the analyte signal and acceptable accuracy of the method.

After the successful validation procedure, the proved CZE-UV method was applied to determine the content of THI and PYR in real pharmaceutical samples. The obtained results are summarised in Table 2. The measured data were in good agreement with the declared content. Only in case of film-coated tablets (B-komplex Sanofi), the determined content of THI was slightly higher than 15% in comparison to the declared one. This variation might be caused due to changes during the storage and manufacture. However, B-komplex Sanofi is classified as a dietary supplement. For such preparation, there is no strict adherence to the active compound content.

In conclusion, the present work illustrates the potential of simple CZE-UV method performed in hydrodynamically closed separation system for the quality control of THI and PYR present in pharmaceutical samples. The advantages of such an analytical system were demonstrated by the excellent performance parameters of the CZE-UV method and its successful application in the drug and dietary supplements' quality control area. This method is suitable for the automation and miniaturisation and it has promising potentialities to be used in the reference and routine pharmaceutical laboratories. Owing to being a rapid, cheap, available and reliable analysis, the presented CZE-UV approach represents a suitable alternative to the well-established analytical methods used in drug and food analysis.

Table 2. THI and PYR concentrations in three pharmaceutical samples determined by the CZE-UV method.

Preparation		Parameters		
		Found ± SD (µg/mL)	RSD (%), n=3	Declared (µg/mL)
Milgamma NA (inj)	THI	53.15 ± 0.26	0.49	50
	PYR	23.01 ± 0.23	0.98	25
Diclovit (cps)	THI	50.81 ± 1.27	2.50	50
	PYR	43.18 ± 1.07	2.48	50
B-komplex Sanofi (tbl flm)	THI	11.59 ± 0.18	1.56	10
	PYR	5.52 ± 0.50	9.00	5

ACKNOWLEDGMENTS

This work was supported by the projects VEGA 1/0463/18, APVV-15-0585, KEGA 027UK-4/2020, FaF UK/2/2021, FaF UK/3/2021 and the grant of Comenius University UK/235/2021 and was carried out in the Toxicologic and Antidoping Center at the Faculty of Pharmacy Comenius University.

CONFLICT OF INTEREST STATEMENT

The authors do not have any conflict of interest concerning the present work.

References

[1] Calderón-Ospina CA, Nava-Mesa MO. B vitamins in the nervous system: Current knowledge of the biochemical modes of action and synergies of thiamine, pyridoxine, and cobalamin. CNS Neurosci Ther. 2020; 26: 5–13.

[2] ICH Harmonised Tripartite Guideline: Validation of Analytical Procedures: Text and Methodology. Step 4 Version. European Medicines Agency, November 2005 (http://www.ich.org/cache/compo/276-254-1.html). Accessed June 9, 2021.

[3] Maráková K, Piešťanský J, Havránek E, Mikuš P, Simultaneous analysis of vitamins B in pharmaceuticals and dietary supplements by capillary electrophoresis hyphenated with triple quadrupole mass spectrometry. Pharmazie. 2014; 69: 663–668.

[4] Maráková K, Piešťanský J, Mikuš P. Determination of drugs for Crohn´s disease treatment in pharmaceuticals by capillary electrophoresis hyphenated with tandem mass spectrometry. Chromatographia. 2017; 80: 537–546.

[5] Maráková K, Piešťanský J, Veizerová L, Galba J, Dokupilová S, Havránek E, Mikuš P. Multidrug analysis of pharmaceutical and urine matrices by on-line coupled capillary electrophoresis and triple quadrupole mass spectrometry. J Sep Sci. 2013; 36: 1806–1816.

[6] Matušková M, Čižmárová I, Mikuš P, Piešťanský J. Stanovenie tiamínu a pyridoxínu vo výživových doplnkoch a nápojoch jednoduchou metódou kapilárnej zónovej elektroforézy v spojení s UV detekciou. Čes. Slov. Farm. 2020; 69: 237–243.

[7] Piešťanský J, Maráková K, Veizerová L, Galba J, Mikuš P. Stanovenie vareniklínu v lieku Champix® dvojdimenzionálnou kapilárnou elektroforézou v spojení s UV detekciou. Čes. Slov. Farm. 2013; 62: 270–275.

[8] Řemínek R, Foret F, Capillary electrophoretic methods for quality control analyses of pharmaceuticals: A review. Electrophoresis. 2021; 42: 19–37.

sciendo

Eur. Pharm. J. 2021, 68(1), 63-65.
ISSN 1338-6786 (online) and ISSN 2453-6725 (print version),
DOI: 10.2478/afpuc-2021-0004

EUROPEAN PHARMACEUTICAL JOURNAL

Drug Technology in Hunting Practice

Original Paper

Laca Megyesi S.[1]✉, Königová A.[1], Molnár L.[2], Várady M.[1], Fedorová M.[3], Eftimová J.[4]

[1]Institute of Parasitology, Slovak Academy of Sciences, Hlinkova 3, 04001 Košice, Slovakia
[2]Clinic for Birds and Exotic Animals, University of Veterinary Medicine and Pharmacy, Košice, Slovakia
[3]Department of Pharmacy and Social Pharmacy
[4]Department of Pharmaceutical Technology, Pharmacognosy and Botany

Received 15 June, 2021, accepted 17 June, 2021

Abstract Antiparasitic therapy in living ratites is based on the right dose and efficacy is only when the drug is pharmaceutically stable and safe. Ivermectin is considered to be the most widely used drug in the treatment of parasitosis in ruminants worlwide. For these reasons, in our study, we focused on the pharmaceutical investigation of ivermectin by SEM analysis of its powder particle shape and size, flow properties of solids (angle of repose, compressibility index, Hausner ratio) and zeta potential.

Keywords *wild ruminants – Galmectin premix – ivermectin – flow properties*

INTRODUCTION

Frequent occurrence of wild and domestic ruminants together on common pastures raises the question about the role of wild species in the transmission of gastrointestinal (GI) nematodes between small ruminants. The similar feeding habits of wild and domestic ruminants may represent a high potential risk for the transmission of GI nematodes from wild to domestic sheep and goats. Hunters are required to estimate the total number of animals and their total weights in hunting districts. The distribution of drugs in the feed may thus be easily inconsistent, so the drugs may be underdosed. Underdosing is one of the most common managerial flaws contributing to the development of anthelmintic resistance (AR) (Torres-Acosta and Hoste, 2008). Ivermectin (IVM) is one of the best known and most widely used antiparasitic drugs in human and veterinary medicine. IVM is a semi-synthetic product obtained from avermectin, naturally synthesised by the microorganism *Streptomyces avermitilis*. It consists of a mixture of two homologues, dihydroavermectin B_{1a} (H_2B_{1a}) and dihydroavermectin B_{1b} (H_2B_{1b}) (Cerkvenik et al., 2001).
The aim of our study was to analyse two samples of Galmectin premix stored at different temperatures and humidity for 1 month using scanning electron microscope (SEM) analyses and flow properties, in order to determine the effect of the external environment on the structure of the premix.

MATERIALS AND METHODS

Chemicals: IVM in Galmectin 0.150 mg/g premix (PHARMAGAL Ltd., Nitra, Slovakia)

Data treatment

Sample No. 1 was stored at 20 °C, 58% humidity in a glass vessel and sample No. 2 was stored at 4.2 °C, 75% humidity in a glass vessel. Samples of the premix (Sample No. 1 and Sample No. 2) for SEM analysis (MIRA3, TESCAN) were observed in the dried state. We placed them on a base plate with a size of about 1 cm^2. According to Kostelanská recommendations (2017), the samples should be coated with a layer of metal with good thermal and electrical conductivity (gold, silver, platinum, carbon or an alloy of platinum and palladium) before observation. In this case, we used a layer of carbon (about 20 nm), which we applied using a sputtering device. The carbon layer provided the samples with a negative charge and a heat circuit in which most of the energy of the accelerated primary electrons was converted. The prepared premix samples were placed in a chamber placed in the lower part of the microscope tube. Samples of the premix were placed on a trigonometric table, near which detectors of individual signals (secondary and reflected electrons) were placed.
Compressibility index is a measure of strength and stability, and Hausner ratio is a measure of the interparticulate friction.

* *E-mail: stefania.megyesiova@uvlf.sk*

Flow character is rated based on compressibility index and Hausner ratio.

$$\text{Compressibility index} = 100(V_0 - V_f)/V_0$$
$$\text{Hausner ratio} = V_o/V_f$$

where: V_0 = original bulk volume of powder; V_f = final tapped volume of powder.

Zeta potential measurement was performed using ZetaSizer ZS device, working on the principle of laser Doppler velocimetry (LDV) in combination with Dynamic Light Scattering (DLS). After switching on, the instrument was calibrated and heated to a measuring temperature of 25 °C. First, the sample was dispersed in 100 ml of distilled water. Then we transferred the solution to the measuring cuvette with a syringe. We used the configuration of the signal passed through the sample. The device automatically evaluated the standard deviation and displayed it together with the zeta potential value in the software program.

RESULTS AND DISCUSSION

SEM analysis of the particle shape of sample No. 1 stored at 20 °C, 58% humidity in a glass vessel revealed an angular particle shape at 500× magnification. Particles with a smooth surface and a regular shape had better flow properties than square-shaped particles that fit together. We confirmed this fact at a magnification of 3,000 times, where we found that the individual particles of the examined sample really fit into each other. At 8,000 and 20,000 times magnification, we confirmed the angular, irregular shape of the particles and also observed small particles on the surface of larger particles.

When comparing the SEM analysis of the particle shape of sample No. 1 and sample No. 2 at 500× magnification, it is clear that in the case of sample No. 2, the individual particles were compacted under the influence of moisture. At 500× magnification of sample No. 2, we could clearly see that the space between the particles had shrunk and they tended to clump together. At 3,000× magnification, we found a more rounded shape of the particles of sample No. 2.

The second part of the SEM analysis was the measurement of individual particles. We measured the particles at 1,500 and 4,000 fold magnification. In sample No. 1, we measured a total of 24 randomly selected particles. The average particle size was 12.24 µm. On evaluating the SEM analysis of the particle size of sample No. 2 at 1,500× magnification, we also observed isolated agglomerates of 42.16 and 39.30 µm. As with sample No. 1, we selected 24 particles at 1,500 and 4,000 fold magnification. The average size of the individual particles was 12.65 µm. According to our calculations, the compressibility index values ranged from 2.85% to 7.69%, which means that the nature of the flow of sample No. 1 was excellent. The Hausner ratio values ranged from 1.02 to 1.08, which again confirms the result of the compressibility index calculation. This result shows that in the case of storage conditions (temperature 20 °C, humidity 58%), the flow properties of the premix do not deteriorate. The compressibility index values of sample No. 2 ranged from 2.98% to 5.00%, which resulted in an excellent flow pattern of the sample. The Hausner ratio values ranged from 1.03 to 1.05, which also indicates the excellent nature of the flow of the examined sample No. 2.

Angle of repose measurement results ° ± SD of sample No. 1 and sample No. 2 were repeated three times for each sample. According to the generally accepted Carr scale, powder with a pour angle below 30° has good flowability, 30°–45° shows some cohesiveness, 45°–55° shows real cohesiveness and powder with a pour angle above 55° is characterised by very high cohesiveness and very limited flowability. It follows from the above that the samples examined by us had a pour angle in the range of 30°–45° and showed certain coherence.

The Zeta potential of both Galmectin 0.150 mg/g premix powder samples examined was measured using a ZetaSizer (Malvern, UK), which recorded the results, and these were subsequently processed into Zeta potential distribution and electrophoretic mobility distribution. When evaluating the results of the analysis, we assumed that if the Zeta potential was in the range of −30 to + 30 mV, then the charge on the surface was too small to prevent contact and the particles tended to agglomerate. The measurement was performed in three cycles, each cycle containing 10 measurements for 10 seconds. The resulting Zeta potential measurement was created as the average of all measurements. The instrument recorded one peak in both cases. Zeta potential of sample No. 1 was −18.7 ± 6.27 mV, so it tended to clump. Zeta potential of sample No. 2 had a value of −17.2 ± 9.22 mV, which showed that similar to sample No. 1, sample No. 2 also tended to clump. Differences in the measured values of Zeta potential of sample No. 1 and sample No. 2 were insignificant, indicating that the effect of external conditions did not affect the stability of the samples.

. The effect of moisture on the powder shape was determined from the SEM analysis. The sample which was exposed to moisture showed a more rounded shape and also the formation of agglomerates. Based on the obtained results of the pharmaceutical analysis, we propose that in hunting practice, premixes have to be stored in well-sealed bags that protect against the effects of moisture.

ACKNOWLEDGEMENT

This study was supported by funds from the Scientific Grant Agency VEGA 2/0099/19.

CONFLICT OF INTEREST STATEMENT

The authors declare that they have no conflicts of interest.

References

[1] Cerkvenik V, Doganoc DZ, Skubic V, Beek WMJ, Keukens HJ. Thermal and long-term freezing stability of ivermectin residues in sheep milk. Eur Food Res Technol. 2001;213:72–6.

[2] Kostelanská K, Gajdziok, J. Elektrónová mikroskopie pro předmět Instrumentální analytické metody ve farmaceutické technologii. Brno: 2017.

[3] Torres-Acosta JFJ, Hoste H. Alternative or improved methods to limit gastro-intestinal parasitism in grazing sheep and goats. Small Rum Res. 2008; 77:159–173.

sciendo

Eur. Pharm. J. 2021, 68(1), 66-71.
ISSN 1338-6786 (online) and ISSN 2453-6725 (print version),
DOI: 10.2478/afpuc-2021-0008

EUROPEAN PHARMACEUTICAL JOURNAL

Phospholipid bilayers in model membranes and drug delivery systems: from physics to pharmacy

Special Issue Article

Uhríková D.✉

Department of Physical Chemistry of Drugs, Faculty of Pharmacy, Comenius University in Bratislava, Odbojárov 10, 832 32 Bratislava, Slovakia

Received 16 June, 2021, accepted 17 June, 2021

Abstract Lipids spontaneously aggregate in an aqueous environment forming supramolecular structures of various architectures known as liquid crystalline mesophases. Their thermodynamic properties determined by dual polar/apolar nature coupled with the possibility to modulate the structural parameters, phase geometry and stability are challenging for applications in drug delivery systems. We review a few examples of functionality of lipid bilayers.

Keywords *lipid bilayer – non-lamellar phases – antimicrobial peptides– lipoplexes – pulmonary surfactant*

Amphiphilic molecules of lipids self-assemble in water to minimise the exposure of their hydrophobic moieties to water. It was found that both the energetics at the lipid–water interface and the lipid molecular shape play a very important role in the aggregation and formation of resultant structures. While the hydrophobic interaction has a tendency to decrease the total surface area, repulsive interactions tend to increase the surface area. These opposing forces give rise to an optimal equilibrium area per lipid molecule. Packing restrictions determine the curvature of lipid monolayer and can also give rise to an optimum aggregate size (Israelachvili et al., 1976). Thus, the hydrophobic effect and structural diversity of lipidic molecules are responsible for the formation of a high variety of their supra-molecular assemblies. Fig. 1 illustrates a few structures of the lyotropic liquid crystalline mesophases formed by lipids: (A) one-dimensional lamellar phase known as multilamellar liposomes (onion-like structure) in excess of water; (B) two-dimensional columnar hexagonal phase and (C) three-dimensional cubic phases of symmetries characterised by space groups. Multilamellar and particularly unilamellar liposomes formed by single lipid bilayer frequently serve as a model system of lipid bilayer of biological membrane. Lipidic mesophases attract attention due to their capability to accommodate a drug into both the water phase and the hydrophobic matrix. Since 1975, when the first demonstration of the improved *in vivo* activity of liposome-entrapped anticancer drug in animal models proved successful treatment of mice bearing leukaemia (Kobayashi et al., 1975), a wide variety of lipidic drug delivery systems have been employed. Here, we review a few examples of functionality of lipid bilayers.

LIPID BILAYERS AS A MODEL OF BIOLOGICAL MEMBRANE

Antimicrobial peptides (AMPs) emerged as an interesting alternative to antibiotics that fight against infectious diseases. AMPs are considered membrane-active agents leading to cell death by acting on the phospholipid membrane. All proposed bactericidal mechanisms have the same main initialisation – adsorption of AMPs onto the membrane due to electrostatic interactions between the cationic peptides and the accessible anionic groups of hydrophilic phospholipid headgroups at the membrane surface. Thereafter, accumulation and positional change eventually lead to the formation of pores, membrane permeabilisation or its micellisation (Teixeira et al., 2012). The interaction must be selective regarding the distinction between mammalian cells and pathogen cells (bacteria, fungi, protozoa). Thus, knowledge of the details of AMPs interaction with lipid bilayers of composition mimicking the pathogen membrane is of great importance to evaluate their antimicrobial activity. Small-angle X-ray and neutron scattering (SAXS and SANS, respectively) studies can

* *E-mail: uhrikova@fpharm.uniba.sk*

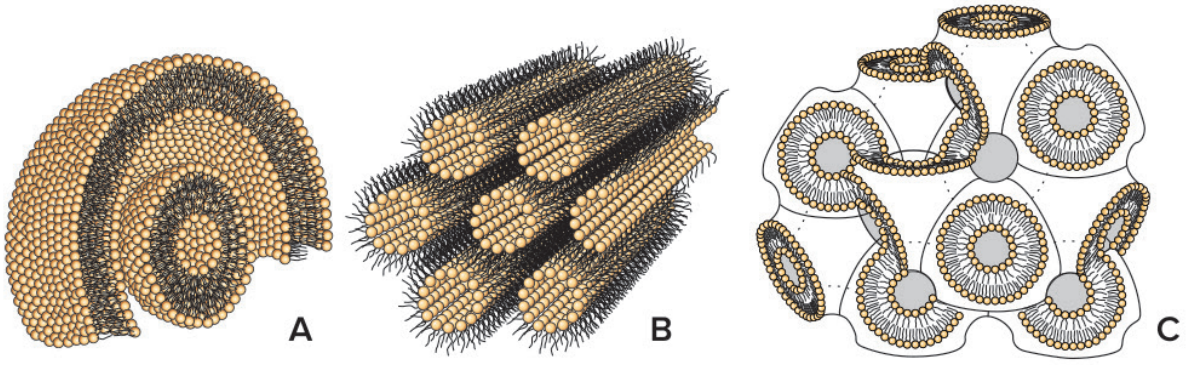

Figure 1. Lyotropic liquid crystalline mesophases: (A) multilamellar vesicles; (B) inverted hexagonal phase; (C) cubic phase of Pn3m space group.

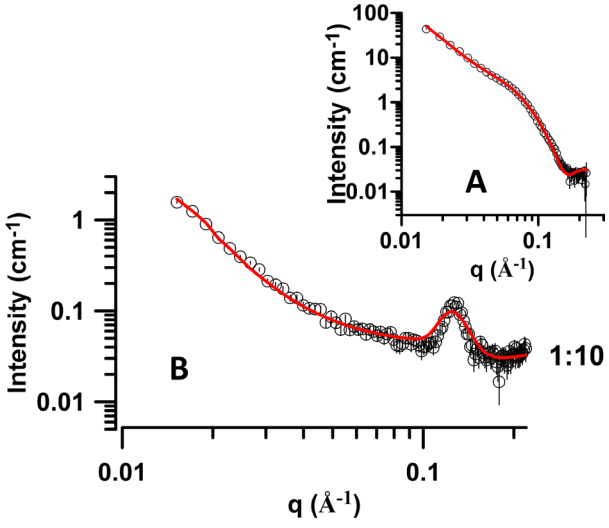

Figure 2. (A) SANS curves of POPE/POPG vesicles; (B) CAM–POPE/POPG at P:L = 1:10 mol/mol (POPE/POPG = 3:1 mol/mol). Full lines represent fitting curves.

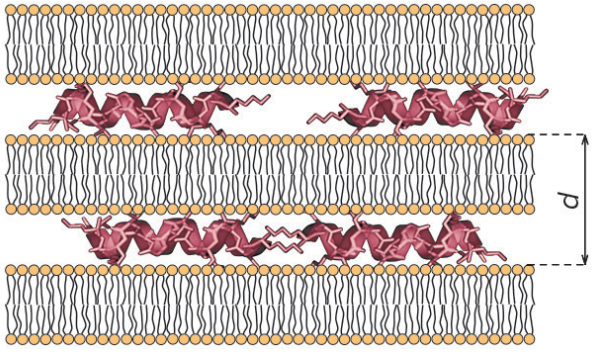

Figure 3. Multilamellar CAM–POPE/POPG structure identified at liquid crystalline state of the lipids (36 °C). d – repeat distance.

give the necessary information on the AMPs' ability to affect the structure and integrity of the membrane.

We studied the interaction of cecropin A–melittin (CAM, nominal charge +6), a hybrid peptide composed of the cationic region of cecropin A and the hydrophobic and non-haemolytic region of melittin with a bacterial model lipid membrane composed of zwitterionic palmitoyl-oleoyl-glycerophosphoethanolamine (POPE) and negatively charged palmitoyl-oleoyl-phosphoglycerol (POPG). SANS and SAXS were used to unravel the mechanism of the peptide antimicrobial activity as described in Silva et al. (2018). Fig. 2A depicts the normalised SANS intensity as a function of the scattering vector *q* of POPE/POPG oligolamellar vesicles with the lipid bilayer thickness being d_L ~ 39.4 Å. SANS data were analysed using SasView software. Fig. 2B shows the *I(q)* of CAM–POPE/POPG mixtures at P:L = 1:10 mol/mol and 36 °C. When the vesicle dispersion is mixed with the CAM peptide, a fine white precipitate spontaneously forms, suggesting massive aggregation and condensation of the lipid bilayers induced by the peptide. CAM interacts strongly with the negatively charged bilayer and induces extensive vesicle disruption, forming a condensed 'onion-like' multilamellar structure with repeat distance $d = 2\pi/q_0$ ~ 50.0 Å as derived from the maximum of the observed peak and confirmed by SAXS (not shown). Fig. 3 shows a sketch of the proposed multilamellar structure of CAM–POPE/POPG mixture. We propose that this peptide exerts its antimicrobial action through extensive membrane disruption, leading to cell death.

In another study (Silva et al., 2013), the bilayer composed of dimyristoylphosphatidylcholine/dimyristoylphosphoglycerol (DMPC/DMPG = 3:1 mol/mol) mimicking the membrane of *Candida albicans* interacted with AMP of the lactoferrin family (LFchimera, nominal charge +12). Fig. 4 shows the SAXS pattern of two bicontinuous cubic phases detected due to disintegration of the membrane by pore-forming mechanism. These results illustrate variedness in the antimicrobial mechanism of AMPs acting on the lipid membrane.

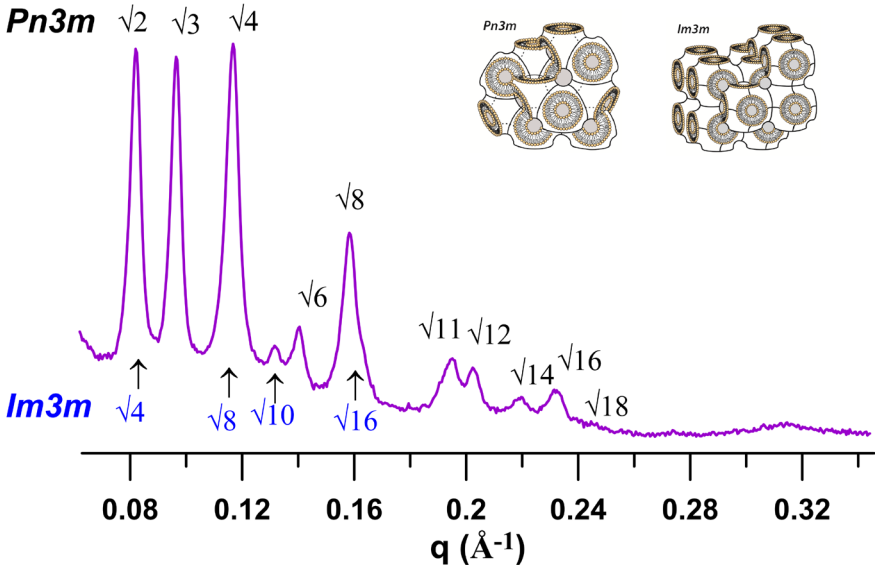

Figure 4. SAXS pattern of a mixture of LFchimera and DMPC/DMPG at P:L = 1:21 mol/mol (t = 24 °C). Peaks of detected cubic phases Pn3m (black) and Im3m (blue) are assigned to spacing $\sqrt{(h^2 + k^2 + l^2)}$, where h, k and l are Miller indices. Models of cubic phases of Pn3m and Im3m space group.

LIPID BILAYERS IN DNA DELIVERY SYSTEM

Lipoplexes are formed due to the electrostatic interaction between positively charged liposomes and DNA polyanion. Positively charged complexes show enhanced interaction with the negatively charged cytoplasmic membrane and, therefore, higher cellular uptake via endocytosis. However, for successful DNA delivery, lipoplexes must escape from the endosome inside the cell and DNA must be released from the complex in cytoplasm. High positive surface charge density of the lipoplex is crucial for a successful endosomal fusion. On the other hand, it can be an obstacle for DNA release from the complex. A way to overcome this problem is to use pH-sensitive surfactants with pK_a between 4.5 and 8. Acidic pH inside of endosome secures lipoplexes' fusion with the endosomal membrane. In the cytoplasm, at neutral pH, the surfactants are uncharged and DNA can be easily released from the lipoplex via dissociation.

We prepared pH-sensitive liposomes composed of homologues of series of *N,N*-dimethyl-alkane-1-amine *N*-oxides (C*n*NO, *n* = 8-18, where *n* is the number of carbon atoms in the alkyl substituent) (Devínsky et al., 1978) and neutral phospholipid dioleoylphosphatidylethanolamine (DOPE) at a molar ratio C*n*NO/DOPE = 0.4 and tested them for *in vitro* transfection activity. Several techniques (SAXS, UV–VIS, zeta potential measurements, confocal microscopy) were applied to characterise the system in an effort to unravel the relationship between the transfection efficiency, structure and composition of the lipoplexes (for details, see Liskayová et al., 2019). Fig. 5 summarises the most important findings underlining the connection between structural changes (studied by SAXS) and transfection activity.

In acidic conditions, DNA–C8NO/DOPE at C8NO/DOPE = 0.4 mol/mol forms a condensed inverted hexagonal phase (H_{II}^C). In this structure, the DNA strands are inserted in hexagonally arranged tubules created by the surfactant/lipid mixture (Fig. 1B). Note that the complexes prepared with C8NO keep their structure in neutral/alkaline solutions also. C*n*NOs with longer hydrophobic alkyl substituent, $n \geq 10$, induce structural changes. SAXS revealed the coexistence of two phases, condensed lamellar L_a^C phase and H_{II}^C in the complexes DNA–C*n*NO/DOPE, $n \geq 10$. Commensurate lattice parameters, the repeat distance d_{LC} of L_a^C phase and the lattice parameter of the H_{II}^C phase ($d_{LC} \approx a_{HC}$) indicate an epitaxial relationship, we abbreviate the structure as L_a^C & H_{II}^C. The connection through the common scattering plane facilitates the transition of the lipid between the two different structures. The structure changed in neutral/slightly alkaline solutions. A lamellar phase (L_a) is a dominant structure in all studied mixtures. In addition, SAXS patterns of complexes DNA-C*n*NO/DOPE, *n*=16 and 18, indicate the presence of a bicontinuous *Pn3m* cubic phase. The lattice parameter a_Q was found to be a_Q ~ 17–18 nm for detected cubic phases. Bicontinuous cubic phases (Q_{II}) are formed by a pair of interpenetrating, but non-contacting aqueous channels separated by a single, continuous lipid bilayer. Even if the lattice parameter of *Pn3m* is rather big (17–18 nm), three-dimensional arrangement of lipid bilayer in the cubic network requires its high negative curvature that might bring difficulties to accommodate bulky DNA molecules. To summarise, the change of pH from acidic to neutral induces phase transition $L_a^C \& H_{II}^C \rightarrow Q_{II} + L_a$, which allows DNA release from the lipoplexes.

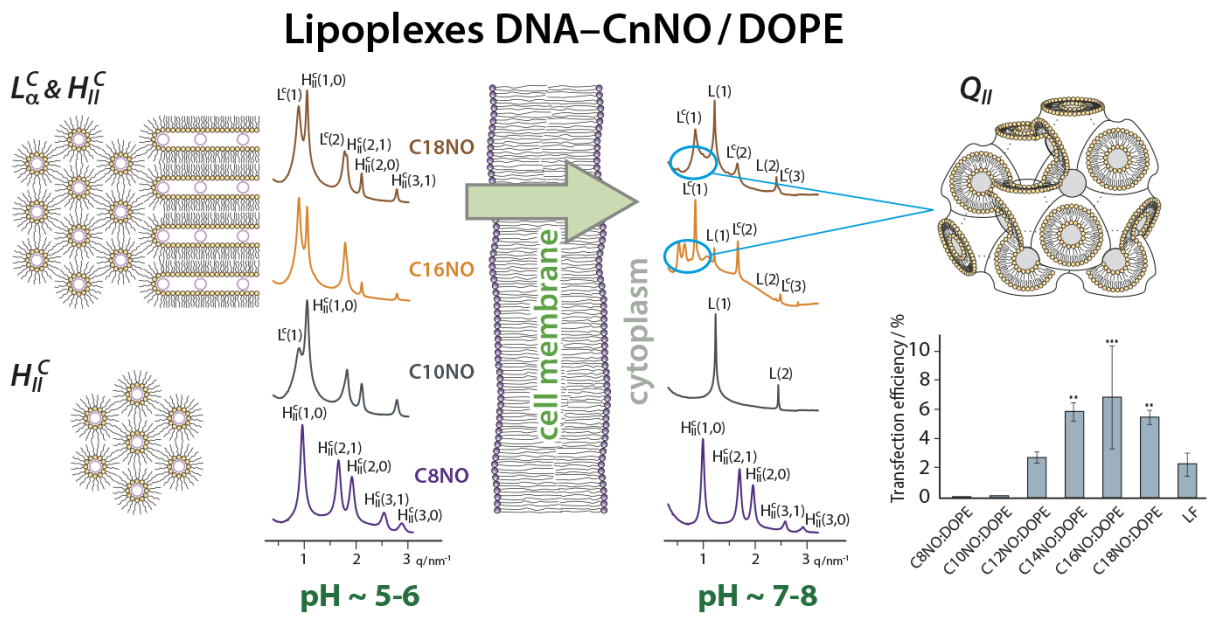

Figure 5. SAXS patterns of DNA–CnNO/DOPE complexes (n = 8, 10, 16 and 18) prepared at CnNO/DOPE = 0.4 mol/mol in aqueous solutions at acidic and neutral/slightly alkaline conditions, respectively. Transfection efficiency of CnNO/DOPE (n = 8–18) complexes tested on U2OS cells.

Transfection efficiency for plasmid DNA (pDNA, EGFP-N1) was tested on human bone osteosarcoma epithelial cells (U2OS line) and evaluated after 24 and 48 hours by flow cytometry. Commercially available Lipofectamine 2000 (LF) was used as a control. Transfection efficiency follows a quasi-parabolic dependence on the length of C*n*NO alkyl substituent *n*, with the maximum found at *n* = 16. The complex of C16NO/DOPE was found to be ~3 times more efficient than LF. Our findings support the hypothesis that the lipids of Q_{II} phase favour membrane pore formation resulting from fusion of the lipoplex cubic structure with endosomal membrane. Pores, in turn, allow for cytoplasmic gene delivery. Due to pH sensitivity of our lipoplexes, we can hypothesise synergy of two processes enhancing transfection: a massive release of DNA during $L_\alpha^C \& H_{II}^C \rightarrow Q_{II} + L_\alpha$ phase transition and its easier internalisation in the cell supported by the propensity of Q_{II} for pore formation.

LIPIDS AS A DRUG

Pulmonary surfactant (PS) is a surface active film lining the alveoli of the lung (Fig. 6A). Its principal function is to lower the surface tension at the air/liquid interface, facilitate the exchange of gasses and stabilise alveoli during breathing. PS is composed of ~90% lipids and 8%–10% of a few specific surfactant-associated proteins. Phospholipids predominate; saturated dipalmitoylphosphatidylcholine (DPPC) is the most abundant in PS of mammals, up to ~50% by mass. Unsaturated phosphatidylcholines (PC) create ~20% and a smaller fraction (~10%) of anionic species such as POPG. A high content of DPPC plays a key function to reach the necessary, extremely low surface tension (<1 mN/m). Hydrophilic SP-A, SP-D and hydrophobic SP-B, SP-C are surfactant-associated specific proteins. SP-B is crucial for proper spreading of the lipid interfacial monolayer. The surface active function of PS is critically dependent on the existence of a multilayered film (~100 nm in thickness) at the air–water interface. An inactivation, deficiency or an absence of PS results in respiratory distress syndrome (RDS) that can be lethal for premature babies. RDS is therapeutically treated by application of PS preparations obtained from animals (exogenous natural), like porcine Curosurf® or bovine Survanta®.

The exogenous natural PS contains at least 50 different phospholipids and a small fraction of hydrophobic proteins (~1–2 wt%) (Calkovska et al., 2016). Morphologically, it is a mixture of various vesicles, from unilamellar through oligolamellar up to multilamellar.

We studied the effect of bacterial toxin, lipopolysaccharide (LPS), on the structure of clinically modified porcine pulmonary surfactant, mimicking pathological conditions. Consecutively, Polymyxin B (PxB), a cyclic amphiphatic antibiotic, was applied. Fig. 6B shows the SAXS patterns of modified porcine surfactant at 37 °C when the mixture is in liquid crystalline state (fluid phase). Two peaks (*L1* and *L2*) belong to a lamellar phase with repeat distance *d* ~ 8.35 nm. LPS affects the multilamellar packing of PS. Longer incubation (~2 hours) generates a large swelling up, which corresponds to a SAXS pattern of large unresolved peak of low intensity with a subtle shoulder at low *q* ~ 0.5 nm^{-1}. The pattern indicates

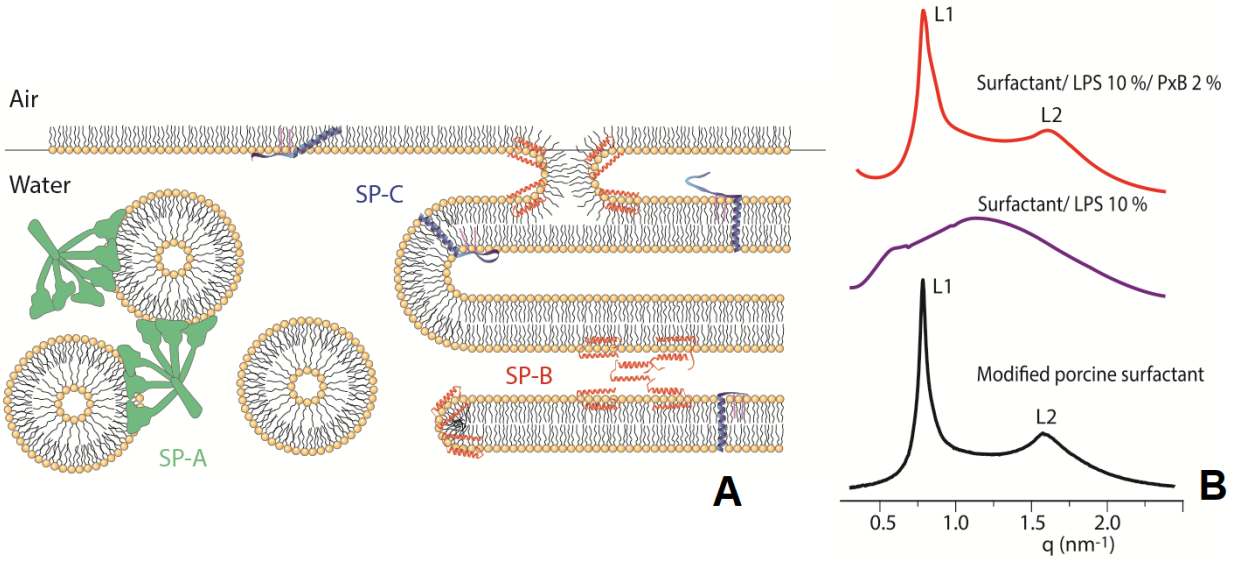

Figure 6. (A) Schematic representation of pulmonary surfactant; (B) SAXS pattern of modified porcine surfactant, surfactant incubated with 10% of LPS for 2 hours and surfactant/LPS 10% with addition of 2% of PxB (at 37 °C).

swelling of a lamellar phase up to periodicity ~12–13 nm. We attribute these structural changes to the PS surface charge unbalance due to LPS insertion. Consecutively, damaged surfactant/LPS 10% was incubated with peptide-based antibiotic PxB. We found that even a small dose of the cationic antibiotic reduces the repeat distance. PS/LPS incubated with 0.5% of PxB for 30 min reduced the repeat distance to $d \sim 8.6$ nm (not shown). Cationic molecule of PxB acts as an inhibitor of structural disarrangement induced by LPS and restores original lamellar packing. Structural changes were confirmed also by optical microscopy.

The study was focused on the mechanism underlying the structural changes in surface-reducing features (for details, see Kolomaznik et al., 2018). The function of 'infected' and consecutively 'treated' PS was tested with pulsating bubble surfactometer. The infected PS (surfactant/LPS 10%) was not able to reach the necessary physiologically relevant low surface tension. Intriguingly, the minimal surface tension decreased alongside with structural recovery when applying PxB (Kolomaznik et al., 2018). The obtained results accurately reflect the situation with a native lung surfactant as confirmed by a recent *in vivo* study (Calkovska et al., 2021) and support the idea of PxB/Curosurf combined therapy in neonatal medicine.

CONCLUDING REMARKS

Amphiphilic molecules of lipids and surfactants self-assemble into structures of various morphologies ranging from micelles, lamellar and non-lamellar phases to microemulsions. Each of these morphologies possesses its own unique physical properties and offers the possibility for pharmaceutical applications. In the text above, we demonstrated just a few examples of 'usability' of phospholipid bilayers: as a model membrane mimicking the lipid bilayer of bacterial membrane in an effort to unravel the mechanisms of AMPs' antimicrobial activity, as a carrier designed for genetic material delivery, and finally, a lipid mixture extracted from animal's lungs that is clinically used in neonatal medicine. Findings presented here result from the collaboration between several institutions and have been published to the full extent in Kolomaznik et al. (2018), Liskayová et al. (2019), Silva et al. (2013) and Silva et al. (2018).

ACKNOWLEDGEMENTS

The author thanks all the co-authors in references (Kolomaznik et al., 2018; Liskayová et al., 2019; Silva et al., 2013, 2018) for their fruitful collaboration. SAXS experiments were performed at BL11-NCD-SWEET beamline at Alba Synchrotron, Barcelona with the collaboration of ALBA staff and at A2 beamline, Doris synchrotron in Hamburg. The research leading to these results has received funding from the JINR project 04-4-1142-2021/2025 and grants from VEGA 1/0223/20, APVV-17-0250 and SK-PT-18-0032.

References

[1] Calkovska A, Haegerstrand-Björkman M, Curstedt T. Restoration of surfactant activity by polymyxin B in lipopolysaccharide potentiated injury of immature rabbit lungs. Scientific Reports 2021; 11: 22

[2] Calkovska A, Linderholm B, Haegerstrand-Björkman M, Pelizzi N, Johansson J, Curstedt T. Phospholipid composition in synthetic surfactants is important for tidal volumes and alveolar stability in surfactant-treated preterm newborn rabbits. Neonatology 2016; 109: 177-185

[3] Devínsky F, Lacko I, Nagy A, Krasnec Ľ. Amine oxides. I. Synthesis, 1H-n.m.r., and Infrared spectra of 4-alkylmorpholine-N-oxides. Chem. Pap. 1978; 32:106-115

[4] Israelachvili JN, Mitchell DJ, Ninham BW. Theory of self-assembly of hydrocarbon amphiphiles into micelles and bilayers. J. Chem. Soc. Faraday Trans 2, Mol. Chem. Phys. 1976; 72:1525-1568

[5] Kobayashi T, Tsukagoshi S, Sakurai K. Enhancement of the cancer chemotherapeutic effect of cytosine arabinoside entrapped in liposomes on mouse leukemia L-1210. Gann 1975; 66:719-720

[6] Kolomaznik M, Liskayova G, Kanjakova N, Hubcik L, Uhrikova D, Calkovska A. The perturbation of pulmonary surfactant by bacterial lipopolysaccharide and its reversal by Polymyxin B: function and structure. Int. J. Mol. Sci. 2018; 19: 1964

[7] Liskayová G, Hubčík L, Búcsi A, Fazekaš T, Martínez JC, Devínsky F, Pisárčik M, Hanulová M, Ritz S, Uhríková D. pH-sensitive N,N-dimethylalkane-1-amine N-oxides in DNA delivery: from structure to transfection efficiency. Langmuir 2019; 35: 13382-13395

[8] Silva T, Adao R, Nazmi K, Bolscher JGM, Funari SS, Uhríková D, Bastos M. Structural diversity and mode of action on lipid membranes of three lactoferrin candidacidal peptides. Biochim. Biophys. Acta 2013; 1828:1329-1339

[9] Silva T, Claro B, Silva BFB, Vale N, Gomes P, Gomes MS, Funari SS, Teixeira J, Uhríková D, Bastos M. Unravelling a mechanism of action for a cecropin -A-Mellitin hybrid antimicrobial peptide: the induced formation of multilamellar lipid stacks. Langmuir 2018; 34:2158-2170

[10] Teixeira V, Feio MJ, Bastos M. Role of lipids in the interaction of antimicrobial peptides with membranes. Prog. Lipid Res. 2012; 51:149–177.

sciendo

Eur. Pharm. J. 2021, 68(1), 72-75.
ISSN 1338-6786 (online) and ISSN 2453-6725 (print version),
DOI: 10.2478/afpuc-2021-0003

EUROPEAN PHARMACEUTICAL JOURNAL

Formulation And Evaluation of Tablets Compressed from Granules Prepared by Thermoplastic Granulation

Special Issue Article

Kľoc D., Wolaschka T.✉, Ruttkay F.

Department of Pharmaceutical Technology, Pharmacognosy and Botany, University of Veterinary Medicine and Pharmacy in Košice, Komenského 73, 041 81 Košice, Slovak Republic

Received 15 June, 2021, accepted 17 June, 2021

Abstract The aim of this formulation study was to determine the effect of the binder used in the preparation of granules by thermoplastic granulation on the release of propranolol from experimental tablets. Another aim was to select suitable excipients and their ratio in the granules to ensure a trouble-free formulation of the tablets. This study proved that the binder affects the flow properties of the granules, disintegration of the tablets and, subsequently, also the method of drug release, which can be used for the preparation of tablets with modified or prolonged drug release.

Keywords *thermoplastic granulation– propranolol dissolution – polyethylene glycol – cetyl stearyl alcohol*

INTRODUCTION

The granulation technique and the binder have an essential influence not only on the granules properties, but also on the properties of the final dosage form. Thermoplastic granulation is a process in which solid particles are converted into agglomerates in the presence of a molten binder. Upon cooling, the binder solidifies again and forms solid bridges between the powder particles. By choosing the right binder material, it is possible to effectively influence the dissolution profile of the final product. When using hydrophilic binders, e.g., polyethylene glycols or poloxamers, a formulation with immediate release is obtained. Instead, lipophilic binders, like waxes, fatty acids or fatty alcohols, are used for manufacturing controlled-release formulations (Keen et al., 2015; Mamidi et al., 2021; Steffens et al., 2020). The aim of this formulation study was to determine the effect of the binder used in the preparation of granules by thermoplastic granulation on the release of propranolol from experimental tablets. Another aim was to select suitable excipients and their ratio in the granules to ensure a trouble-free formulation of the tablets.

MATERIALS AND METHODS

Chemicals

Propranolol (Fagron, Olomouc, Czech Republic), polyethylene glycol 1500 (PEG 1500) (Fagron), cetyl stearyl alcohol (CSA) (Fagron), colloidal silicon dioxide (CSD) (Fagron), lactose (LAC) (Dr. Kulich Pharma, Hradec Králové, Czech Republic), microcrystalline cellulose (MCC) (Centralchem, Bratislava, Slovakia), concentrated hydrochloric acid (HCl) (Centralchem), potassium dihydrogen phosphate (KH_2PO_4) (Centralchem), stearic acid (Galvex, Banská Bystrica, Slovakia), sodium hydroxide (NaOH) (Mikrochem, Pezinok, Slovakia)

Granule preparation

Materials sifted through a 1.00-mm sieve were homogenised in a ceramic mortar with a rough base and a ceramic pestle. The granulation mixture was melted for 30 minutes at 80 °C in a Memmert UNB400 oven (Memmert, Schwabach, Germany). The mixture was stirred every 10 minutes. After cooling, the granulation mixture was extruded through a sieve with a mesh size of 1 mm. CSD and stearic acid were added extragranular to the resulting granules as glidants and anti-adhesives. This way, we prepared four types of granules, A3, A4, B3 and B4, with the composition given in Table 1.

Determination of flowability

Fifty grams of granules was poured loosely into the hopper of Erweka GDT (ERWEKA GmbH, Heusenstamm, Germany). After start-up, the instrument recorded the time it took for

* *E-mail: tomas.wolaschka@uvlf.sk*

Table 1. Composition of granules in percentages by weight.

	A3 (%)	A4 (%)	B3 (%)	B4 (%)
LAC	33	28	33	28
MCC	33	28	33	28
PEG 1500	28	38	-	-
CSA	-	-	28	38
Stearic acid	1.5	1.5	1.5	1.5
CSD	1.5	1.5	1.5	1.5
Propranolol	3	3	3	3

the sample to flow. The measurement was repeated 3 times for each sample.

Determination angle of repose

Fifty grams of granules was poured continuously onto the inside of the funnel, which was placed 4 cm above the presumed top of the cone. The granules was allowed to flow freely on a solid base. The height (*h*) and the radius (*r*) of the resulting cone were measured and the angle of repose was calculated using Equation 1. The test was repeated 3 times for each sample.

$$\alpha = arc\ tg\ \frac{h}{r}\ [°] \quad (1)$$

Carr compressibility index and Hausner ratio

One hundred millilitres (V_0) of granules was poured freely into the measuring cylinder and its weight was measured. Subsequently, 10, 50 and 100 taps on the solid surface were performed, after which the compacted volume (V_f) was recorded. Based on the values V_0 and V_f after 100 taps, the compressibility index was calculated using Equation 2 and the Hausner ratio was calculated using Equation 3. The test was repeated 3 times with each sample.

$$\text{Carr compressibility index} = 100\frac{V_0 - V_f}{V_0} \quad (2)$$

$$\text{Hausner ratio} = \frac{V_0}{V_{100}} \quad (3)$$

Tablet preparation

Tablets were compressed on a Romaco AM 8 rotary press (Romaco, Milan, Italy). The compression pressure was approximately 85 MPa for all granules. The height of the upper die was set to 15 mm.

Weight uniformity of tablets

Weight uniformity of the prepared tablets was performed according to the European Pharmacopoeia 10.5 (European Pharmacopoeia, 2010).

Tablet disintegration

Tablet disintegration was evaluated using Erweka ZT3-2 (ERWEKA GmbH). One tablet was placed in each of the six tubes of the device and the medium was placed in a beaker. Also, 0.1 mol/l HCl and phosphate buffer with pH 6.8 were used as media. The whole system was tempered to 37 °C. In both media, the test was run for 60 minutes at a frequency of vertical movement of the hanging device with 30 oscillations per minute.

Basket tablet dissolution

A Hanson SR8 PLUS dissolution device (Teledyne Hanson Research, Chatsworth, CA, USA) was used to dissolve the tablets. The device consists of eight containers and baskets. Seven propranolol tablets were placed in the baskets, one on each basket. A tablet with the same excipients but without the drug was placed in the last one. The distance between the basket and the inner bottom of the container was 25 mm. The baskets with the tablet rotated about their own axis at a speed of 50 turns per minute. The whole system was tempered to 37 °C. At intervals of 5, 10, 15, 22, 30, 42, 55 65, 70, 75, 82, 105, 120, 180, 240, 300, 360, 540, 720 and 1440 minutes, 2 ml of solution was collected from each of the eight vessels using a syringe with a needle into the prepared microtubes. The missing 2 ml of solution was replaced with pure dissolution liquid. The dissolution medium consisted of 750 ml of 0.1 mol/l HCl, to which a mixture of 46 ml of 0.2 mol/l NaOH, 200 ml of 0.2 mol/l KH_2PO_4 and 4 ml H_2O was added after 60 minutes of dissolution. The amount of propranolol in the samples was determined spectrophotometrically at a wavelength of 290 nm with the spectrophotometer Cary 60 (Agilent technologies, Santa Clara, CA, USA). Korsmeyer–Peppas dissolution model was used to describe the release kinetics from the tablets.

RESULTS AND DISCUSSION

In this formulation study, four types of granules were prepared by thermoplastic granulation. Granules A3 and A4 contained PEG 1500 and granules B3 and B4 contained CSA as the binder. PEGs are stable hydrophilic substances that are widely used in different types of pharmaceutical formulations, including parenteral, topical, ophthalmic, oral and rectal dosage forms. In solid drug formulations, PEGs with high molecular weight are used as binders in granulation to provide strength and plasticity to the granules. At high concentrations, they have the ability to prolong disintegration, which can be used to prepare dosage forms with delayed disintegration time. On the other hand, CSA is a lipophilic mixture of solid aliphatic alcohols consisting mainly of stearyl alcohols and cetyl alcohols. CSA is used mainly in cosmetics and topical pharmaceuticals. In addition, CSA can be used to control or slow the dissolution rate of tablets containing well or sparingly water-soluble drugs (Rowe et al., 2009).

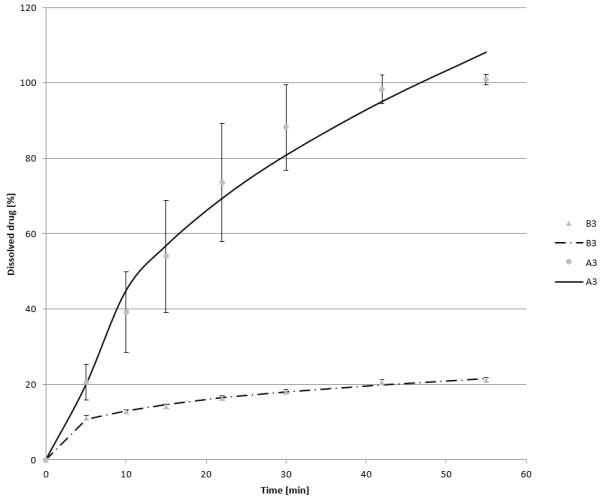

Figure 1. Dissolution profile of tablets A3, B3 in the acidic medium.

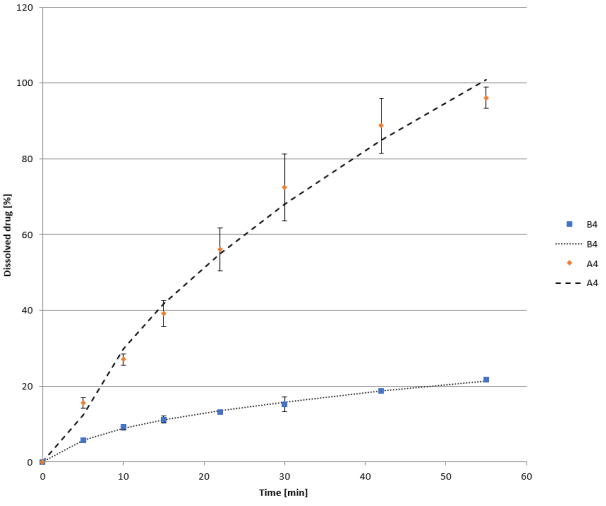

Figure 2. Dissolution profile of tablets A4, B4 in the acidic medium.

The prerequisites for tablet compression without technological problems are good flow properties of the powders or granules. Therefore, in this study, extragranular excipients were added to the base granules. CSD, which is widely used in the manufacture of powders, capsules and tablets, has been used as a lubricant; while it improves the flow properties of powders, it also has a beneficial effect on the mechanical properties and disintegration of tablets. Stearic acid was used to prevent the tablet from sticking to the dies (Jonat et al., 2006, Komárek et al., 2006). After addition of extragranular excipients, the flowability of samples A3, A4, B3 and B4 was 6.60 ± 0.00, 15.73 ± 0.3, 6.93 ± 0.23 and 15.47 ± 0.42 seconds. It follows that the flowability was affected by the amount of binder and not its character. Angle of repose of samples A3, A4, B3 was 34.14° ± 0.04°,

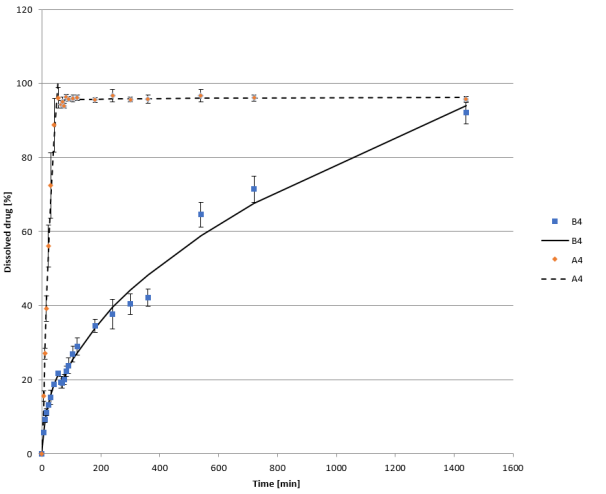

Figure 3. Dissolution profile of tablets A3, B3 during the whole time dissolution.

34.81° ± 0.00°, 35.09° ± 0.05°, which represents good flow properties of the granules. For sample B4 with the angle of repose 36.57° ± 0.01°, the flow property was adequate. The Carr compressibility index of samples A3, A4, B3 and B4 was 9%, 10%, 15% and 11% and the Hausner ratio was 1.10, 1.11, 1.18 and 1.12. These values show that the flow character was excellent in samples A3 and A4, good in sample B3 and adequate in sample B4.

The preparation of tablets from these granules did not cause technological problems, the dies were filled sufficiently, and there was no sticking of the tablets to the walls of the die and the surface of the dies. At the same press setting, the average weight of the tablets was A3, A4, B3, B4, 567, 534, 628 and 629 mg. Each batch of tablets passed the weight uniformity test, where the average deviation for all types of tablets was between 1% and 2%. In the disintegration test, tablets A3, A4 and B3 disintegrated completely in HCl as well as in buffer within 60 minutes. B4 tablets retained their shape in both liquids throughout the test.

Dissolution profiles clearly showed that the drug was released significantly faster from tablets A3 and A4, for which the release half-life was calculated to be 12.56 ± 6.10 and 19.10 ± 2.31 minutes. The faster drug release was due to the hydrophilic properties of PEG. In the aqueous solution, water was transferred to PEG, which led to disintegration of the tablets. In contrast, the release half-life of propranolol for tablets B3 and B4 was 186.17 ± 9.90 and 332.44 ± 27.47 minutes. Due to the lipophilicity of CSA, the drug was released gradually because the dissolution fluid transfer was not accelerated by the hydrophilicity of the binder. The difference in the release rate of propranolol depending on the binder is clearly seen on the dissolution curves in acidic HCl medium (Figs 1 and 2) and during the whole dissolution time (60 minutes HCl + remaining time in phosphate buffer with pH 6.8) as shown in the graphs in Figs 3 and 4.

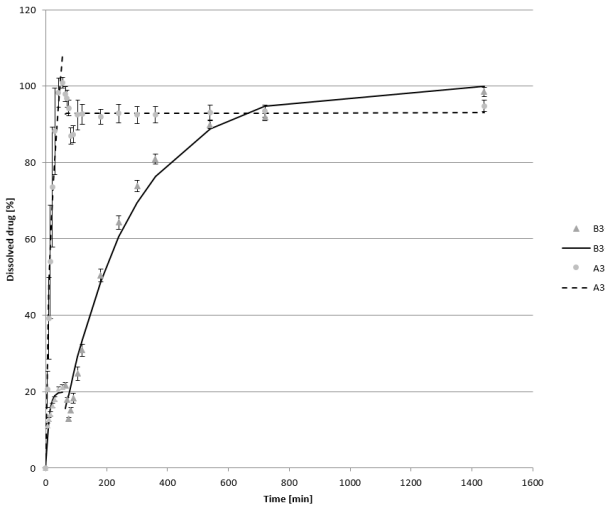

Figure 4. Dissolution profile of tablets A4, B4 during the whole time dissolution.

The effect of binder concentration on the release of propranolol from tablets was evaluated using a difference factor (f_1) and a similarity factor (f_2). The difference factor (f_1) measures the percent error between two curves over all time points. The percent error is zero when the test and drug reference profiles are identical and increases proportionally with the dissimilarity between the two dissolution profiles. The similarity factor is a logarithmic transformation of the sum-squared error of differences between the test and reference samples over all time points. The f_2 can take values between 0 and 100. A value of 100 means that the dissolution profiles are identical and a value of 0 indicates a complete mismatch in the dissolution profiles. The similarity factor and the difference factor were adopted by the Food and Drug Administration (FDA) and the European Medicines Agency (EMA) as a criterion for assessing the similarity between two in vitro dissolution profiles. The FDA and the EMA consider the dissolution profiles to be similar if f_1 is less than 15 and f_2 is greater than 50 (Costa and Sousa Lobo, 2001). When comparing samples A4 (reference sample) and A3 (test sample), the value of f_1 was 7.77 ± 2.66 and f_2 was 54.47 ± 9.89. It follows that the drug release from these samples is similar. From this, it can be concluded that the concentration of PEG 1500 did not have a significant effect on the release of propranolol from the experimental tablets. When comparing the dissolution profiles of tablets B3 (test sample) and B4 (reference sample), the values of f_1 and f_2 were 26.87 ± 1.64 and 41.18 ± 1.65, which differs slightly from the values at which it can be argued that the dissolution profiles are similar. Based on these values, it can be concluded that the concentration of CSA slightly affects the release of propranolol from the experimental tablets.

This formulation study has shown that the character and concentration of the binder affects the properties of the granules and tablets. The binder affects the flow properties of granules, disintegration of the tablets and, subsequently, also the method of drug release, which can be used for the preparation of tablets with modified or prolonged drug release.

ACKNOWLEDGMENT

The work was designed thanks to the support provided by the project from the structural fund, "Renewal of research and development infrastructure and instrumentation at UVLF, ITMS 26210120028."

References

[1] Costa P, Sousa Lobo JM. Modeling and comparison of dissolution profiles. Vol. 13, European Journal of Pharmaceutical Sciences. Elsevier; 2001. p. 123–33.

[2] European Pharmacopoeia. Uniformity of mass of single-dose preparations. Eur Pharmacopoeia. 2010;(1):291–2.

[3] Jonat S, Albers P, Gray A, Schmidt PC. Investigation of the glidant properties of compacted colloidal silicon dioxide by angle of repose and X-ray photoelectron spectroscopy. Eur J Pharm Biopharm. 2006;63(3):356–9.

[4] Keen JM, Foley CJ, Hughey JR, Bennett RC, Jannin V, Rosiaux Y, et al. Continuous twin screw melt granulation of glyceryl behenate: Development of controlled release tramadol hydrochloride tablets for improved safety. Int J Pharm [Internet]. Elsevier B.V.; 2015;487(1–2):72–80. Available from: http://dx.doi.org/10.1016/j.ijpharm.2015.03.058

[5] Komárek P, Rabišková M, Chalabala M, Kopecký F, Vitková M, Řehula M, et al. Technologie léku. Praha: Galén; 2006.

[6] Mamidi HK, Palekar S, Nukala PK, Mishra SM, Patki M, Fu Y, et al. Process optimization of twin-screw melt granulation of fenofibrate using design of experiment (DoE). Int J Pharm [Internet]. Elsevier B.V.; 2021;593(September 2020):120101. Available from: https://doi.org/10.1016/j.ijpharm.2020.120101

[7] Rowe RC, Sheskey PJ, and Owen SC. Handbook of pharmaceutical excipients. London: Pharmaceutical Press; 2006.

[8] Steffens KE, Brenner MB, Hartig MU, Monschke M, Wagner KG. Melt granulation: A comparison of granules produced via high-shear mixing and twin-screw granulation. Int J Pharm [Internet]. Elsevier B.V.; 2020;591(March):119941. Available from: https://doi.org/10.1016/j.ijpharm.2020.119941

sciendo

Eur. Pharm. J. 2021, 68(1), 76-79.
ISSN 1338-6786 (online) and ISSN 2453-6725 (print version),
DOI: 10.2478/afpuc-2021-0009

EUROPEAN PHARMACEUTICAL JOURNAL

Purification of Murine Gammaherpesvirus 68 With Use of Differential Centrifugation

Special Issue Article

Hodoši R.[1], Nováková E.[1,2], Šupolíková M.[1,3]✉

[1]Department of Microbiology and Virology, Faculty of Natural Sciences, Comenius University in Bratislava, Ilkovičova 6, Mlynská dolina, 842 15, Bratislava, Slovak republic
[2]Slovak Academy of Sciences, Biomedical Research Center, Institute of Virology, Dúbravská cesta 9, 845 05 Bratislava, Slovak republic
[3]Department of Galenic Pharmacy, Faculty of Pharmacy, Comenius University in Bratislava, Odbojárov 10 832 32 Bratislava 3, Slovak Republic

Received 14 June, 2021, accepted 17 June, 2021

Abstract The method for separation of viral particles in a concentrated form from the environment is called virus purification. Viruses are required to be purified for a range of studies in which it is necessary to distinguish the properties or structure of a virus from the host cells or culture media, including analysis of viral polypeptide structures and membrane glycoprotein function. Our objective was to purify murine gammaherpesvirus 68 (MHV-68, MuHV-4) using the centrifuge, equipment and other materials available in our laboratory. After infection of baby hamster kidney 21 (BHK-21) cells with MHV-68 with the multiplicity of infection (MI) of 0.01 and following virus multiplication, we repeatedly froze and thawed the cell culture to disrupt the cells and release the virus particles into the culture medium. We used low-speed centrifugation (3000 rpm at 4°C) to separate the viral particles from cell debris. Subsequently, we transferred the supernatant containing virus particles to a fresh centrifuge tube and centrifuged at a speed of 8000 rpm (8801 *g*) and 11,000 rpm (=16,639 *g*) and at 4°C. We tested different centrifugation durations of 2, 4, 6 and 8 hours. To evaluate the quality of the obtained purified MHV-68 virus by this method and compare it to purified MHV-68 sample acquired by conventional ultracentrifugation on sucrose cushion (30%, w/v), we used the SDS-PAGE separation method using a 4%–20% (w/v) and 6%–14% (w/v) gradient gel. We obtained the best results with 6-hour-long centrifugation at 11,000 rpm. In conclusion, we managed to optimise virus purification method using the equipment available in our laboratory and prepared purified MHV-68 virus in sufficient concentration for determination of MHV-68 virus proteins.

Keywords *MHV-68 – purification – virus proteins – SDS-PAGE*

INTRODUCTION

The aim of the virus purification method is to separate it from all particles of cellular origin and culture media (Mistríková *et al.*, 2016). Viruses need to be purified for many studies in which it is necessary to distinguish the properties or structure of a virus from the properties or structure of host cells (or culture media), such as analysis of the structure of viral polypeptides or the function of membrane glycoproteins (Killington *et al.,* 1996). Differential (ultra)centrifugation (Fig. 1) is a common technique used to purify particles of defined size (i.e., virions). It is based on differences in the sedimentation rate of particles in suspension, which depends not only on their size, density and morphology, but also on the properties of the medium in which the virions are located and the force applied during centrifugation (Killington *et al.,* 1996; Taulbe and Furst, 2005). By using a density gradient centrifugation technique (particle separation is achieved by density gradient sedimentation), it is possible to achieve a more accurate separation of biological particles of similar dimensions but different densities. A large number of gradient materials are available, such as various dextrans and sucrose, or commercially available, for example, Percoll, Ficoll and others (Taulbe and Furst, 2005). The aim of our experimental work in the presented paper was to prepare purified murine gammaherpesvirus 68 (MHV-68, MuHV-4) propagated on the stabilised baby hamster kidney 21 (BHK-21) cell line and use it for further research. Using laboratory instrumentation, ultracentrifuge and other necessary materials available in our laboratory, we performed and optimised the MHV-68 purification method.

* *E-mail: hodosi3@uniba.sk*

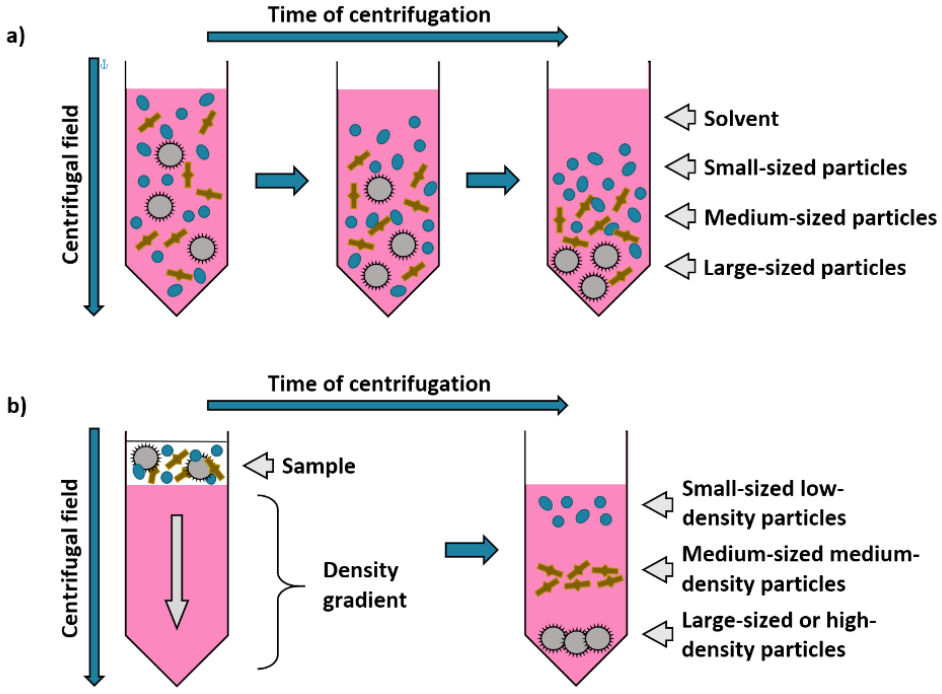

Figure 1. Diagram of particle behaviour during differential centrifugation and density gradient centrifugation. a) During the differential centrifugation of a suspension of particles in a centrifugal field, the movement of the particles depends on their density, shape and size. b) To separate the biological particles by means of a density gradient, the samples are layered on the prepared gradient before centrifugation. To achieve separation, the sample is centrifuged, until the isopycnic position for the desired particles in the gradient is achieved.

MATERIALS AND METHODS

We used baby hamster kidney 21 (BHK-21) cells to propagate MHV-68 virus. Cells were cultured in Dulbecco's Modified Eagle Medium **(**DMEM) medium (Lonza, Belgium) supplemented with 7% fetal bovine serum (FBS; Sigma Aldrich, USA), 1% PSA (antibiotics – 100 U/ml penicillin–streptomycin and 100 µg/ml amphotericin) and 1% glutamine (Sigma Aldrich, USA) at 37°C in the presence of 5% CO^2. After virus adsorption, we replaced DMEM with 7% FBS with DMEM with 2% FBS. Cells were infected with MHV-68 virus at a multiplicity of infection of 0.1 and cultured until a cytopathic effect was developed. The virus/cell suspension was frozen and thawed 3 times (–80°C). We transferred the virus–medium solution from the culture flasks to 50-ml centrifuge tubes and centrifuged for 30 min at 2000 rpm at 4°C (low-speed centrifugation to remove cell debris). After centrifugation, we transferred the supernatant to a new centrifuge tube and centrifuged. We tested four different durations of 2, 4, 6 and 8 hours and two different centrifugation speeds of 8000 rpm (8801 *g*) and 11,000 rpm (16,639 *g*) at 4°C in an Eppendorf 5804 R centrifuge with an FA-45-6-30 rotor – primary high-speed centrifugation. After this centrifugation, we removed the supernatant, resuspended the pellet in 25 ml phosphate-buffered saline (PBS) and centrifuged for 2 hours at 11,000 rpm (16,639 *g*) at 4°C (secondary high-speed centrifugation) in an Eppendorf 5804 R centrifuge with an FA-45-6-30 rotor. After removing the supernatant, we resuspended the virus pellet in 1 ml PBS, filled into microtubes in volume of 100 µl and froze at –80°C. The purification process is schematically shown in Fig. 2.

To evaluate the quality of the obtained samples, we used the sodium dodecyl sulphate–polyacrylamide gel electrophoresis (SDS-PAGE) separation method using a gradient gel. To create a gradient separating gel, we prepared two bis-acrylamide solutions with different densities: one with the lowest gradient density (4% w/v and 6% w/v) and the second one with the highest gradient density (20% w/v and 16% w/v). Following this, we drew up the lower density solution (4% w/v and 6% w/v) into a serological pipette and then a higher density solution (20% w/v and 16% w/v) in the ratio of 1:1. The total volume must correspond to the volume of the gel cast (BioRad mini-PROTEAN gel cast has a volume of 5 ml). Next, we drew up approximately 1 ml of air into the serological pipette containing gel solutions and allowed the air bubble to ascend to the surface. The air bubble travel mixes the solution and forms a density gradient within pipette. Lastly, we applied the solution to the cast evenly and overlaid it with 99.6% w/v isopropanol and let it polymerise.

RESULTS AND DISCUSSION

For viral protein separation, we used gradient SDS-PAGE in the density range of 4%–20% (w/v) and 6%–16% (w/v),

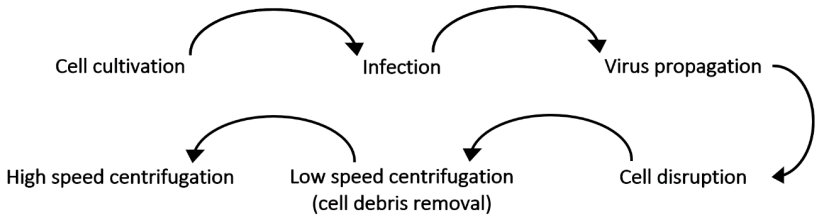

Figure 2. Schematic diagram of virus purification steps.

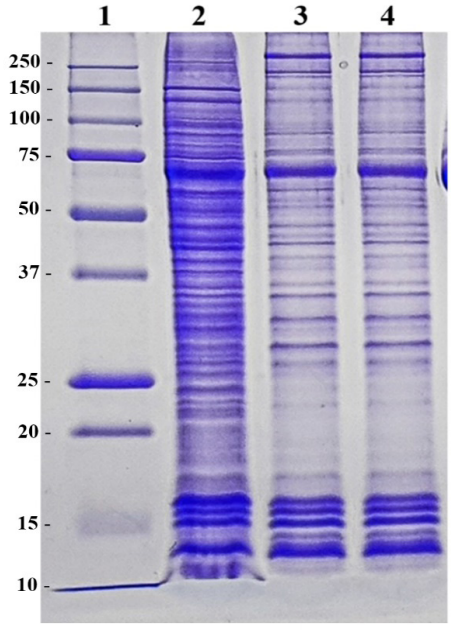

Figure 3. Polypeptide profile of purified MHV-68 in gradient SDS-PAGE (6%–14%, w/v). Lane 1: ladder (Precision Plus Protein™ Dual Xtra); lane 2: purified MHV-68 (centrifuged 6 hours) – 10 µl/lane; lane 3: purified MHV-68 (centrifuged 6 hours) – 5 µl/lane; lane 4: purified MHV-68 (centrifuged 6 hours) – 3 µl/lane.

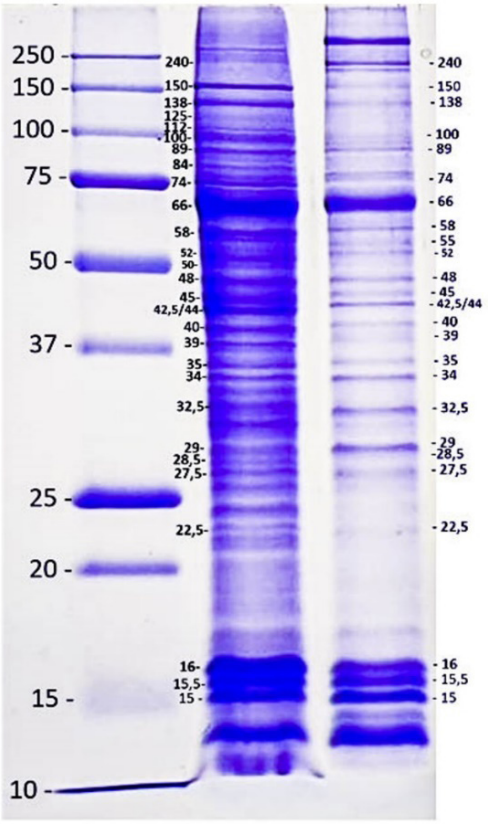

Figure 4. Molecular weights (in kDa) of viral proteins of purified MHV-68, gradient SDS-PAGE (6%–14% w/v). Lane 1: ladder (Precision Plus Protein™ Dual Xtra); lane 2: purified MHV-68 (centrifuged 6 hours) – 12 µl/lane; lane 3: purified MHV-68 (centrifuged 6 hours) – 6 µl/lane.

considering the large range of molecular weights of the individual MHV-68 proteins (from 15 to 240 kDa). Samples obtained by centrifugation at 8000 rpm were unsuitable for further analysis due to insufficient concentration of MHV-68 proteins (data not shown). We obtained improved results by increasing the centrifugation speed to 11,000 rpm. Centrifugation of 2 and 4 hours was not sufficient to concentrate the virus in the pellet (data not shown). By extending the centrifugation interval to 6 hours, we obtained MHV-68 purification at a sufficient concentration, resulting in a polypeptide profile of viral proteins of specific size. We applied purified MHV-68 after 6-hour-long centrifugation at 11,000 rpm in various volumes on gradient SDS-PAGE with a density range of 6%–14% (w/v) (Fig. 3). Protein profile of purified murine gammaherpesvirus obtained by ultracentrifugation on sucrose cushion (Reichel *et al.*, 1991) was comparable to MHV-68 purified by our method (after 6-hour-long centrifugation at 11,000 rpm).

The next step was to determine the approximate molecular weight (in kDa) of the viral proteins of the obtained purified MHV-68. Fig. 4 shows in more detail the protein profile of the obtained purified MHV-68. We determined the molecular weight of individual proteins according to Reichel et al. (1991). In conclusion, we were able to prepare purified MHV-68 virus and determine the approximate molecular weight of viral proteins using available instruments and methods in our laboratory. We obtained the best results with primary centrifugation duration of 6 hours at a centrifugation speed of 11,000 rpm (16,639 *g*) at 4°C (in our case, 6 hours of primary and 2 hours of secondary high-speed centrifugation was sufficient to purify MHV-68 virus).

ACKNOWLEDGMENT

This research was carried out with the financial support from VEGA 1/0061/18 and UK/240/2021.

References

[1] Mistríková M., Stančeková M., Kostrábová A. (2016) Základné laboratórne techniky používané vo virológii. 3. prepracované vydanie, Bratislava, Univerzita Komenského, strany 39-41, ISBN 9788022342087

[2] Killington R.A., Stokes A., Hierholzer J.C. (1996) 4 - Virus purification. In: Mahy B.W.J. (ed.), Kangro H.O. (ed.), Virology Methods Manual, Academic Press, strany 71-89, ISBN 9780124653306

[3] Taulbee D.N., Furst A. (2005) – Centrifugation | Preparative. In: Worsfold P. (ed.), Townshend A. (ed.), Poole C (ed.), Encyclopedia of Analytical Science (Second Edition), Elsevier, strany 469-481, ISBN 9780123693976

[4] Reichel M, Matis J, Lesso J. Stancekova, M. (1991). Polypeptides synthesized in rabbit cells infected with murine herpesvirus (MHV): a comparison of proteins specified by various MHV strains. Acta virologiea 35, 268 275

sciendo

Eur. Pharm. J. 2021, 68(1), 80-83.
ISSN 1338-6786 (online) and ISSN 2453-6725 (print version),
DOI: 10.2478/afpuc-2021-0007

EUROPEAN PHARMACEUTICAL JOURNAL

Transdermal Patches For Delivery of Beta-Blockers

Special Issue Article

Rohaľová S., Guman M., Wolaschka T.✉

Department of Pharmaceutical Technology, Pharmacognosy and Botany, University of Veterinary Medicine and Pharmacy in Košice, Komenského 73, 041 81 Košice, Slovak Republic

Received 15 June, 2021, accepted 17 June, 2021

Abstract Transdermal matrices containing 1.258 mg/cm^2 of propranolol and consisting of ethylcellulose (EC), castor oil, and hydroxypropylmethylcellulose (HPMC) or halloysite (HA) were prepared. They were evaluated by tests such as folding endurance, moisture content and absorption, and paddle dissolution test. Of the total amount of propranolol in the samples (20 mg), 28.41% ± 3.30% was released from the EC film after 24 hours, the addition of HA 20.94% ± 1.52% (f_1 = 61.82 ± 7.70, f_2 = 53.61 ± 4.25) or HPMC 36.05% ± 6.18% (f_1 = 34.48 ± 8.79, f_2 = 65.02 ± 5.33). The dissolution profiles of HA and HPMC films were compared with each other (f_1 = 51.35 ± 12.56, f_2 = 59.20 ± 9.43).

Keywords *ethylcellulose – halloysite – hypromellose – propranolol – transdermal therapeutic system*

INTRODUCTION

Beta-blockers are one of the most used molecules in the therapy of cardiovascular diseases. They are mainly formulated as conventional dosage forms (Aquil et al., 2006). Management of cardiovascular diseases often requires, besides a change of lifestyle, also a long-term pharmacotherapy. This kind of therapy can lead to insufficient patient compliance because of dosage frequency. Orally administered beta-blockers are characterised by the need for doses that are more frequent, significant first-pass effects and variable bioavailability. Transdermal patches prolong the time interval of therapeutic plasma levels, which decreases the incidence of side effects and the dosage frequency. Transdermally administered drugs avoid the hepatic first-pass effect, which increases their bioavailability. Another advantage of transdermal patches is their easy application, which can also contribute to higher patient compliance (Ahad et al., 2015).

Model drug propranolol is significantly hepatically metabolised, which causes low bioavailability 30%–35% after oral administration. Its elimination half-life is 2–6 hours and the partition coefficient logP is 3.03 (Calatayud-Pascual et al., 2018). Thanks to these properties, propranolol is suitable for transdermal administration.

METHODS

Chemicals: Propranolol hydrochloride was purchased from Fagron, a.s. (Olomouc, Czech Republic), ethylcellulose (EC) from Acros Organics (New Jersey, PA, USA), hydroxypropylmethylcellulose (HPMC) from Dr. Kulich Pharma, s.r.o (Hradec Králové, Czech Republic) and halloysite (HA) nanoclay from Aldrich Chemistry (Saint-Louis, MO, USA).

Film preparation was carried out by solvent casting method. Composition of the films is shown in Table 1. The dispersions were prepared by mixing EC in ethanol with castor oil as a plasticiser for 5 minutes at 750 rpm. Propranolol was dissolved in ethanol and added to the dispersion. Either HPMC or HA was added to the prepared dispersions and the mixing was continued for 15 minutes at 750 rpm. Films were poured into Petri dishes previously wiped out with glycerine. HA-containing films underwent incorporation of the drug in a vacuum, which was applied 3 times for 5 minutes. Films were dried (UNB400; Memmert, Schwabach, Germany) after 12 hours at 60 °C and covered with funnels.

Folding endurance was determined by repeatedly folding the film at the same place until visible damage was caused. The number of times the films could be folded without breaking gives the folding endurance value. We considered

* *E-mail: tomas.wolaschka@uvlf.sk*

Table 1. Composition of formulations (in grams).

Film	Propranolol	Ethanol	Castor oil	Ethylcellulose	Halloysite	Hypromellose
E	0.02	10	0.162	0.36	-	-
Ha1	0.02	10	0.162	0.36	0.0225	-
Ha2	0.02	10	0.162	0.36	0.0450	-
HPMC1	0.02	10	0.162	0.36		0.0225
HPMC2	0.02	10	0.162	0.36		0.0450

the film as favourable if it lasted without obvious damage after a hundred folds (Sanap et al., 2008).

Percentage moisture content was calculated using Equation (1), where m_1 is the initial weight of a film and m_2 is the final weight of the same film after being kept in a desiccator with silica gel for 24 hours at room temperature (Arora & Mukherjee, 2002).

$$\% = \frac{m_1 - m_2}{m_2} \ 100 \quad (1)$$

Percentage moisture uptake was calculated using Equation (2), where m_1 is the initial weight of a film and m_2 is the final weight of the same film after being kept in a desiccator with a saturated solution of sodium chloride instead of potassium chloride for 24 hours at room temperature (Arora & Mukherjee, 2002).

$$\% = \frac{m_2 - m_1}{m_1} \ 100 \quad (2)$$

Dissolution test was carried out using a paddle apparatus (50 rpm) with the addition of a modified disc assembly in acetate buffer with pH 4.5 tempered at 32 °C ± 0.5 °C (Ph. Eur. 10.4, 2021). Fourteen samples were collected for 24 hours (SR8 Plus; Hanson Research, Los Angeles, CA, USA).

RESULTS AND DISCUSSION

Folding endurance was the main criterion taken into consideration when formulating the films. Firstly, it was noted that EC films require a plasticiser. Out of castor oil, polyethylene glycol and glycerine, the addition of 0.162 g of castor oil increased the number of folds to 100. Moreover, the amount of EC was increased to 0.36 g to obtain more compact and flexible films. These films remained intact after 400 folds. For homogeneity of the films, it was necessary to direct the evaporating ethanol into a funnel during the drying process.

The addition of 0.0225 or 0.045 g of HPMC caused 0.85% (p = 0.004) or 0.95% (p = 0.002) increase in moisture content and 0.95% (p = 0.278) and 1.93% (p = 0.078) increase in moisture uptake, respectively. In our case, similar to what Dey et al. (2009) had mentioned, HPMC as a hydrophilic polymer increased the water content. HA addition did not cause a statistically significant difference in either moisture content or uptake.

We monitored the amount of propranolol released by dissolution in acetate buffer of pH 4.5 for 24 hours and calculated the similarity (f_2) and difference (f_1) factors to compare the dissolution profiles. Of the total amount of propranolol in the samples, 28.41% ± 3.30% was released from the EC film after 24 hours, the addition of HA 20.94% ± 1.52% (f_1 = 61.82 ± 7.70, f_2 = 53.61 ± 4.25) (Fig. 1) or HPMC 36.05% ± 6.18% (f_1 = 34.48 ± 8.79, f_2 = 65.02 ± 5.33) (Fig. 2). The dissolution profiles of Ha1 and HPMC1 films were compared with each other (f_1 = 51.35 ± 12.56, f_2 = 59.20 ± 9.43). The Food and Drug Administration and the European Medicines Agency consider the dissolution profiles to be similar if f_1 is less than 15 and f_2 is greater than 50 (Costa & Sousa Lobo, 2001). All similarity factors of the dissolution profiles of the films were above 50, and also, all difference factors were considerably above 15; we can therefore conclude that these profiles are not similar.

According to the coefficient of determination (R_2), the drug followed Higuchi model in case of HPMC1 film (R_2 = 0.9805 ± 0.0057) and Korsmeyer–Peppas model in case of Ha1 film (R_2 = 0.9715 ± 0.0032). Release exponents (n) of Ha and HPMC films were in the range 0.5 < n < 1.0, which indicates non-Fickian diffusion of the drug. Based on the percentage of propranolol released from the formulations and their dissolution profiles, it can be stated that HA and HPMC are release rate modifiers in the prepared films. As Dey et al. (2009) had stated, the introduction of hydrophilic HPMC increased the dissolution rate in the case of water-soluble propranolol. However, such small amount of HPMC did not cause the initial burst effect unlike the case of the mentioned paper. HA is known for drug loading of cationic compounds and providing them prolonged release, possibly reducing the burst effect (Levis & Deasy, 2003). Both of these effects are demonstrated in Fig. 1.

In conclusion, we have prepared matrix-type propranolol patches without adhesives, which, to our knowledge, is novel in terms of composition. We have confirmed the possibility of alteration of the dissolution rate with the use of excipients such as HPMC for increasing and HA for decreasing the

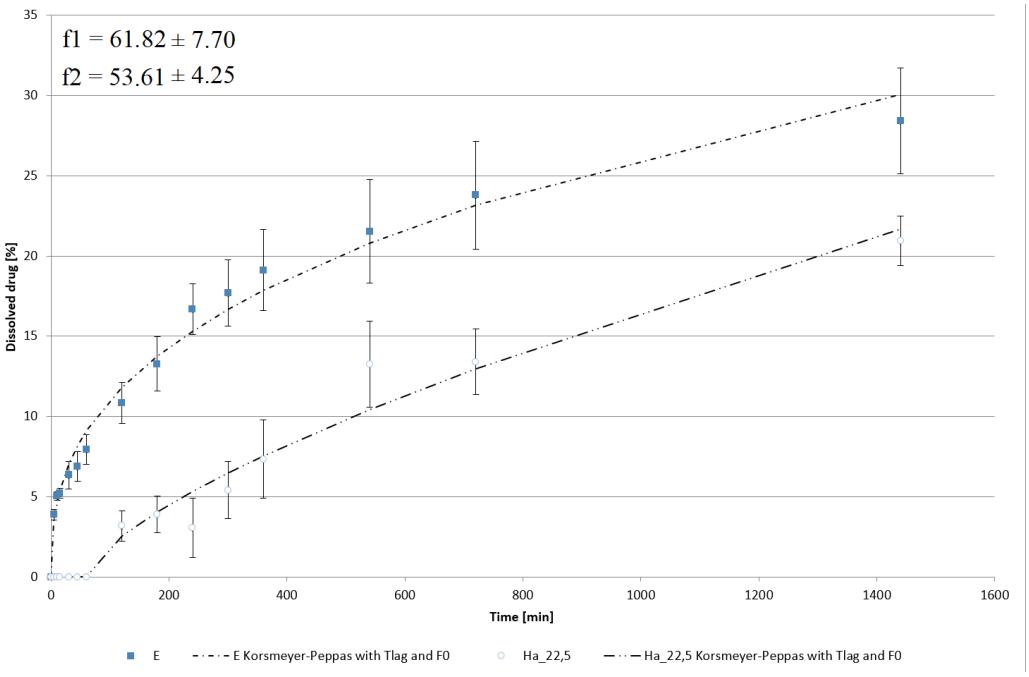

Figure 1. Dissolution profiles of formulations E and Ha1 compared.

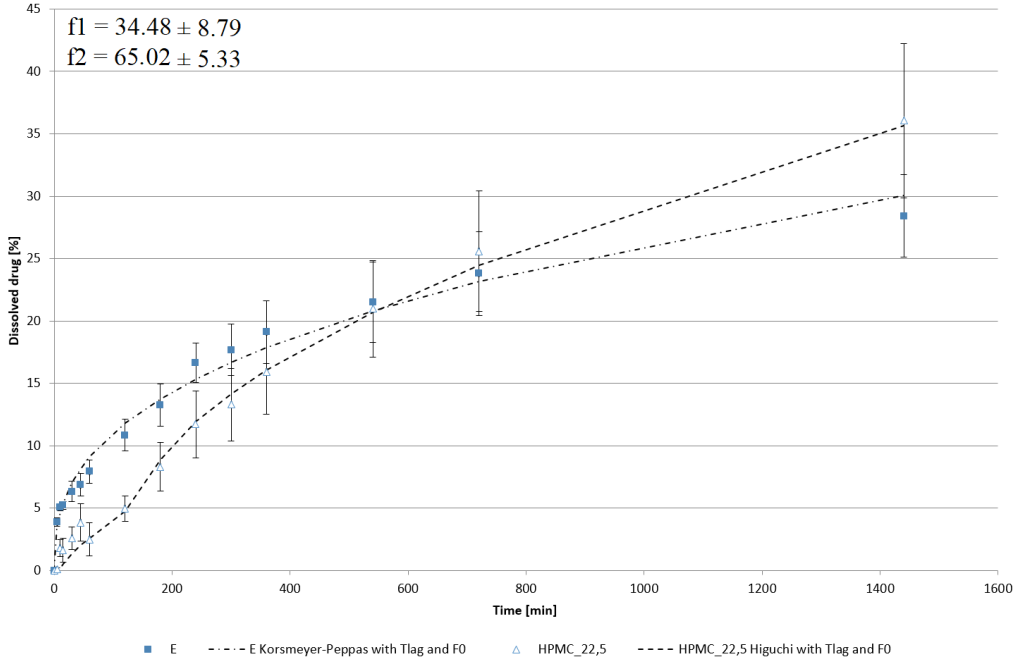

Figure 2. Dissolution profiles of formulations E and HPMC1 compared.

dissolution rate. However, since the daily dose of propranolol usually starts at 40–80 mg, the enhancement of dissolution rate should be considered keeping in mind the possible burst effect of hydrophilic polymers.

ACKNOWLEDGEMENT

The work was supported by the project from the structural funds 'Renewal of research and development infrastructure and instrumentation at UVLF, ITMS 26210120028'.

References

[1] Ahad A, Al-Jenoobi FI, Al-Mohizea AM, Akhtar N, Raish M, Aqil M. Systemic delivery of β-blockers via transdermal route for hypertension. Saudi Pharm J. 2015;23(6):587–602.

[2] Aqil M, Sultana Y, Ali A. Transdermal delivery of β -blockers. Expert Opin Drug Deliv. 2006;3(3):405–18.

[3] Arora P, Mukherjee B. Design, development, physicochemical, and in vitro and in vivo evaluation of transdermal patches containing diclofenac diethylammonium salt. J Pharm Sci. 2002;91(9):2076–89.

[4] Calatayud-Pascual MA, Sebastian-Morelló M, Balaguer-Fernández C, Delgado-Charro MB, López-Castellano A, Merino V. Influence of chemical enhancers and iontophoresis on the in vitro transdermal permeation of propranolol: Evaluation by dermatopharmacokinetics. Pharmaceutics. 2018;10(4).

[5] Costa P, Sousa Lobo JM. Modeling and Comparison of Dissolution Profiles. Eur J Pharm Sci. 2001;13(2):123-133.

[6] Dey BK, Kar PK, Nath LK. Formulation design, preparation and in vitro – in vivo evaluation of propranolol hydrochloride transdermal patches using hydrophilic and hydrophobic polymer complex. Research J. Pharm. and Tech. 2009;2(1):155–160.

[7] European pharmacopoeia 10.4. 2.9.4. Dissolution test for transdermal patches. (https://pheur.edqm.eu/app/10-4/content/10-4/20904E.htm?highlight=on&terms=dissolution). Revised April 2021. Accessed June 7, 2021.

[8] Levis SR, Deasy PB. Use of coated microtubular halloysite for the sustained release of diltiazem hydrochloride and propranolol hydrochloride. Int J Pharm. 2003;253(1–2):145–57.

[9] Sanap GS, Dama GY, Hande AS et al. Preparation of transdermal monolithic systems of indapamide by solvent casting method and the use of vegetable oils as permeation enhancer. Int J Green Pharm. 2008;2(2):129.